

**POLITECNICO DI TORINO**

Collegio di Ingegneria Chimica e dei Materiali

**Corso di Laurea Magistrale  
in Ingegneria Chimica e dei Processi Sostenibili**

Tesi di Laurea Magistrale

**Impact of freezing on the activity of an  
active pharmaceutical ingredient**



**Relatore**

prof. Roberto Pisano

**Candidato**

Maria Valeria Fornaro

Marzo 2018



*To my beloved family  
and boyfriend...*



## Introduzione

La liofilizzazione è una tra le tecnologie di processo più utilizzate dalle industrie alimentari e farmaceutiche per preservare le proprietà di sostanze termolabili o principi attivi, quali ad esempio le proteine, che possono destabilizzarsi se conservate in soluzioni acquose o se vengono trattate con processi termici che lavorano ad alte temperature. La liofilizzazione, anche conosciuta come crioessiccamento, permette di ridurre l'umidità residua della sostanza tramite congelamento della stessa, e sublimazione del ghiaccio sottovuoto. Il processo consta di tre fasi: congelamento, essiccamento primario ed essiccamento secondario.

Durante il congelamento, la temperatura viene diminuita per permettere la totale cristallizzazione dell'acqua. Tale fase è regolata dal grado di sottoraffreddamento e dal fenomeno di nucleazione. Per permettere la formazione dei cristalli di ghiaccio occorre sottoraffreddare il sistema, in quanto la nucleazione è un processo attivato e richiede energia affinché i primi nuclei cristallini possano interagire tra loro, aggregarsi, per poi accrescersi. La temperatura di nucleazione,  $T_n$ , determina il numero e la dimensione dei nuclei cristallini che vengono a formarsi; temperature più basse inducono alla formazione di molti e piccoli cristalli di ghiaccio rispetto temperature di nucleazione più alte che inducono pochi nuclei cristallini ad accrescersi. Poiché il fenomeno è stocastico, non tutti i flaconi enucleano alla stessa temperatura e, pertanto, possono presentare strutture diverse. Anche il metodo di congelamento e la velocità di raffreddamento sono determinanti nel definire la struttura del prodotto congelato. Esistono, inoltre, diverse tecniche che permettono di controllare il processo di nucleazione, al fine di ottenere caratteristiche quanto più comuni possibili tra i prodotti congelati.

Dopo il congelamento, la temperatura dei ripiani del liofilizzatore viene aumentata, mentre la pressione viene diminuita al di sotto di quella atmosferica così da indurre la sublimazione del ghiaccio (essiccamento primario). Una più grande dimensione dei cristalli di ghiaccio facilita la sublimazione poiché permette di diminuire i tempi e i consumi energetici di questa fase, la più lunga dell'intero processo, di ridurre gli stress sul principio attivo legato alle condizioni del processo; ad esempio, alcune proteine tendono a denaturarsi irreversibilmente all'interfaccia soluto/ghiaccio. I parametri di processo (temperatura e pressione) vengono stabiliti in modo da ottimizzare l'essiccamento primario evitando che la temperatura al fronte di sublimazione superi la temperatura di collasso del prodotto. Al tal fine, esistono diversi modelli matematici che si prefiggono di individuare le combinazioni ottimali dei parametri di processo, temperatura dei ripiani,  $T_s$ , e pressione in camera,  $P_c$ , per l'essiccamento primario.

Infine, in un comune processo di liofilizzazione, spesso è richiesta una seconda fase di essiccamento (essiccamento secondario) che richiede temperature più alte, a volte anche maggiori gradi di vuoto, per desorbire parte dell'acqua adsorbita sulla struttura porosa.

### Obiettivo della tesi

L'obiettivo di questo lavoro di tesi è stato quello di studiare come la fase di congelamento possa influire su tre diversi aspetti del processo di liofilizzazione: la struttura del prodotto, la stabilità di un principio attivo farmaceutico (API), e l'ottimizzazione dell'essiccamento primario. A tal fine, sono stati condotti una serie di esperimenti, in parte presso il laboratorio di liofilizzazione del dipartimento DISAT del Politecnico di Torino ed in parte presso il dipartimento di farmacia dell'Università di Ghent (Belgio). I risultati sono stati riportati in tre sezioni differenti in cui si analizzano i tre differenti aspetti studiati in questa tesi.

In una prima sezione, due metodi di congelamento, che si distinguono per la diversa configurazione dei flaconi, sospesi dai ripiani o su di essi appoggiati, sono stati utilizzati per confrontare come può variare la struttura del prodotto in termini di intra-eterogeneità ed eterogeneità del lotto. Inizialmente, si è determinato il range di variabilità delle temperature di nucleazione al variare anche di due protocolli di raffreddamento diversi, uno più veloce (HCR) ed uno più lento (LCR); poi, per il protocollo HCR, alcuni campioni liofilizzati sono stati analizzati al microscopio elettronico (SEM), e sono state stimate le curve distributive del diametro medio dei pori all'interno del lotto. Infine, sfruttando queste conoscenze e per entrambe le configurazioni dei flaconi, sono stati determinati il coefficiente di resistenza al trasferimento di materia,  $R_p$ , e la sua variabilità.

Nella seconda sezione, l'enzima alcol deidrogenasi (ADH) è stato scelto come proteina-modello al fine di valutare l'impatto che il metodo di congelamento ed il protocollo di raffreddamento hanno sulla sua stabilità, valutata in termini di attività residua, per campioni sottoposti a cicli di congelamento-scongelo e cicli di liofilizzazione. Inoltre, per valutare anche l'impatto della formulazione, sono state considerate due diverse concentrazioni di enzima e la presenza o meno di un protettore, scelto tra PEG e saccarosio. In più, si è cercato di stabilire se vi è una correlazione tra la temperatura di nucleazione e l'attività dell'ADH sia per i cicli di congelamento-scongelo che per quelli di liofilizzazione.

Infine, nella terza sezione, si è utilizzato un modello matematico per determinare il Design Space dinamico durante l'essiccamento primario, con l'inclusione, o meno, nel modello delle incertezze di alcune variabili. Il modello si pone l'obiettivo di determinare il profilo dinamico di  $T_s$  e  $P_c$  che ottimizzi la fase di essiccamento primario in termini di tempo (ed energia) e considerando tre diversi rischi di fallimento (RoF 1%, 50%, 99%); il RoF è definito come la probabilità che in uno o più flaconi possa verificarsi il collasso del prodotto e viene stabilito a partire da un'analisi di incertezza. Per studiare l'influenza del metodo di congelamento, le simulazioni sono state condotte prendendo come caso studio una formulazione placebo sottoposta a due differenti protocolli di raffreddamento (primo caso studio), o una formulazione contenente ADH (secondo caso studio). In ultima analisi, sono stati effettuati alcuni cicli di convalida a verifica delle predizioni.

### Struttura dell'elaborato

Il seguente elaborato è stato diviso in 5 capitoli. Il primo capitolo introduce il lettore al processo di liofilizzazione, e cosa esso comporti nel caso in cui il prodotto contenga un principio attivo (API). Ci si è focalizzati principalmente sulla descrizione della fase di congelamento, su cosa influenza e quali sono i diversi metodi, applicati su scala di laboratorio o industriale, e se prevedono o meno di controllare la temperatura di nucleazione. Inoltre, si è descritto in maniera più approfondita cosa spinge una proteina a disattivarsi durante le fasi di congelamento ed essiccamento, quali sono le probabili cause e come poter migliorarne la stabilità introducendo dei crio- e lio-protettori.

I metodi e i relativi risultati sperimentali sono suddivisi in tre capitoli (capitolo 2,3,4). Il capitolo 2 tratta l'impatto del congelamento sulla struttura del prodotto, a seguire, nel capitolo 3 si documenta lo studio sulla stabilità dell'enzima ADH sottoposto a cicli di congelamento-scongelo e cicli di liofilizzazione, infine, nel capitolo 4, si è cercato di valutare l'impatto del congelamento e delle incertezze di alcuni parametri di input sull'ottimizzazione del ciclo tramite Design Space dinamico.

In conclusione, il capitolo 5 riepiloga il lavoro svolto e riassume i principali risultati ottenuti.

## **Impatto del congelamento sulla struttura del prodotto**

Per determinare l'influenza che il congelamento può avere sulla struttura del prodotto, sono stati confrontati due metodi di congelamento che si distinguono per la configurazione dei flaconi, sospesi dai ripiani o su di essi appoggiati. Inizialmente, sono state determinate le temperature di nucleazione per ogni flacone secondo due protocolli di raffreddamento diverso, uno più veloce (HCR) ed uno più lento (LCR). Poi, per il protocollo HCR, dei campioni liofilizzati sono stati analizzati al microscopio elettronico (SEM) per correlare la variabilità della dimensione dei pori con la temperatura di nucleazione. Dalla dimensione dei pori si è proceduto a calcolare il coefficiente di resistenza al trasferimento di materia,  $R_p$ , e la sua variabilità, per i flaconi sospesi e non sospesi. Inoltre, dato che la soluzione utilizzata conteneva mannitolo, in alcuni campioni liofilizzati sono stati identificati i polimorfi del mannitolo tramite un'analisi diffrattometrica ai raggi X (XRD).

### Materiali e metodi di congelamento

Tutte le prove hanno previsto l'uso di soluzioni acquose di mannitolo al 5% in peso, utilizzando acqua per iniezione e filtrando le soluzioni con filtri di 0.2  $\mu\text{m}$ . I flaconi sono stati riempiti con 3 ml della soluzione preparata.

Per sospendere i flaconi dai ripiani del liofilizzatore si è utilizzato un supporto in plexiglass costituito da due barre che trattengono i flaconi e che sono rialzate tramite delle viti di sostegno regolabili. Sono stati inseriti 14 flaconi non sospesi e 14 sospesi sui quattro ripiani della camera del liofilizzatore (LyoBeta 25, Tesla, Spagna). La diversa disposizione dei flaconi influisce sul meccanismo di trasferimento del calore. Se i flaconi sono appoggiati sui ripiani del liofilizzatore, la conduzione è il meccanismo principale di trasferimento di calore. Viceversa, convezione e irraggiamento prevalgono per i flaconi sospesi.

Il protocollo HCR, prevedeva di raffreddare la temperatura dei ripiani da 20°C a -55°C il più velocemente possibile, nei limiti di potenza del sistema di refrigerazione; il secondo protocollo, invece, prevedeva di raffreddare fino a -55°C in 6 ore.

#### Curve distributive della temperatura di nucleazione

Per determinare la temperatura di nucleazione,  $T_n$ , di ogni campione è stato utilizzato un metodo semplice ma sufficientemente accurato per gli scopi di questo lavoro di tesi. Esso prevede di misurare direttamente la temperatura di nucleazione di alcuni campioni tramite l'utilizzo di termocoppie, collegate ad un software di rilevamento, e di determinare la temperatura di nucleazione degli altri campioni sfruttando la conoscenza dei loro tempi di nucleazione che venivano registrati tramite l'installazione di alcune webcam davanti la camera del liofilizzatore.

Essendo la nucleazione un processo esotermico, la temperatura aumenta durante la nucleazione per poi nuovamente diminuire a fenomeno ultimato. Un profilo termico continuo viene quindi estrapolato per non considerare il picco di nucleazione, permettendo così di determinare i valori di temperatura per gli altri campioni. Le prove di congelamento sono state ripetute più volte al fine di avere un numero soddisfacente di valori di  $T_n$  per permettere di determinare delle curve gaussiane delle temperature di nucleazione. Inoltre, poiché la ripetibilità delle prove non è ovvia, i valori delle temperature di nucleazione sono state normalizzate rispetto il valore medio di  $T_n$  per ogni configurazione (flaconi sospesi e non sospesi) in ogni ciclo. In questo modo sono state determinate anche delle curve di distribuzione normalizzate.

#### Caratterizzazione morfologica e curve distributive del diametro medio dei pori

Relativamente al solo protocollo HCR, 5 liofilizzati per ciascuna configurazione sono stati analizzati al SEM. Al fine di rilevare come varia la morfologia della matrice porosa lungo lo spessore della torta essiccata, i rilevamenti sono stati effettuati in tre posizioni diverse (fondo, centro, top). Per ogni immagine SEM, è stato calcolato il poro medio e la corrispondente deviazione standard approssimando i pori a delle ellissi e calcolando, quindi, un diametro medio equivalente. Infine, è stato attribuito un valore medio del poro per quel determinato campione alla quale è associata una temperatura di nucleazione.

Conoscendo le curve distributive delle temperature di nucleazione, si è poi passata da una distribuzione discreta dei diametri medi dei pori ad una continua, estrapolando una funzione che interpola linearmente i 5 punti disponibili per ogni configurazione. Tramite questa funzione, si sono ottenute, quindi, le curve distributive del diametro medio dei pori per le due configurazioni dei flaconi.

#### Determinazione di $R_p$ e sua variabilità

Il coefficiente di resistenza al trasferimento di materia nello strato essiccato durante l'essiccamento primario,  $R_p$ , è stato sia determinato sperimentalmente, e confrontato con il valore teorico che si ricava attraverso un modello che correla  $R_p$  al diametro dei pori e allo spessore dello strato essiccato. Noto il diametro dei pori e la loro varianza, è stato dunque calcolato un  $R_p$  medio e la rispettiva variabilità. Inoltre,  $R_p$  è stato anche calcolato individualmente per ogni campione analizzato al SEM, considerando che il diametro all'interno del prodotto non è costante, e conoscendo tre valori medi e rispettive deviazioni standard lungo lo spessore. In questo modo si è determinata l'intra-variabilità di  $R_p$  per ciascun prodotto. Infine, i valori di  $R_p$  medio dei prodotti analizzati al SEM sono stati plottati in un unico grafico in funzione della temperatura di nucleazione.

## Determinazione della struttura cristallina del liofilizzato

I prodotti sono stati analizzati tramite analisi XRD poiché il mannitolo può cristallizzare in tre forme diverse (polimorfi). Il polimorfo  $\beta$  è quello stabile, mentre i polimorfi  $\alpha$  e  $\delta$  sono metastabili. Gli spettri sono stati confrontati con i picchi di riferimento che caratterizzano i tre polimorfi per determinare qualitativamente quali forme sono presenti e se vi è una differenza tra la struttura cristallina dei flaconi sospesi e di quelli non sospesi.

## Risultati

### Curve distributive di $T_n$

Tramite i profili di temperatura, la velocità di raffreddamento è stata misurata per entrambe le configurazioni nei due diversi protocolli. È stata rilevata una velocità media di  $0.85^\circ\text{C}/\text{min}$  per i flaconi non sospesi, ed una di  $0.55^\circ\text{C}/\text{min}$  per i flaconi sospesi nel protocollo HCR. Relativamente all'altro protocollo (LCR), le velocità sono simili e rispettivamente di  $0.2^\circ\text{C}/\text{min}$  e  $0.15^\circ\text{C}/\text{min}$ .

Analizzando le curve distributive relative al primo caso, il range di  $T_n$  varia maggiormente per i flaconi non sospesi rispetto a quelli sospesi. Tale divergenza è molto meno pronunciata per il protocollo LCR dato che le due configurazioni sono caratterizzate quasi dalla stessa velocità di raffreddamento.

Inoltre, la temperatura media di nucleazione si abbassa di qualche grado al variare del protocollo, passando da  $-10$  a  $-13^\circ\text{C}$  per i flaconi non sospesi, e da  $-15^\circ\text{C}$  a  $-16^\circ\text{C}$  per quelli sospesi.

Per determinare le curve di distribuzione sono stati effettuati più cicli. La determinazione delle temperature di nucleazione soffre della ripetibilità delle prove. Nonostante la camera sia sempre stata pulita, le soluzioni sempre filtrate e sono sempre stati utilizzati dei flaconi di vetro nuovi, la ripetibilità delle prove non è ovvia. Inoltre, in ambito industriale questi range possono essere ancora maggiori perché si lavora in condizioni "dust free" (assenza di polvere) e il fenomeno di nucleazione risulta puramente stocastico.

### Morfologia e curve distributive di $D_p$

Dalle analisi SEM è stato evidenziato che, a seguito del protocollo HCR, i liofilizzati dei campioni sospesi mostrano pori di maggiori dimensioni e omogenei all'interno della struttura porosa. Invece, i flaconi non sospesi mostrano dimensioni dei pori minori e molto variabili all'interno. Dalle curve di distribuzione del diametro medio, risulta che i flaconi sospesi sono caratterizzati da un diametro medio del poro di circa  $97\ \mu\text{m}$ , mentre quelli non sospesi di circa  $41\ \mu\text{m}$ .

### $R_p$ e sua variabilità

Dal valore sperimentale di  $R_p$  e dal calcolo teorico, si rivela come  $R_p$  per i flaconi non sospesi sia maggiore, il che comporta maggiori tempi di essiccamento primario. Sfruttando i dati delle curve di distribuzione dei  $D_p$  medi, è stata determinata la variabilità di  $R_p$  globale, con valori di incertezza maggiori per i flaconi non sospesi. L'incertezza sui flaconi sospesi è, invece, quasi trascurabile. Calcolando  $R_p$  per ogni campione liofilizzato ed analizzato al SEM, al variare di  $D_p$  all'interno della struttura porosa, si nota come l'intra-variabilità di  $R_p$  sia molto più elevata per i flaconi non sospesi che per i sospesi. Infine, anche dal diagramma di  $R_p$  medio in funzione di  $T_n$ , la variabilità è maggiore per i flaconi non sospesi, e si nota come al diminuire della temperatura di nucleazione  $R_p$  aumenti.

### Struttura fisica dei prodotti liofilizzati

Dalle analisi XRD, i flaconi non sospesi rilevano essere costituiti quasi dal solo polimorfo  $\beta$  del mannitolo, ossia dalla forma stabile, mentre i flaconi sospesi rilevano anche una presenza, non trascurabile, della forma metastabile  $\alpha$  oltre la forma  $\beta$ .

## **Impatto del congelamento sull'enzima ADH**

Si è scelto di lavorare con la proteina alcol deidrogenasi (ADH) come ingrediente attivo delle formulazioni da testare. Si sono sottoposti i campioni a cicli di congelamento-scongelo e di liofilizzazione lavorando con il metodo convenzionale dei flaconi non sospesi con due velocità di raffreddamento (1°C/min e 0.1 °C/min), o utilizzando un congelamento rapido tramite immersione dei campioni in azoto liquido per pochi minuti. Inoltre, è stata variata la concentrazione della proteina (0.1 mg/ml o 0.01 mg/ml), includendo o meno uno stabilizzante scelto tra PEG e saccarosio. Infine, la temperatura di nucleazione è stata monitorata per valutarne l'impatto sull'attività residua dell'enzima.

### Materiali e metodi

Sono state preparate soluzioni placebo (i) di sola acqua, (ii) con 2.5%(w/v) di PEG, (iii) con 2.5% (w/v) di saccarosio utilizzando acqua per iniezione. Le soluzioni sono state filtrate con filtro di 1.2 µm. La proteina ADH veniva aggiunta in concentrazione di 0.1 mg/ml o 0.01 mg/ml solo dopo la filtrazione per evitare di perdere alcune sue molecole. Qualora si doveva testare l'effetto della concentrazione sull'attività dell'ADH lavorando con lo stesso ciclo, la formulazione più concentrata (0.1mg/ml) veniva opportunamente diluita con la rispettiva soluzione placebo per ottenere una concentrazione finale di 0.01 mg/ml. I flaconi di vetro venivano riempiti con 3ml delle soluzioni preparate.

La proteina è stata sottoposta a cicli di congelamento-scongelo e cicli di liofilizzazione.

Riguardo i primi, con velocità di 1°C/min, la temperatura dei ripiani veniva diminuita da 20°C a -40°C in 1 ora e 15 minuti; con velocità di 0.1°C/min i tempi di congelamento erano di 12 ore e 15 minuti. Prima di scongelare i campioni il ciclo prevedeva una fase di stoccaggio di quasi 14 ore. Al termine di essa, i campioni venivano prelevati e scongelati in un bagno d'acqua a 15°C.

Alcuni campioni inoltre sono stati congelati immergendoli in azoto liquido per 1 minuto e mezzo, poi i campioni venivano o stoccati a -40°C per 15 ore o direttamente scongelati.

Per i cicli di liofilizzazione, la pressione della camera veniva impostata a 10Pa, mentre la temperatura veniva alzata a -32°C in 42 ore. Seguiva poi l'essiccamento secondario, aumentando la temperatura a 20°C in 9 ore e restandoci per almeno 12 ore.

Per determinare l'impatto della temperatura di nucleazione al termine del processo di liofilizzazione per la formulazione ADH (0.01 mg/ml) e saccarosio (2.5% w/v) il ciclo prevedeva di raffreddare i campioni da 20°C a -40°C a 0.1°C/min o 1°C/min. I campioni venivano stoccati a -40°C per un'ora prima di diminuire la pressione a 10Pa. Durante l'essiccamento primario la temperatura veniva aumentata fino a -28°C in 38 h e poi nuovamente aumentata a 20°C in 8 ore durante l'essiccamento secondario, per restare a 20°C per almeno 12 ore.

### Misura dell'attività dell'enzima

L'attività biologica dell'ADH è stata testata tramite analisi spettrofotometrica durante la reazione di conversione dell'etanolo in aldeide mediata dall'enzima ADH e dal coenzima NAD<sup>+</sup>. La misura dell'attività veniva effettuata su di un campione di riferimento non sottoposto al processo, e su tutti gli altri campioni al termine del ciclo. I campioni liofilizzati venivano ricostituiti con l'aggiunta di 3 ml di acqua pura. Per ogni campione si è misurata l'attività mediata tra 12 rilevamenti. Si è calcolata l'attività residua dei campioni tramite valore relativo percentuale rispetto l'attività del campione di riferimento.

Il kit di attività prevedeva di diluire l'enzima ad una concentrazione di 1.25 µg/ml con una soluzione di 0.1% w/v di siero albumina (BSA) in 10mM di buffer sodio fosfato con pH 7.5. La miscela di reazione conteneva inoltre 90 µl di 50mM di sodio pirofosfato (pH 8.8), 21 µl di etanolo (35%v/v), 100 µl di 15mM β-NADH e 18 µl della soluzione diluita di ADH.

### Risultati

#### Dopo i cicli di congelamento-scongelo

Riguardo la stabilità dell'enzima ADH, i test permettono di concludere come questa molecola sia tollerante agli stress di congelamento, ma si disattiva durante il ciclo completo di liofilizzazione, tale che è necessario aggiungere un lioprotettore in soluzione. L'ADH è tollerante al congelamento perché conservava circa l'80-90% della sua attività dopo il ciclo congelamento-scongelo in assenza di protettori. Inoltre, lavorare con una maggiore concentrazione di proteina ha permesso di preservare ancora di più l'attività rispetto le formulazioni contenente la concentrazione minore. Non vi è stato trovato alcun impatto dei metodi di congelamento, della velocità di raffreddamento e della temperatura di nucleazione durante i cicli di congelamento-scongelo. Poiché l'ADH non soffre degli stress dovuti alla formazione del ghiaccio durante il congelamento, la dimensione del cristallo di ghiaccio non è causa di disattivazione dell'ADH. Questo comportamento è probabilmente dovuto all'assenza di un'interfaccia che potesse compromettere irreversibilmente la denaturazione della proteina.

### Dopo i cicli di liofilizzazione

In relazione alla formulazione, è stato scoperto che il PEG non è in grado di proteggere l'ADH durante l'essiccamento. In effetti, l'attività recuperata è addirittura inferiore rispetto al caso di una formulazione di acqua e ADH. Invece, c'è una buona ripresa dell'attività se nella formulazione si aggiunge il saccarosio. Inoltre, la formulazione migliore risulta sempre quella contenente più enzima.

Al fine di stabilire se esiste una correlazione tra la temperatura di nucleazione e l'attività enzimatica per i prodotti liofilizzati, è stata scelta la formulazione con la minore concentrazione di enzima e con saccarosio come protettore. Tale scelta si spiega poiché la proteina sembra essere più sensibile a basse concentrazioni ed il saccarosio potrebbe influenzare l'attività dell'enzima per la creazione di un'interfaccia durante l'essiccamento primario. Dopo l'essiccamento, utilizzando una velocità di raffreddamento di 1°C/min, si è verificata una diminuzione dell'attività dell'ADH con il diminuire della temperatura di nucleazione, cioè presenza di pori più piccoli e quindi di maggiore interfaccia proteina/soluto. Invece, con velocità di raffreddamento di 0.1 °C/min, la temperatura di nucleazione sembra non influenzare l'attività enzimatica probabilmente a causa della maggiore uniformità della struttura del liofilizzato e soprattutto della dimensione maggiore dei pori.

## **Impatto del congelamento sull'ottimizzazione del ciclo attraverso Design Space dinamico**

Un modello meccanicistico è stato utilizzato per determinare il Design Space, ovvero lo spazio configurazionale dei parametri di processo, temperatura dei ripiani e pressione in camera ( $T_s$  e  $P_c$ ) con cui condurre l'essiccamento primario. Il modello ha l'obiettivo di determinare il profilo dinamico di  $T_s$  e  $P_c$  che ottimizzi la fase di essiccamento primario in termini di tempo (ed energia) e considerando tre diversi rischi di fallimento (1%, 50%, 99%) definiti come la probabilità che in uno o più flaconi possa verificarsi il collasso del prodotto. Il rischio di fallimento viene stabilito a partire da un'analisi di incertezza di alcune variabili di input e di processo. Due casi studio sono stati analizzati; nel primo, le simulazioni sono state condotte su di una formulazione placebo utilizzando due protocolli di raffreddamento diverso, nel secondo caso, si è lavorato con una formulazione contenente ADH. Inoltre, alcuni cicli di convalida sono stati effettuati a verifica delle predizioni del modello.

### Materiali

Sono state preparate due soluzioni:

- 1) 1% (w/v) di saccarosio, 4% (w/v) di mannitolo in 0.05 M di soluzione tampone sodio fosfato (pH 7.4)
- 2) 2.5% (w/v) di saccarosio, 0.01 mg / ml di alcol deidrogenasi (ADH).

Il tampone salino di 0.05M è stato preparato miscelando 1.65 g di sodio fosfato bibasico ( $\text{Na}_2\text{HPO}_4$ ) e 0.53 g di sodio fosfato monobasico diidrato ( $\text{NaH}_2\text{PO}_4 \cdot 2 \text{H}_2\text{O}$ ) in 300 ml di acqua per iniezione. Questa soluzione tampone è stata utilizzata per preparare la formulazione finale aggiungendo mannitolo (4%w/v) e saccarosio (1% w/v). Poi,

il pH veniva misurato per verificare che il target 7.4 non fosse alterato. La soluzione veniva filtrata con un filtro di 0.2  $\mu\text{m}$ .

La soluzione contenente ADH è stata preparata come riportato nella sezione 2 (Impatto del congelamento sull'enzima ADH).

Per la validazione del modello, ogni test è stato eseguito nel liofilizzatore (LyoBeta 25, Tesla, Spagna) con un totale di 100 flaconi di vetro riempiti con 3 ml della formulazione studiata e posti direttamente su un solo ripiano utilizzando una disposizione quadrata.

Si noti che, per la convalida del secondo caso studio, non tutte le fiale contenevano la proteina, ma solo 10 fiale. Due di queste, posizionate una sul bordo ed una al centro della disposizione quadrata, contenevano le termocoppie per monitorare la temperatura del prodotto; le altre 8 fiale sono state posizionate casualmente nella disposizione quadrata. Questo aggiustamento non ha influenzato la validazione dei test perché la bassa presenza della proteina non influisce sulle proprietà termiche della formulazione.

### Misura della temperatura critica

Uno dei limiti che il modello tiene in considerazione è la temperatura critica del prodotto,  $T_{cr}$ . Per evitare il collasso, avere rapida ricostituzione del prodotto essiccato ed una struttura estetica accettabile, la temperatura del prodotto sul fronte di sublimazione,  $T_i$ , non deve superare la temperatura di collasso,  $T_c$ , durante l'essiccamento primario.

In generale, poiché la temperatura di transizione vetrosa,  $T_g'$ , è leggermente inferiore a  $T_c$ , nel modello  $T_{cr}$  è stata impostata uguale a  $T_g'$ , introducendo, in questo modo, un ampio margine di sicurezza.

Per la prima formulazione, la temperatura di collasso al punto medio ( $T_{c-50}$ ) è stata utilizzata come  $T_{cr}$ , prendendo tale valore dalla letteratura. Questa temperatura è stata calcolata come la media tra l'inizio della temperatura di collasso ( $T_{oc}$ ) e la temperatura di collasso finale ( $T_{fc}$ ) misurate tramite "freeze-drying microscopy" (FDM).

Invece, la temperatura di transizione vetrosa,  $T_g'$ , misurata con la calorimetria differenziale a scansione modulata (MDSC) è stata utilizzata come temperatura critica per il secondo caso. Il campione è stato inizialmente raffreddato fino a -90 °C ed è stato mantenuto a quella temperatura per 5 minuti; poi, la temperatura è stata aumentata fino a 0 °C con una velocità di riscaldamento di 2°C/min.

È importante prendere in considerazione il metodo utilizzato per misurare la temperatura critica.  $T_c$  può dipendere dalla metodologia di misurazione, dalla variazione della velocità di sublimazione e dalla variazione dell'area superficiale del prodotto essiccato. Ad esempio, il valore  $T_{c-50}$ , originato dall'analisi FDM, è generalmente superiore a  $T_g'$  misurata tramite DSC. Inoltre, La temperatura di collasso osservata in una fiala durante la liofilizzazione spesso è superiore di 1-3 °C rispetto i valori calcolati con strumentazioni di laboratorio.

### Modello di Design Space dinamico

Questo modello meccanicistico, sviluppato presso l'università di Ghent, si basa su equazioni di massa ed energia che descrivono il processo di sublimazione durante l'essiccamento primario. Esso è costruito verificando che  $T_i$  sia sempre inferiore a  $T_{cr}$  (parametro di input del modello) durante tutto l'essiccamento primario e modellando i parametri di processo  $P_c$  e  $T_s$  per avere una massima efficienza di sublimazione (ottimizzazione del ciclo). Inoltre, verifica anche che durante la simulazione il fenomeno "choked flow" non sia presente.

Il modello si basa sulle seguenti semplificazioni: considera il fronte di sublimazione planare e che l'energia trasferita sia utilizzata solo per la sublimazione del ghiaccio, quindi ipotizzando uno stato stazionario. Inoltre, il carico computazionale è limitato da una griglia di calcolo per  $P_c$  e  $T_s$ . I limiti per  $P_c$  sono stati impostati a 10 Pa e 14 Pa, mentre l'intervallo per  $T_s$  cambia durante il processo in funzione della rampa di temperatura massima di 1°C/min che l'apparecchiatura può sopportare.

Se le incertezze non sono incluse come parametri di input, il modello calcola i profili di  $T_c$  e  $P_c$  come segue: ad ogni passo temporale, viene creata una griglia ( $T_s$ - $P_c$ ). Per ogni punto della griglia, che significa per ciascuna combinazione di  $T_s$  e  $P_c$ , viene calcolata la velocità di sublimazione e vengono verificate le due condizioni limite ( $T_i < T_{cr}$  e il criterio "choked flow"). Se almeno una delle due condizioni non viene verificata, per quel punto della griglia viene associata una velocità di sublimazione uguale a zero. Alla fine, viene selezionata la combinazione  $T_s$ - $P_c$  alla quale corrisponde la massima velocità di sublimazione (ottimizzazione del processo). La simulazione

continua con un nuovo intervallo temporale fino a quando lo strato di prodotto essiccato  $L_d$  raggiunge il valore dello spessore totale  $L_t$ .

### Analisi delle incertezze

Le incertezze possono derivare da diversi motivi, ad esempio:

- 1) Il modello meccanicistico contiene un grado di incertezza perché si basa su assunzioni e semplificazioni della realtà.
- 2) La griglia di calcolo introduce altre incertezze a causa degli errori numerici inclusi nei calcoli.
- 3) I parametri utilizzati nel modello meccanicistico sono spesso una stima (basata su dati di letteratura o determinata sperimentalmente) e la loro incertezza è originata da varie fonti.

Per valutare l'impatto dell'incertezza sulla determinazione dello spazio di progettazione, il modello utilizza la "tecnica di campionamento Sobol" che crea un insieme di combinazioni tra le variabili di input e i parametri di processo, caratterizzati o da un limite inferiore ed uno superiore o da un range di incertezza rispetto il loro valore medio. È stata inclusa nel modello l'incertezza di 8 fattori e, poiché  $L_d$  è sia una variabile di input che di output, la propagazione dell'errore sulla stima dello spessore dello strato essiccato in funzione del tempo di essiccamento primario è stata inclusa nell'analisi di incertezza.

Tra gli otto fattori è stato incluso  $R_p$ . In particolare, per il primo caso studio si è utilizzato un modello matematico che, noto il protocollo di congelamento e le temperature di nucleazione, predice la morfologia dei pori lungo lo strato di prodotto essiccato. Dalla morfologia si risale dunque al valore di  $R_p$  e sua incertezza. Nel secondo caso, invece,  $R_p$  è stato determinato sperimentalmente.

Gli 8 fattori sono stati variati insieme ottenendo 1000 combinazioni. Ad ogni passo temporale, e per ogni punto della griglia  $T_s-P_c$ , sono state eseguite 1000 simulazioni ottenendo 1000 valori diversi per  $T_i$  (per quel punto di griglia). I valori di  $T_i$  venivano ordinati dal valore più piccolo a quello più grande (per ciascun punto di griglia), fissando  $T_i$  al valore corrispondente al percentile superiore " $\alpha$ " (delle distribuzioni ordinate dei 1000 valori di  $T_i$ ). Proseguendo, la velocità di sublimazione veniva calcolata in ciascun punto della griglia, impostata a 0 se le condizioni limite non erano rispettate. Infine, per ciascuna fase temporale, è stata scelta la combinazione  $P_c-T_s$  con la massima velocità di sublimazione. In questo modo, esiste una probabilità di  $1-\alpha$  che la temperatura effettiva superi  $T_i$  calcolata dal modello e il rischio di fallimento associato,  $R_{of}$ , è  $1-\alpha\%$ .

Ad esempio, se  $T_i$  è fissata al percentile superiore del 99%, il rischio di fallimento è dell'1%. Al contrario, il rischio di fallimento del 99% corrisponde alla scelta del percentile superiore dell'1% di  $T_i$ .

Secondo questa metodologia, se il  $R_{of}$  è più alto (es. 99%  $R_{of}$ ), il Design Space diventa più ampio poiché molte combinazioni di  $T_s-P_c$  rispettano le due limitazioni (poiché il percentile superiore dell'1% è stato selezionato per ciascuna punto di griglia) e i valori di  $T_s$  e  $P_c$  possono essere impostati a valori più spinti, inducendo velocità di sublimazione più elevata e tempo di essiccamento primario più corto. Invece, con un valore più conservativo del  $R_{of}$ ,  $T_s$  è inferiore e il tempo del processo aumenta.

### Risultati

Le simulazioni hanno rivelato che l'inclusione di un livello di incertezza ha influito sul tempo di essiccamento primario e sulla qualità dei prodotti finali. Se le incertezze non venivano incluse nel modello, la probabilità di fallimento era superiore al 50% e più vicino al 99%. In termini generali, è ovvio che lavorare con un rischio più elevato di fallimento comporta un più alto tasso di sublimazione, diminuendo il tempo di essiccamento primario ma aumentando la probabilità che possa avvenire il di uno o più campioni.

Confrontando le previsioni dei protocolli HCR e LCR per il primo caso studio è stato confermato che il metodo di congelamento ha un impatto sull'ottimizzazione del ciclo anche tramite Design Space. Infatti, la predizione del tempo di essiccamento primario è inferiore con il protocollo LCR a causa della dimensione più grande dei pori che ha ridotto la resistenza di trasferimento di materia  $R_p$ .

Riguardo il secondo caso studio, sono state effettuate due convalide delle previsioni del modello (50% e 99%  $R_{of}$ ). Con questi esperimenti, è stato possibile dimostrare che l'incertezza della temperatura critica  $T_{cr}$  è importante e una sua sottostima rende le previsioni molto conservative (il collasso non si è mai verificato). Inoltre, nel secondo caso studio, la durata dell'essiccamento primario misurato sperimentalmente tenendo valori fissi di  $P_c$  e  $T_s$  è stato

confrontato con due cicli progettati con il design space dinamico, risultando più lungo. Il risultato ha dimostrato, quindi, che il Design Space dinamico ha permesso di ottimizzare il ciclo in termini di tempo (ed energia) garantendo alcuni attributi critici che dipendono dal livello di incertezza che si vuole includere nel modello.

## **Conclusioni**

In conclusione, da questi risultati emerge l'importanza che il congelamento ha sul processo di liofilizzazione e sulle caratteristiche del prodotto finale.

Certamente, lavorare con metodi di congelamento che inducono la formazione di cristalli di ghiaccio più grandi ed uniformi è un beneficio, perché riduce i tempi di essiccamento e, inoltre, potrebbe favorire la stabilità di molecole sensibili, come le proteine. Ad esempio, in questo lavoro di tesi, l'ADH, sembra disattivarsi maggiormente in presenza di maggiore area superficiale durante l'essiccamento, benché in generale risulti particolarmente resistente agli stress dovuti al congelamento. Infine, si è dimostrato che il protocollo di congelamento ha un impatto non trascurabile sull'ottimizzazione di processo attraverso la costruzione del Design Space dinamico.

Questo lavoro di tesi, può essere, quindi, considerato preliminare ad altre future ricerche in tale ambito, come, ad esempio, lo studio dell'impatto del congelamento su altri principi attivi, o il miglioramento del modello matematico alla base del Design Space includendo, tra i parametri di incertezza, anche quello relativo alla temperatura critica del prodotto.



# Index

<b>1. Freeze-drying of proteins.....</b>	<b>1</b>
1.1. Introduction .....	1
1.2. Freeze-drying process.....	2
1.2.1. Freezing.....	2
1.2.2. Primary drying.....	4
1.2.3. Secondary Drying.....	6
1.3. Freezing methods and consequences on quality attributes of biopharmaceuticals.....	6
1.4. Lyophilization plants.....	9
1.4.1. Batch lyophilization .....	10
1.4.2. Continuous lyophilization .....	11
1.5. Protein Stabilization .....	12
1.5.1. Denaturation stresses during lyophilization .....	13
1.5.2. Mechanisms of stabilization.....	15
1.5.3. Excipients for cryo- and lyo-protection.....	17
1.6. Motivation of the thesis.....	19
List of symbols .....	20
References .....	21
<b>2. Impact of the freezing method on inter and intra-vial variability .....</b>	<b>25</b>
2.1. Introduction .....	25
2.2. Materials and methods.....	25
2.2.1. Preparation of the solution.....	25
2.2.2. Freezing methods: conventional shelf-ramped and suspended-vial freezing .....	26
2.2.3. Product characterization .....	27
2.3. Results and discussions .....	30
2.3.1. Nucleation temperature distribution .....	30
2.3.2. Characterization of the product morphology.....	33

2.3.3.	Variability of mass transfer resistance .....	39
2.3.4.	Characterization of Mannitol formulation.....	43
2.4.	Conclusions .....	46
	List of symbols .....	47
	References .....	48
<b>3.</b>	<b>Impact of the freezing method on ADH activity recovery .....</b>	<b>51</b>
3.1	Introduction .....	51
3.2	Materials and methods.....	51
3.2.1	Preparation of the solutions.....	51
3.2.2	Inactivation tests: freeze-thawing and freeze-drying of ADH solutions .....	51
3.2.3	Measurement of enzymatic recovered activity .....	53
3.3	Results and discussions .....	55
3.3.1	After Freezing-thawing .....	55
3.3.2.	After Freeze-drying .....	59
3.4.	Conclusions .....	64
	Abbreviations .....	65
	References .....	65
<b>4.</b>	<b>Impact of freezing on cycle design: optimization via dynamic Design Space. ....</b>	<b>67</b>
4.1.	Introduction .....	67
4.2.	Material and Methods.....	68
4.2.1.	Preparation of the solutions and freezing protocols .....	68
4.2.2.	Measure of the critical temperature ( $T_{cr}$ ).....	69
4.2.3.	Model formulation for primary drying .....	69
4.2.4.	Uncertainty analysis .....	71
4.3.	Results and discussion.....	74
4.3.1.	Freeze-drying of the mannitol-based formulation .....	74
4.3.2.	Freeze-drying of the sucrose-based formulation .....	78

4.4. Conclusions .....	81
List of symbols .....	81
References .....	83
<b>5. Conclusions .....</b>	<b>87</b>
<b>Acknowledgments.....</b>	<b>91</b>



# Chapter 1

## 1. Freeze-drying of proteins

### 1.1. Introduction

Proteins are becoming an important class of drugs in human health care. They are large, complex molecules that play many critical roles in the body; for example, antibodies, enzymes, cell messengers, structural components and transporters within the cell and throughout the body are proteins.

The preservation of the biological material in a stable state is an elemental demand in biological and medical science, agriculture, and biotechnology. For bioactive macromolecules, such as proteins, freeze-drying is the most commonly used method of preservation and extension of shelf life. Indeed, many proteins have limited long-term storage stability in the aqueous state because they are susceptible to chemical degradations by both reactions, e.g., deamidation, oxidation, as well as physical degradations, e.g., aggregation and precipitation in liquid formulations.

Despite lyophilization is the most used method for preparing solid protein pharmaceuticals, during the process the proteins are exposed to different stresses, such as freezing and drying stresses, which consequently impact on the efficacy and performance of the final product (Wang, 2000). Thus, the freeze-drying process, as well as the protein formulation, have to be optimized to enhance the preservation of the protein function. An overview of the process is shown in Figure 1.1.

In this chapter, the main aspects of the freeze-drying process and protein stabilization during freezing and freeze-drying are briefly discussed.

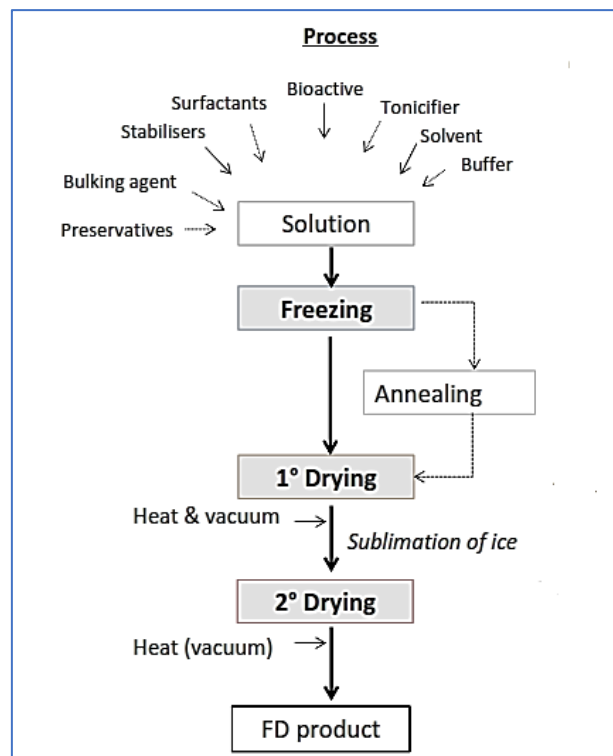


Figure 1.1 An overview of the freeze-drying process for biopharmaceuticals formulations.

## 1.2. Freeze-drying process

Lyophilization, or freeze-drying, is a process in which the solvent (usually water) is first frozen and then removed by sublimation under vacuum conditions. Freeze drying includes three main steps: freezing, primary drying, and secondary drying. Freezing involves the reduction in the product temperature to induce crystallization of the water and some excipients. The second stage is primary drying, sometimes preceded by an additional step called annealing or thermal cycling. During primary drying, the chamber pressure is reduced, and heat is provided to the product to trigger ice sublimation. In the end, the desorption of residual moisture from the product takes place during secondary drying.

### 1.2.1. Freezing

The development and the optimization of the lyophilization process are typically focused on the primary drying step since it is the longest step of the process. However, the freezing step is equally important because it impacts on the microstructure of the porous dried cake determining both the quality of the final product and the processing characteristics such as the rates of primary and secondary drying (Kasper and Friess, 2011). Therefore, it is essential to know the physical events associated with the freezing process, such as supercooling, ice crystallization and ice crystal growth, concentration and crystallization of the solute. These events are represented in Figure 1.2.

Ice, water, and water vapour coexist in equilibrium at the triple point (0.01 °C; 0.6 KPa). When pure water is cooled at atmospheric pressure, it does not freeze spontaneously at its equilibrium freezing point, but a supercooling is necessary because nucleation process is an activated phenomenon. Supercooling always occurs during freezing and it is defined as the difference between the equilibrium ice formation temperature and the actual temperature at which ice crystals first form (Kasper and Friess, 2011). Before that, crystals can develop, and several microscopic solid entities, nuclei, that act as centers of crystallization, must exist in the solution. The formation of a stable nucleus is a rare event because is due to the simultaneous collision of a critical number of molecules. The probability of these nuclei to growth in both number and size is more pronounced at lowered temperatures. Once the critical mass of nuclei is reached, ice crystallization occurs rapidly in the entire system.

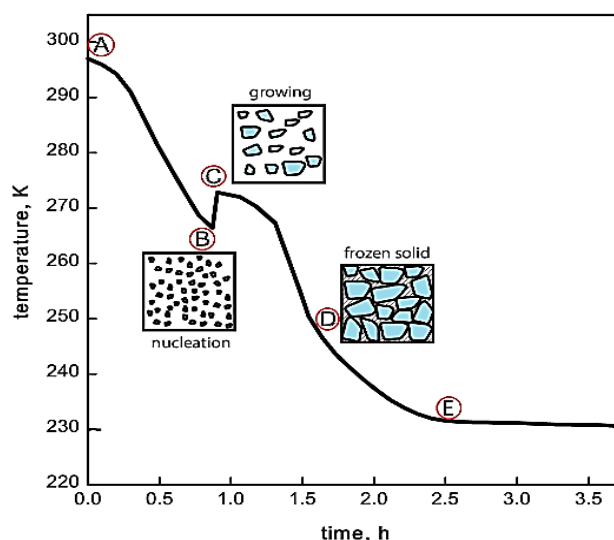


**Figure 1.2** Temperature profile of an aqueous solution of sucrose (5% by weight) during the shelf-ramped freezing. Three events are observable: (AB) supercooling, (BC) nucleation, (CD) crystal growth. (Reprinted with modifications from Pisano and Capozzi, 2017).

The freezing step can be divided into three phases: it initially involves the “supercooling” of the solution until “ice nucleation” occurs, which is followed by “ice growth”. The kinetics of ice nucleation and crystal growth determine the physical state and the morphology of the frozen cake and consequently the final properties of the freeze-dried product.

In general, it can be distinguished homogeneous nucleation from heterogeneous nucleation. The energetic gap to overcome for heterogeneous nucleation is lower than homogeneous process. In term of supercooling, homogeneous nucleation of water appears at a temperature to be at about  $-40\text{ }^{\circ}\text{C}$ , while heterogeneous nucleation occurs with temperature often in the range of  $-10\text{ }^{\circ}\text{C}$  to  $-20\text{ }^{\circ}\text{C}$ . However, in all pharmaceutical solutions the observed nucleation is heterogeneous, meaning that the formation of ice involves some “foreign impurities” that act like clusters such as particulate contaminants present in the water or on the surface of the vial, or some large molecules like proteins within the solution (Kasper and Friess, 2011). Nucleation is a stochastic phenomenon, and, hence, it influences the intra-vial uniformity and the homogeneity within a batch. The nucleation temperature influences the number of ice nuclei formed. If the nucleation starts at a lower temperature, a high degree of supercooling is involved, and the number of ice crystals formed is greater. These crystals will have small dimensions and will conduct to dried products with small pores and high superficial area; meanwhile, with a lower degree of supercooling larger crystals are formed.

Cooling rate, defined as the rate at which a solution is cooled, also impact on the structure of the frozen material. A moderate cooling rate is recommended for pharmaceutical freeze-drying, resulting in moderate supercooling ( $-10$  to  $-15\text{ }^{\circ}\text{C}$ ), moderate surface area cake ( $<1\text{m}^2\text{g}^{-1}$ ), a reasonable fast freezing rate and a reasonable variability among vials (Tang and Pikal, 2004). The slow cooling rate can induce a gradient of concentration of solute within the vial.

Most important, the degree of supercooling should be uniform, both within a given vial and within the entire batch of vials. In practise, this is not so easy to obtain, because of the variations in the cooling process and in the product nucleation temperature. If necessary, a tempering process (annealing) may be followed to assure uniformity and greater dimensions in ice crystals (Searles *et.al.*, 2001).

In Figure 1.3 a general state diagram for an aqueous binary formulation is schematized. As the ice crystals form and grow, the solution becomes more and more concentrated in the solute. If the solute forms a eutectic phase with water, there will be present ice and freeze-concentrated solution. The lowest temperature at which the solute remains as liquid is called eutectic temperature  $T_{eu}$ . Below  $T_{eu}$ , pure ice and a solid mixture of water and solute are in equilibrium and the system is completely solidified.

If the solute does not crystallize (i.e., does not form a true eutectic), it is transformed into a rigid glass when the system is brought below the glass transition temperature of the amorphous phase ( $T_g'$ ). This phenomenon is called glassification or vitrification and it causes an increase in the viscosity of the solution. The amorphous phase consists of uncrystallized solute and uncrystallized water.  $T_g'$  describes the temperature at which there is a fundamental change in the physical properties of the product, which does not reflect a change in state, but rather a change in the macromolecular mobility. Below  $T_g'$ , product mobility is severely restricted. Compounds that do not form true eutectic are difficult to dry successfully. In amorphous solution, the unfrozen water is linked to the solute and a desorption stage is required to remove it.

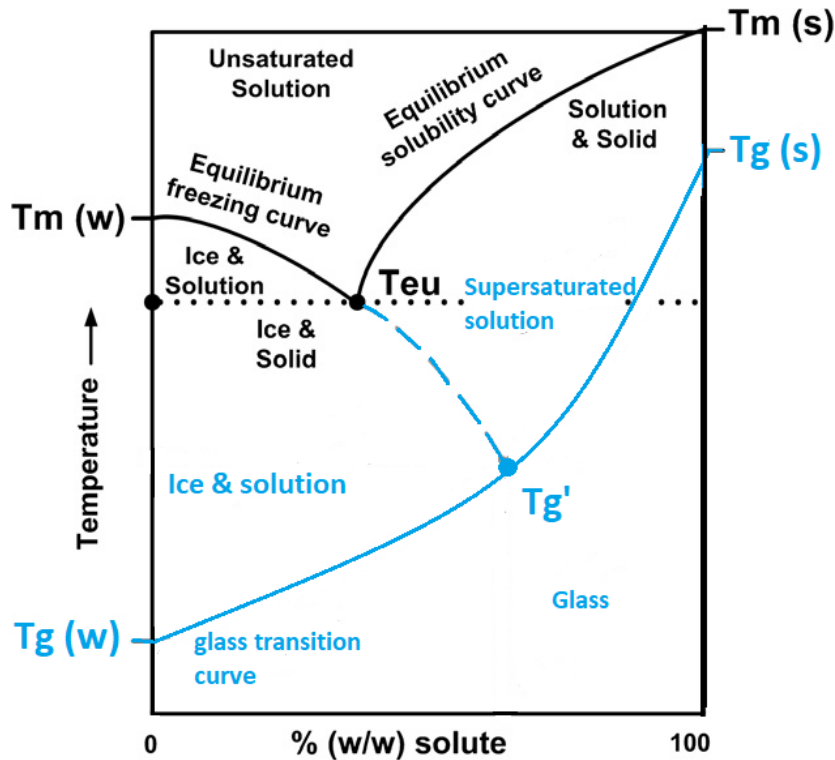


**Figure 1.3** State diagram from a water (w)/solute (s) system. (Reprinted from Kasper and Friess, 2011 with modifications).

## 1.2.2 Primary drying

During primary drying, ice sublimation occurred by lowering chamber pressure and supplying heat to the product. The sublimated water moves from a region of relative high pressure to a region of low pressure in the freeze-dryer condenser. At the same time heat is provided to the product increasing shelf temperature. In Figure 1.4, heat and mass transfer occurring during primary drying are schematized.

In order to enhance process efficiency during primary drying, it is possible to control two parameters, shelf temperature and chamber pressure. These parameters are chosen to work with as high as possible sublimation rate. To ensure the necessary energy for sublimation, the control of shelf temperature is essential. If shelf temperature is too low, there may not be sufficient heat transfer to allow ice sublimation whereas, if it is too high, product temperature can go above the collapse temperature  $T_c$ . Thus, chamber pressure is also an important parameter, because it may set to facilitate sublimation and control the thermal transfer between vials and the shelf. Modulating  $T_s$  and  $P_c$ , it is possible to reduce the primary drying time and optimise the cycle.

Another parameter that is crucial for the design of primary drying is the collapse temperature,  $T_c$ , defined as the temperature at which a structural loss of the product occurs. In general,  $T_c$  is several degrees higher than  $T_g'$ . If the product temperature exceeds this critical temperature, crystalline melting or amorphous collapse will occur. The cake-collapse in general compromises the storage stability because the final product tends to retain higher moisture content than a product dried without collapse (Chang and Patro, 2004).

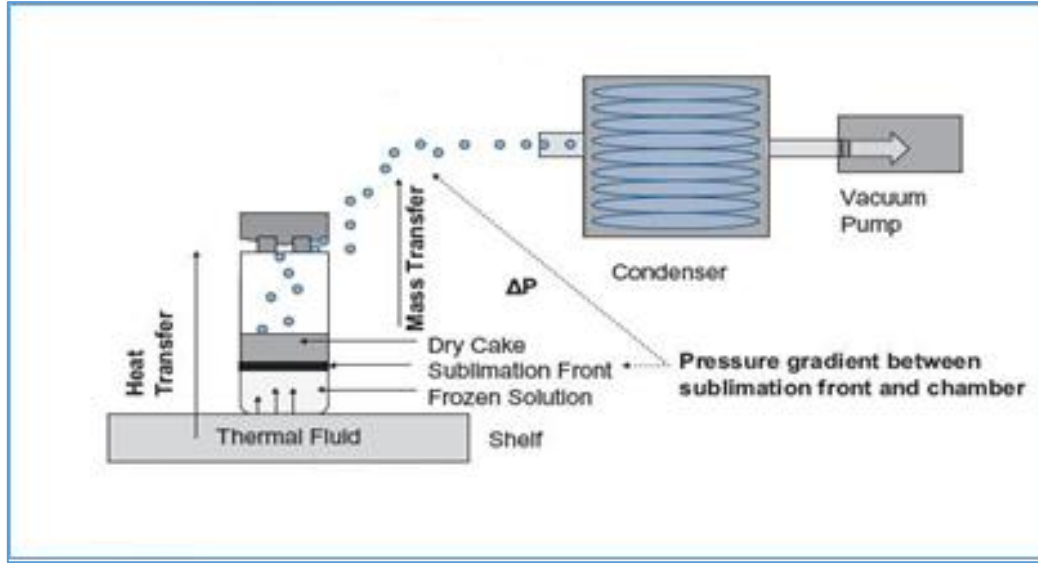


**Figure 1.4** Schematic of heat and mass transfer in the freeze dryer (Khainrar et al., 2013 with modifications).

Unfortunately, as the sublimation front is limited by the collapse temperature of the product  $T_c$  (or the eutectic temperature  $T_{eu}$  for crystalline material), the shelf temperature and the chamber pressure must be set up so that the product temperature does not exceed the collapse temperature.

Mass transfer involves the resistance of flow water vapour through the various mass transfer barriers, which are the resistance of the dried-product, the resistance of the semistoppered vial and resistance to the transfer from the drying chamber to the condenser. The resistance of dried product is generally prevalent and accounts for over 90% of the total resistance to mass transfer (Vecchio C., 2010).

The sublimation rate per vial may be expressed as follows,

$$\frac{dm}{dt} = \frac{P_0 - P_c}{R_p + R_s} \quad (1.2)$$

where  $P_0$  is the equilibrium vapour pressure over ice at the product temperature and  $P_c$  the chamber pressure,  $R_p$  is the dry product layer resistance to vapour transfer, while  $R_s$  is the resistance of the stopper. As  $P_0$  increases exponentially with temperature, the sublimation rate increases dramatically as the product temperature increases. The temperature of the frozen interface determines the vapour pressure of the ice and the driving force for sublimation.

Heat transfer flow can be expressed as follows:

$$\frac{dq}{dt} = a_v K_v (T_s - T_b) \quad (1.3)$$

where  $dq/dt$  is the heat flow from shelves to the product in the vial,  $a_v$  is the cross-sectional area of the vials calculated from the vial outlet diameter,  $T_s$  is the temperature of the shelf,  $T_b$  is the temperature of the product at the bottom centre vial and  $K_v$  is the overall vials heat-transfer coefficient between the vial and the equipment.

As the chamber pressure increases,  $K_v$  increases as well, thereby transporting more heat to the product at a fixed shelf temperature and increasing the product temperature. The general rule is that chamber

pressure should be significantly lower than the vapour pressure of ice at the target product temperature (in the range of 10-30% of the vapour pressure of ice).

Primary drying ends when all ice in all product containers has been removed. Different ways to indicate the end of primary drying may be applied. At the end of the primary drying stage, no ice is present in the vials, and as no heat is removed by sublimation, the product temperature increases till it reaches the shelf temperature, and the vapour composition in the freeze-drying chamber changes from essentially all water to mostly nitrogen (Pikal *et al.*, 1983).

So, temperature sensors (such as thermocouples) can indicate the end of sublimation for the monitored vial. However, the majority of vials in the batch do not contain thermocouples, and their behaviour can be significantly different from that of the vial without thermocouples. In general, vials with thermocouples nucleated before the other samples.

The pressure rise test is another method for the determination of the primary drying endpoint. If the slope of the pressure rise curve significantly exceeded that given by the equipment leakage, ice must be present.

The molar flux of nitrogen may be used to control the chamber pressure. Indeed, the gas composition is essentially all water vapour during primary drying. When essentially all of the vials have finished primary drying, the gas composition changes from mostly water vapour to nitrogen. Hence, a sharp drop in water vapour composition during primary drying can be used as an indication of the end point of primary drying. The point where the Pirani pressure starts to sharply decrease (i.e., onset) indicates that the gas composition is changing from mostly water vapour to nitrogen (Patel *et al.*, 2010).

### 1.2.3 Secondary Drying

In secondary drying, 'unfrozen' water is removed by desorption from the dried cake. In particular for biopharmaceutical products, the absence of water is important for protein activity and its stability during storage. But at the same time, over-drying of protein-based products can cause the loss of protein activity. Therefore, ideally, a final moisture content of between 1 to 3 % v/v is preferred (Townns 1995). Achievement of this target moisture content indicates the end of the secondary drying process.

Three parameters affect secondary drying: shelf temperature, specific surface area and porosity of the cake structure. Shelf temperature is set up between 25-60 °C, depending on dehydration sensitivity of the active protein in the product. The temperature is usually higher than primary drying temperature and it is recommended to be between  $T_g'$  and  $T_c$  for optimum secondary drying. The last two parameters are directly correlated to freezing rate because the dimension of pore size depends on the respective ice crystals. However, the dimension of pores and the specific surface area are inversely correlated. Indeed, although larger pores provide easier and faster diffusion, the surface area is smaller and desorption rates are therefore lower. Because the glass transition temperature,  $T_g'$ , is a function of the moisture content, how  $T_g'$  changes with the decrease of moisture during primary and secondary drying is necessary to optimize this last step. Some advanced techniques, such as dynamic vapour sorption (DVS), allow to characterize the moisture sorption properties and can be used to optimize secondary drying (Liu, 2006). However, the optimization of the process generally aims to reduce primary drying time.

## 1.3. Freezing methods and consequences on quality attributes of biopharmaceuticals

The quality attributes of biopharmaceutical products are influenced by several factors, such as the process conditions, formulation composition, filling volume and properties of the glass vials. Freezing

is probably the step mainly influences the quality of the product, because it impacts on the following phases of the process, on the residual moisture content and reconstitution time. The manner in which a sample is frozen greatly affects the size and the shape of the ice crystals and, hence, the morphology of the final cake and the capacity to remove water from the frozen sample once the vacuum is applied.

Freezing also influences the homogeneity of the whole batch, which is a fundamental characteristic of commercial products. The batch non- uniformity is caused by the stochastic nature of nucleation; in fact, vials do not nucleate at the same time. The best way to produce a homogeneous batch is to directly control the ice nucleation temperature in all the vials of a batch during freezing. However, the intra-vial heterogeneity often occurs and results in changes in sublimation rate during primary drying.

In order to control the process, several methods have already been developed to influence ice nucleation. Some of these allow controlling nucleation temperature, e.g ice fog technique, electrofreezing, vacuum-induced surface, (Kasper and Friess, 2011). The main freezing methods are briefly summarized below.

#### *Shelf-ramped freezing*

The most common freezing method consists of placing the vials in the freeze-drier shelves and increasing temperature with a linear ramp. The cooling rate is relatively slow (0.1 °C/min up to 5 °C/min) because of the limited thermal conductivity between vials and shelf. In some cases, vials are loaded on the cooled shelves, or more simply loaded at ambient temperatures. The equilibration at a lowered shelf temperature (5-10°C) or room temperature for about 15-30 before the shelf temperature is linearly decreased induces more homogeneous conditions among vials. Nucleation temperature is not controlled with this method. Moreover, different vials may show a different degree of supercooling resulting in a great variability in the batch.

#### *Spin freezing*

Spin freezing is an alternative freezing approach where the vials are rotated rapidly along their longitudinal axis. The cooling and freezing of the solution are achieved by using a flow of sterile gas with a controllable temperature around the rotating vial. Consequently, the resulting frozen product will be spread over a larger vial surface compare to traditional freeze-drying (Meyer et al., 2015).

#### *Gap freezing*

In the gap freezing vials are suspended from the shelf through a rising system. With this configuration the thermal conduction from the shelf to the bottom of the vial is irrelevant and natural convection and radiation are prevalent. As a result of this, uniform freezing of the solution occurs without significant gradients of temperature in the vial. This uniform condition promotes the formation of large crystals and pores, which then accelerate the primary drying process. Indeed, the largest pore size results in a lowest mass transfer resistance for ice sublimation.

#### *Annealing*

Annealing in freeze-drying is a process hold step with which the shelf temperature is raised at a specific value above the glass transition temperature. It usually follows the freezing step and the temperature of the system is maintained above  $T_g'$  for several hours for maximum crystallization to occur by the phenomenon of "Oswald ripening". Larger ice crystals with more homogenous size distributions among vials may be obtained via annealing. During annealing, the smallest ice crystals melt. After this hold step, annealed samples are usually frozen again, but small crystals do not reform because the largest crystals, that have not melt during annealing, become nucleation sites for addition crystallization. Thus, the melting of small crystals brings to an enhancement of the larger crystals which allow faster drying. Indeed, annealing is usually applied to speed up primary drying time by a factor of up to 3.5 (Searles *et al.* 2001).

Annealing can also be applied to allow the crystallisation of the certain excipients (e.g. mannitol and glycine) otherwise, if these compounds term to crystallize during storage they may compromise the long-term stability of the pharmaceutical product since the moisture associated with it may be released to the protein product, thereby creating potential stability issues (Chang and Patro 2004). Nevertheless, some negative aspects were been reported in the application of annealing and they include the increase of the secondary drying times and the residual moisture content in the final product due to the decrease in surface area and relative unknown effect on protein structure and stability (Schwegman *et al.* 2005).

#### *Quench freezing*

Using quench freezing, the solution is frozen by immersion of the vials in liquid nitrogen or a refrigerated heat transfer liquid (e.g. dry ice in alcohol) or by spraying liquid nitrogen. Ice crystals formation begins on both the vial wall and bottom, where the heat transfer media has contact. This freezing method results in a lowered degree of supercooling. Because the sample temperature is decreased quickly, small ice crystals are formed as it is possible to observe in Figure 1.5. However, this faster cooling method actually induces supercooling only in a small sample volume before nucleation starts and freezes by directional solidification.

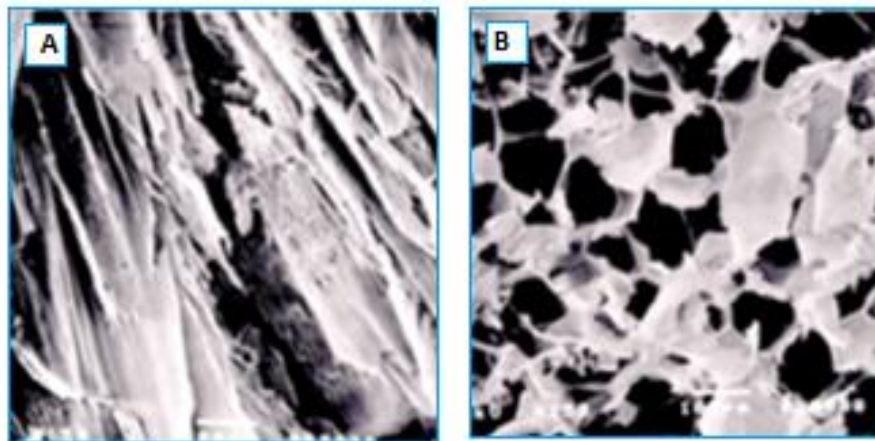


**Figure 1.5** SEM picture of dextran samples that were lyophilized with different freezing processes. Picture A shows the sample frozen by a liquid nitrogen quench and picture B shows the supercooled sample. Cake A showed larger surface area than cake B (Reprinted by Chang and Patro, 2004, with modifications).

#### *Ice fog technique*

A recent advance in the freezing process is the ‘controlled nucleation’ methods. One of this is the ice fog technique. Here, while vials are cooled on the freeze-dryer, a flow of cold nitrogen is released into the chamber, generating an ice fog because of the high humidity. The ice fog, consisting of small ice particles suspended in the vapour phase, penetrates into the vials, where ice nucleation starts at the solution surface. Because the small particles of the ice fog do not reach all the vials simultaneously, inter-vial heterogeneity occurs. Therefore, Patel *et al.* introduced a variation in the ice fog method in which a reduced pressure in the chamber was applied to enable a faster and more uniform freezing (Patel *et al.*, 2010). This method is not yet implemented in large scale.

#### *Electrofreezing*

It is an external freezing method in which ice nucleation is induced by applying an external static electric field and then the samples are further cooled. The instrument generates a high voltage pulse on a platinum electrode which initiates ice crystallization. The nucleation can be started at the desired

temperature with the advantage of not contaminating the solution with external substances. Application of homogeneous and static electric fields during freezing of water has been reported to have a beneficial effect on nucleus formation by inducing nucleation at relatively high temperatures.

#### *Ultrasound-controlled ice nucleation*

A kind of ultrasound waves with low frequency (20e 100 kHz) and high intensity (generally higher than  $1 \text{ W cm}^2$ ), has proven to be useful in controlling the crystallization during freezing. There are different theories about the activation of nucleation with this method. One of this argued that the collapse of the cavitating bubble generated high pressure which increased the equilibrium freezing temperature of water and thus increased the supercooling which is the driving force of ice nucleation (Saclier *et al.*, 2010). However, Zhang et al. have found that flow streams of stable cavitation bubbles and molecular segregation due to the pressure gradient of cavitation bubbles could also cause nucleation (Zhang *et al.*, 2003). A significant intra vial heterogeneity of ice crystal distribution with smaller ice crystals at the vial bottom compared to larger ice crystals at the top was observed by applying ultrasound-induced ice nucleation.

#### *Vacuum-induced surface freezing*

This method is based on the fact the evaporation of water is favored at low pressure. During evaporation, the local temperature in the water surface is reduced and consequently, a thin film of ice is formed. After this, the chamber pressure is released to atmospheric pressure to inhibit melting of the ice film on the surface. At the same time temperature is been decrease. In this way, it seems that dendritic and large ice crystals are formed.

#### *Depressurization technique*

With this method, pressure is released instantaneously throughout the product, and subsequently, a decrease in its temperature is produced. Pressure can be released slowly, over several minutes, or quickly, in 1–2 s. (Otero and Sanz,2000). Supercooling, and hence also ice nucleation, takes place just after pressure release. The extents of supercooling induce high nucleation rates which promote the instantaneous crystallization of a percentage of water in the sample. Phase transition times are thus considerably reduced, resulting in granular ice crystals homogeneously distributed.

#### *Addition of ice nucleating agents*

Ice nucleation agents (INAs) promote heterogeneous nucleation that occurs at a higher temperature compared to samples that do not contain INAs. The most studied agent is silver iodine (AgI). It has a similar structure at ice, but the nucleation process is also due to an electric mechanism. This method does not permit to obtain a lower heterogeneity, but it just increases the average nucleation temperature. Moreover, INAs are often used in food science, but they do not find large application in the lyophilization of pharmaceutical products.

## **1.4. Lyophilization plants**

Pharmaceutical industry traditionally worked with batch processes for several years, which is therefore quite consuming in terms of time and money. On the contrary, the food industry, which has to ensure high productivity, is progressively shifted from batch processes to semi-continuous and continuous operations. Using continuous processes allows to reduce the time and improve the quality product and

thus, in the last years, the Food and Drug Administration is promoting the industries to pursue this direction (Arsiccio 2016).

Batch processes are characterized by longer time and greater energy than continuous processes. In addition, it is difficult to achieve uniform process conditions with batch configuration. For a given throughput, the size of the equipment is significantly greater. In addition, continuous processes work almost always in stationary conditions, facilitating the monitoring of operations. Therefore, continuous production is currently a subject of great interest.

### 1.4.1. Batch lyophilization

As shown in Figure 1.6, a freeze dryer consists of a chamber with shelves onto which vials are loaded, a refrigeration system to supply energy, a condenser and a vacuum pump that can reduce chamber pressure to subatmospheric values. Chamber pressure is maintained at its setpoint by introducing an inert, dry gas in a controlled manner (normally nitrogen gas). The product is loaded onto the shelves, whose temperature is controlled via a heat transfer fluid (e.g., silicone oil) that circulates through them. The temperature of the heat transfer fluid is controlled via the refrigeration system. The freeze-drying equipment also has provisions for defrosting the condenser and computer interface to input, monitor, and control the cycle parameters via a Programmable Logic Control (PLC), (Chang and Patro 2004).

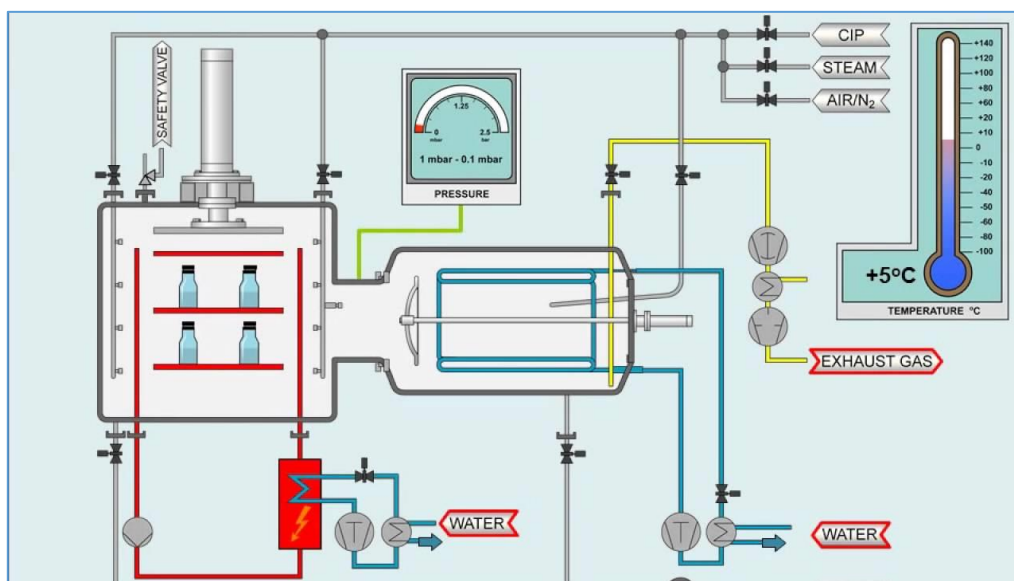


Figure 1.6 Components of a freeze-dryer

There are many disadvantages using batch processing. The freezing phase cannot be controlled at the level of individual vials and it impacts on the homogeneity of the production and drying time. The size of the ice crystals varies from vial to vial in the same batch and this results in different sublimation rates. The heat transfer to the drying chamber is different for samples placed in different positions. Into the equipment, for example, samples on the edge of the shelf are exposed to a flux of radiant energy that is more intensive than the vials placed in the center of the shelves. Moreover, a batch process is slow and expensive. Filling, loading, and unloading are typically longer with a serious risk of contamination: storage not only occupies large amounts of space but also requires high standards of cleanliness and sterility, resulting in a significant increase in overall costs. Moreover, process monitoring at the level of the single sample is not achievable.

### 1.4.2. Continuous lyophilization

One of the alternatives for the continuous lyophilization of pharmaceuticals was proposed by Rey. Rey proposed to divide the solution to be lyophilized in single spherical granules. It is possible to divide the system into four sections. The first section aims to freeze the solution in spherical granules. In the second section, there is a heated vibrating tray that delivers the individual granules in a temperature and pressure environment set up for allowing the sublimation of the ice from the product. Then, the granules pass into a secondary drying chamber and are distributed in sterilized flasks. The schematic of the equipment proposed by Rey is shown in Figure 1.7.

Thanks to the small size of the granules, the primary drying times are considerably reduced compared to the traditional processes. However, the application of this process is difficult to achieve. In addition, another limit is linked to the inability to maintain sterilization conditions in the system. In this regard, Rey proposed the insertion of a post-treatment sterilization after the lyophilization. This treatment is still studied as it could lead to the deactivation of the active molecules.

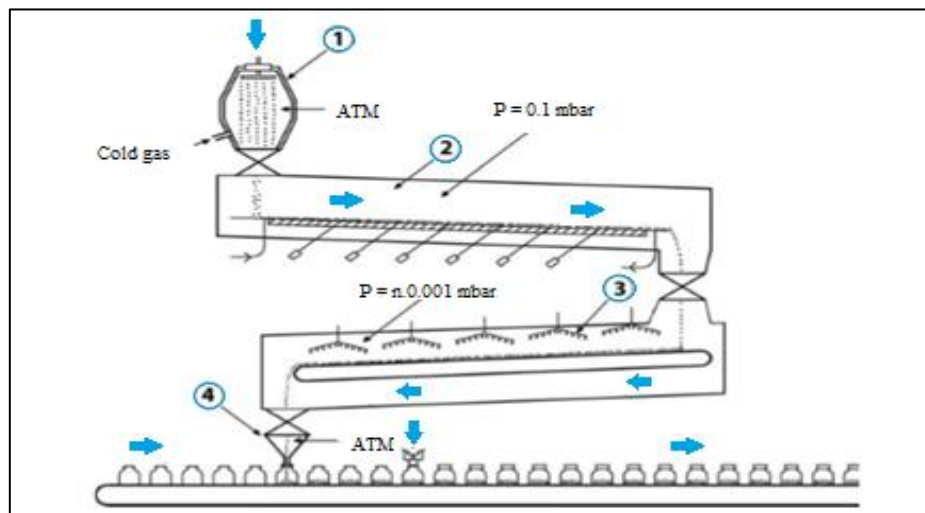


**Figure 1.7** Schematic of a pharmaceutical continuous freeze-drying plant. The system displays four sections (Reprinted from Rey, 2004 with modifications).

A recent approach is based on the use of the so-called spin-freezing. As explained in the previous sections, spin-freezing consists in rapidly rotating the flakes, filled in with a liquid formulation, around their longitudinal axis. Figure 1.8 shows a continuous spin freezing system connected to a continuous drying system. The resulting frozen product will be dispersed on the entire surface of the flask. The following steps, primary and secondary drying, can be conducted in two successive chambers where a conveyor belt, with appropriate pockets for accommodating the vials, allows the handling of the vials and the heat exchange necessary for the process. Movimentation between rooms at different temperatures and pressures takes place through an appropriate load-lock system, necessary to keep the process running (De Meyer *et al.*, 2015).

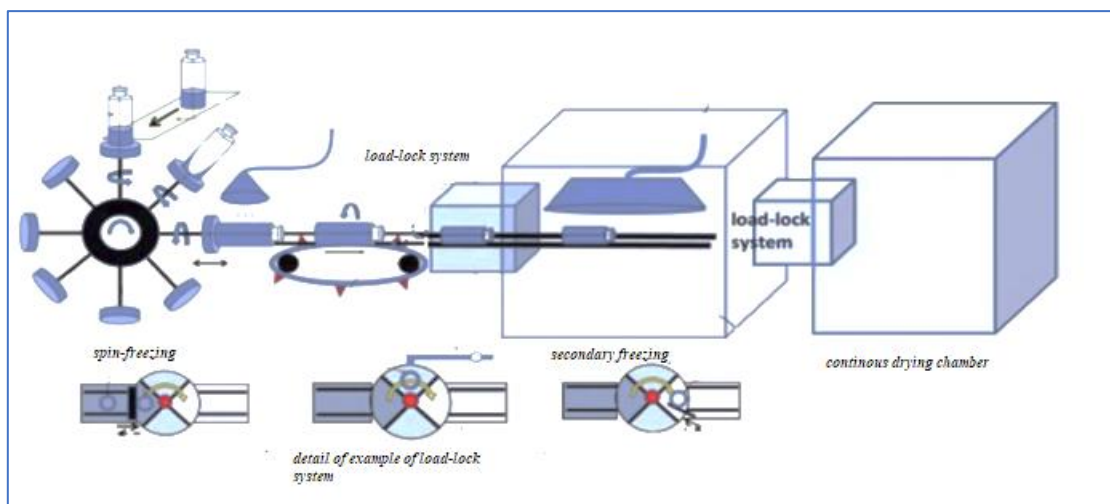


**Figure 1.8** Continuous freezing system connected to a continuous drying system. (Reprinted from De Meyer *et al.*, 2015, with modifications).

## 1.5. Protein Stabilization

As pharmaceutical products require many months and years as storage periods, an alternative to increment the stability of the protein for more long time is provided by the removal of water to form a solid through the lyophilization process. However, some proteins can be deactivated during freeze-drying, and even if the protein is stable and active after the lyophilization, it may suffer damage during storage. Stability problems are normally minimized by a combination of appropriate process control and formulation optimization.

As reported by Pikal, it has to be distinguished the “protein stability” from the “pharmaceutical stability”. Protein stability refers to the ability of protein staying in the native conformation without shift the equilibrium between native and unfolded in favor of the unfolded state. This stability leans on thermodynamic principles. Instead, pharmaceutical stability is commonly used to describe the ability of a protein to not be degraded, meaning that it does not change in primary structure, conformation or physical change (i.e., aggregation) when it is processed, distributed and used (Pikal, 2004).

Protein can be destabilized by the thermodynamic or kinetic mechanism. A stabilizer that allows increasing the equilibrium free energy between stable native state and unstable unfolded conformation operates via a thermodynamic stabilization. The “solute exclusion hypothesis” and the “water substitute hypothesis” are respectively used to explain the stabilizing effect during freezing and drying as thermodynamic mechanisms. On the opposite, the “vitrification hypothesis” is based on the kinetic mechanism according to which the rate of the degradation processes is really slow because the system is in the glassy state and the protein is almost immobilized.

Most protein stability studies have focussed their interpretation either on a thermodynamic mechanism or on a pure kinetic mechanism, and consequently, there are some controversies and confusions over which mechanism is “correct” (Pikal, 2004).

Anyway, the creation of pharmaceutical formulation, adding stabilizers, bulking agents, buffer salts and another kind of excipients has to be optimized for each protein. Several experimental studies are conducted in an attempt to find the best formulation. There are general guidelines how to proceed in the selection of excipients, but the most part of the work is still experimental.

### 1.5.1. Denaturation stresses during lyophilization

Because of the marginal stability of some proteins, the freeze-drying process generates various stresses to denature proteins. These factors are summarized below and include cold denaturation, freeze-concentration, the formation of the ice-water interface, pH changes, crystallization of solutes, phase separation and dehydration stresses.

#### *Cold denaturation*

During freezing the temperature is decreased and this event can denature the protein. Indeed, proteins may unfold with an increase in temperature (heat denaturation) or with a decrease in temperature. The cold denaturation is probably due to an increase in the solubility of nonpolar groups in aqueous solutions when the temperature is generally lower than 0 °C. The cold denaturation temperature is influenced by the pH of the solution, concentration of the protein and the presence of additives (Bhatnagar *et al.*, 2007). Some observations about the study of cold denaturation on different enzymes suggested that this stress mechanism is less relevant than the others (i.e. ice formation, freeze-concentrations) since the estimated cold denaturation temperature is often well below freeze-drying temperatures. Moreover, adding stabilizers decreases widely the cold temperature.

#### *Freeze-Concentration*

During freezing water starts crystallizing by inducing the concentration of the solutes to increase. At the same time, the viscosity increases leading to the development of other stresses. In the example reported in Figure 1.9, at the end of freezing, the viscosity is about seven orders of magnitude higher than for the starting solution (Pikal, 2004). Although the reactions rate decreases with a decrease of temperature, degradation reactions are accelerated by the increasing of solute concentration. The increase in the rate of a chemical reaction in a partially frozen state could reach several orders of magnitude relative to that in solution (Wang, 2000).

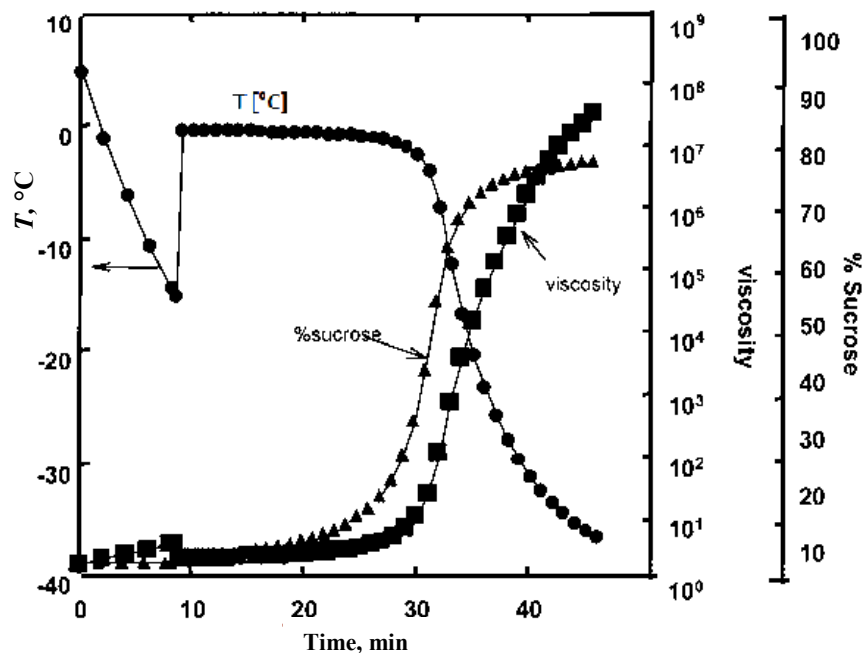


**Figure 1.9** Time profile of temperature, concentration, and viscosity during freezing of 3% sucrose (Reprinted from Pikal, 2004, with modifications).

### *Formation of ice-water interface*

When the solution is frozen ice-water interface is created. Proteins can be adsorbed to the interface and can be denatured by surface-induced stresses. Using freezing protocol, that induces a large ice-water interface such as quench freezing, affects dramatically the stability of the protein in the native configuration (Wang 2000). Indeed, working with a high degree of supercooling, the number of ice crystals increases, thereby increasing the aqueous-ice interfacial area. Obviously, the formation of ice itself would be a significant “stress” during freezing since the adsorbed protein on the ice crystals can suffer the loss of conformational stability (Pikal,2004).

### *pH changes*

Some proteins are pH sensitive and a small drop in pH during freezing can partially denature the protein also in the presence of stabilizers such as sucrose and trehalose. The changing of pH may be produced by the decrease of temperature, freeze-concentration, but the most important cause is the crystallization of buffer salts that provokes large shifts of the pH in the solutions. In particular, sodium phosphate buffers showed a decrease in pH about 3-4 units for the precipitation of the dibasic salt, while potassium phosphate buffers exhibit a modest increase in pH due to precipitation of the monobasic salt of potassium phosphate during freezing. If the concentration of buffers is lower, the pH shift is less dramatic (Pikal,2004).

### *Crystallization of Solutes*

Crystallization of non-buffer components such as glycine, raffinose, mannitol, and polyethylene glycol from frozen solutions can result in the loss of protein structure and activity, how demonstrated with mannitol and raffinose crystallization when the frozen solutions were annealed (Bhatnagar *et al.*, 2007). Despite this, the ability of solutes to crystallize during freezing has been used to provide a macroscopic support for an amorphous system and to perform primary drying above the collapse temperature of the amorphous phase without observation of structural collapse of the product.

### *Phase separation*

Phase separation may occur when the concentration of solutes increases during freezing in presence of electrolytes, such as polymer, polysaccharide, protein, etc. Freezing polymer solutions may cause phase separation because polymers change their solubility at cold temperature creating a large excess of interface and, hence, denaturing the protein. Some studies have found that mannitol minimized phase separation because crystallized segregating the freeze-concentrate into microscopic domains (Bhatnagar *et al.*, 2007).

### *Dehydration stresses*

The hydration shell that covers the protein surface is removed during lyophilization provoking stresses on the protein which may lose the native structure. Protein denaturation may be also due to a significant difference in moisture distribution caused by dehydration stresses. Not only denaturation but also protein aggregation can occur during freeze-drying since protein can transfer protons to ionized carboxyl groups when part of its hydration shell is removed. Protons transfer reduce the charge density facilitating protein aggregation among hydrophobic groups. Moreover, if water molecules are an integral part of an active site in proteins, removal of these functional water molecules during drying inactivates proteins.

### 1.5.2. Mechanisms of stabilization

Since freeze-drying and freeze-thawing cause different kind of stresses on the protein, the mechanisms of protein stabilization by excipients are not the same. In the last two decades, more tests have been conducted by researchers in order to identify the prevalent mechanisms or interpreting the phenomena in terms of thermodynamic and/or kinetic rules. However, it is difficult to associate the right mechanism of stabilization because many factors and denaturation stresses are involved at the same time. In this section the “solute exclusion hypothesis”, the “vitrification hypothesis” and the “water substitute hypothesis”, that are the principal mechanisms of stabilization, are presented and discussed.

#### *During freezing and freeze-thawing*

Two different explanations on the mechanism that stabilizes proteins have been found by investigating several proteins during freezing and freeze-thawing. In the past, some researchers (Arawaka *et.al*, 1982)), studied the stress mechanisms in an unfrozen protein solution and discovered that adding solutes in the solution affect positively the protein stability. It was observed that solutes were preferentially excluded from contact with the surface of the protein. Thus, as Timasheff and his colleagues explained, the presence of these solutes in a protein solution created a thermodynamically unfavorable situation since the chemical potentials of both the protein and the additive were increased (Carpenter and Crow 1988). This enhancement is more relevant when the protein increases in the surface area, that means it is unfolded. The additions of sugars provoke a positive free-energy increase between the native and the denatured states as shown in Figure 1.10. For this reason, the contact of sugar when protein is unfolded is thermodynamically more unfavorable than the native configuration of protein. This must be reflected in the equilibrium constant, which, in sugar solutions, will shift to a value favouring the native conditions (Arawaka and Thimasheff, 1982).

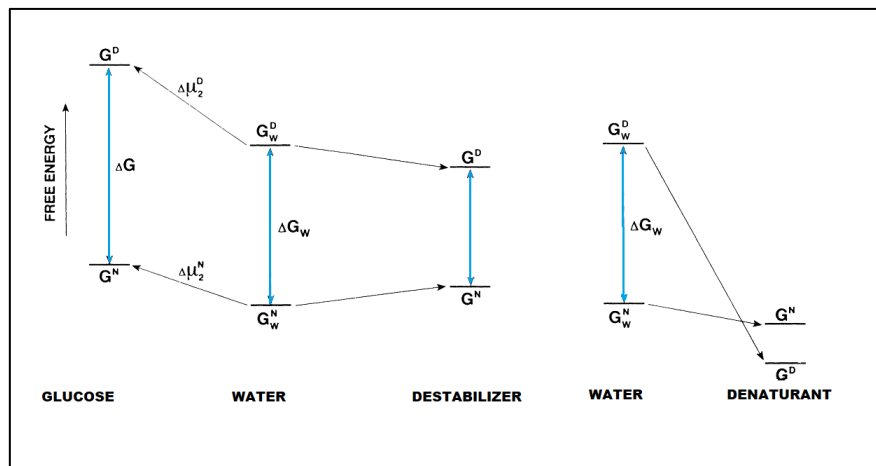


**Figure 1.10** Free energy diagram of a protein in different solvent systems (Arakawa *et al*, 2001, with modifications).

Some years later, Carpenter and Crow tested different classes of solutes (sugars, polyols, amino acids, methylamines, and lyotropic salts) during freeze-thawing discovering that these compounds have in common only the propriety to be preferentially excluded from contact with the surface of protein in aqueous solution.

More recently a kinetic mechanism was introduced to explain the mechanism of protein stabilization during freeze-thawing and drying. This latter theory is based on the “vitrification hypothesis” whereby the increasing of viscosity, due to freeze-concentration and the decrease of temperature, reduces

mobility and all dynamic processes. In this situation unfolding and refolding of proteins are very slow, so the validity of the solute exclusion theory has been questioned, considering its plausibility only when the concentrations are modest and the viscosities are low (Pikal 2004, Bhatnagar 2007). With this point of view, a cryoprotectant can be seen as the agent that slows the rate of inactivation without affecting the free energy of denaturation. This theory has been introduced to explain protein stabilization during freezing as well as during drying.

#### *During Drying*

In order to investigate the kind of mechanism which is responsible of the partial protection of proteins during drying, Carpenter and Crow conducted trials with different kinds of solute and working with phosphofructokinase (PFK). They discovered that sugars were able to protect the protein during drying but the preferential exclusion from contact with the surface of the protein is not the stabilizing mechanism against stresses caused by dehydration. So, they suggested that sugars molecule formed hydrogen bonds with protein molecules substituting the water molecules. Indeed, before drying, proteins have a monolayer of water on the protein surface providing thermodynamic stability. When some of these water molecules are removed from the protein surface during drying, the protein may change configuration because the protein tends to transfer protons to ionized carboxyl groups and thus abolishes as many charges as possible in the protein.

According to this theory, sugars may be used as lyoprotectants because they are also able to preserve proteins during freezing. Increasing the concentration of the sugar may increase protein stabilization during freezing but decreases the protection against drying because at initial high concentrations sugars can crystallize and hence not be available to hydrogen bond substituents. Using different co-solute as cryoprotectants and lyoprotectants may be a solution how showed by Carpenter et al. that developed a formulation with PEG as a cryoprotectant and various sugars used as lyoprotectants. They found that adding polyethylene glycol, the stability of freeze-dried phosphofructokinase increased rather than using only sugars. An example is reported in Figure 1.11.

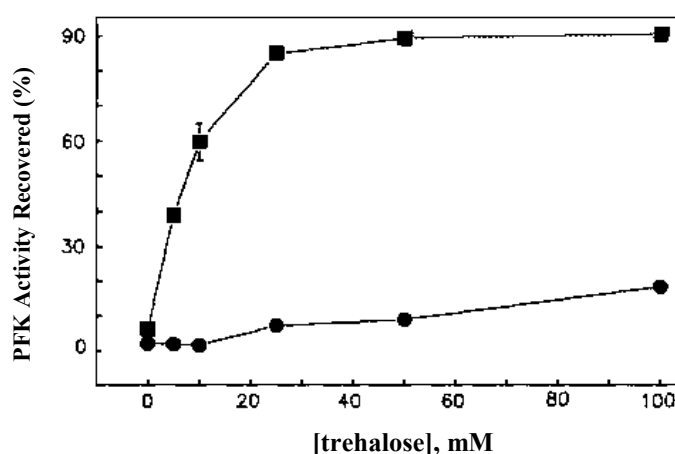


**Figure 1.11** Comparison of the influence of trehalose alone (●) and trehalose with 1% (w/v) PEG (■) on the stability of freeze-dried PFK (Reprinted by Carpenter et al., 1993, with modifications).

In literature another theory about the mechanism of stabilization of proteins is available. It is the “glass dynamic hypothesis” or “vitrification hypothesis” already reported to explain the kinetic hindrance to the motion of the protein during freezing stresses. The molecular rigidity of the system prevents equilibrium changes to occur between the native and un-folded state. It is possible to maintain the native

structure of the protein into a rigid inert glassy solid in which any molecular motions are inhibited. Therefore, compounds with good glass properties and amorphous solutes are suitable as stabilizers in protein formulations. This is a plausible hypothesis, but it is probably not the only mechanism that acts for stabilizing proteins. However, an amorphous state of solute molecules appears important to allow maximal hydrogen bonding between the solute molecules and proteins (Arawaka *et al.*, 2001).

### 1.5.3. Excipients for cryo- and lyo-protection

Freeze-drying a protein without losing the protein activity and guaranteeing good quality of final product is possible only if some excipients are added to the protein solution before freeze-drying. The insertion of some additives in the protein solution is technically called “formulation” that has to be optimized in order to find the better compounds, and their quantities, which allow stabilizing protein during freeze-drying and storage. Additives may play the role of cryoprotectants if they protect the protein during freezing, or lyoprotectants if they are able to stabilize the protein during dehydration.

The recovery and functional activity of the freeze-dried proteins, the appearance and residual moisture content should be assessed after the process so that it is possible to provide the optimal design of the formulation. However, the formulation should be designed with some considerations on the physical processing conditions in order to provide the highest collapse temperature that allows reducing the drying cycle time.

In this section, additives are subdivided according to their role in stabilizing the protein and a brief description for each of these is included.

#### Stabilizers

The first and most important class of additives is the stabilizer which should protect protein during freezing and during dehydration. A stabilizer for a solid protein product should be at least partially amorphous and able to replace water, forming intimate hydrogen bonds with the protein. Formation of an amorphous glassy state is considered to be a prerequisite, not a guarantee, for protein stability (Wang 2000).

#### *Sugars/polyols*

Many sugars and polyols are used as cryoprotectants and lyoprotectants. The effect of stabilization during drying is the same for sugars and polyols since they have the hydroxyl functional groups that can form hydrogen bonds to the surface of protein when water is lost during drying. The most effective stabilizers during the lyophilization are disaccharides, in particular, sucrose and trehalose since they have higher glass transition temperature, while reducing sugars should be avoided because they can degrade proteins during storage for the reaction between carbonyls of the sugars and free amino groups on the protein (Millard reaction). Trehalose has higher  $T_g'$  than sucrose and is also more resistant to acid hydrolysis, but sucrose seems to be more efficient in the inhibition of unfolding during freeze-drying since trehalose tends to separate from protein (Carpenter *et al.*, 1997). In Table 1.5 the main sugars and polyols used as protectants are reported.

#### *Polymers*

Polymers are used as stabilizers in combination with sugars during lyophilization because they can act as cryoprotectants or lyoprotectants for preferential exclusion, surface activity, steric hindrance of protein-protein interactions and/or increased solution viscosity limiting protein structural movement. Moreover, they keep constant the pH of solutions. Unfortunately, polymers do not provide stability during storage. The most used polymer is dextran. It has been reported that dextran stabilizes protein

increasing the glass transition temperature of protein formulation and inhibits crystallization of mannitol. The disadvantage of using polymers is due to the probability of causing phase separation because of steric hindrance that cannot permit efficient hydrogen bond with protein. An alternative is to use both polymers and sugars together as protectors. Sugars substitute hydrogen bond of water with the protein, while polymers increase the  $T_g'$  of a protein formulation and inhibit crystallization of other excipients.

**Table 1.5** Sugars and polyols used in freeze-drying formulations for proteins (Liu *et al.*, 2015).

Type	Name	Formula	MW(g/mol)	$T_g'$ (°C)	$T_c$ (°C)
<b>Mono-saccharide</b>	Glucose	C <sub>6</sub> H <sub>12</sub> O <sub>6</sub>	180.16	-43	-41
	Galactose			-41	
	Mannose			-41	
	Fructose			-42	
	Ribose	C <sub>5</sub> H <sub>10</sub> O <sub>5</sub>	150.13	-47	
	Xylose			-48	
<b>Oligo-saccharide</b>	Sucrose	C <sub>12</sub> H <sub>22</sub> O <sub>11</sub>	342.30	-32	-31
	Lactose				-30.5
	Maltose monohydrate	C <sub>12</sub> H <sub>22</sub> O <sub>11</sub> *H <sub>2</sub> O	360.32	-30	
	Trehalose dehydrate	C <sub>12</sub> H <sub>22</sub> O <sub>11</sub> *2H <sub>2</sub> O	378.34		-29
	Raffinose pentahydrated	C <sub>18</sub> H <sub>32</sub> O <sub>16</sub> *5H <sub>2</sub> O	594.53		-26
<b>Poly-saccharide</b>	Mannitol	C <sub>6</sub> H <sub>14</sub> O <sub>6</sub>	182.17	-27	
	Glycerol	C <sub>3</sub> H <sub>8</sub> O <sub>3</sub>	92.09	-65	
	Sorbitol	C <sub>6</sub> H <sub>14</sub> O <sub>6</sub>	182.17	-44	-54
	Xylitol	C <sub>5</sub> H <sub>12</sub> O <sub>5</sub>	152.15	-47	
	Inositol	C <sub>6</sub> H <sub>12</sub> O <sub>6</sub>	180.16		

### *Proteins itself*

It is still not clear why increasing protein concentration stabilizes the protein itself during freezing and or freeze-drying. Some investigators thought that unfolding of proteins at high concentrations during freezing may be temporarily inhibited by steric repulsion of close protein molecules, while another hypothesis argued that not all protein molecules are involved in the stress adsorption on ice-water interface since the surface area of ice water interface is finite. Moreover, keeping high the protein concentration, the  $T_g'$  of the entire formulation increases, preventing collapse. In addition, favorable protein-protein interactions may contribute to the increased protein stability at high concentrations (Wang, 2000).

### **Bulking agents**

Mannitol, sorbitol, and glycine do not provide protection during lyophilization, but they are used as bulking agents to provide physical and mechanical stabilization to the final dried formulation. Mostly if the product has a relatively low mass of protein per vial, it will necessary to have a bulking agent to prevent the loss of the protein from the vial during freeze-drying. Bulking agents usually crystallize during lyophilization and form a mechanically strong cake. However, it must be realized that crystalline

excipients when used alone will usually not provide adequate stability for most proteins (Carpenter and Crow 1997). Bulking agents can improve product elegance, improve formulation dissolutions and prevent product collapse.

Mannitol sorbitol and glycine are good bulking agents because they have a high eutectic temperature, allowing efficient freeze-drying. Crystallization of bulking agents is inhibited by the presence of other amorphous excipients, such as sucrose. In order to allow the crystallization, bulking agents are added at relative high concentration.

### **Buffer salts**

Many proteins in solution are stable only in a narrow pH range. The pH of the solution can affect the protein stability during lyophilization and during long-term storage. Therefore, the solution pH must be optimal to minimize protein denaturation. In order to maintain the solution pH of the formulation, buffer salts are used since they cover a wide range of pH. The principal buffering agents are acetate, citrate, glycine, histidine, phosphate and Tris. If the molecule is pH sensitive, it is suggested to avoid sodium phosphate buffer because it can crystallize causing a significant drop in pH during freezing which in turn affects the stability of the protein. The cooling rate, active ingredients or other excipients in the solution may affect the crystallization of some buffers. Indeed, increasing the initial cooling rate and limiting the duration of annealing steps can reduce the tendency of salt to crystallize.

### **Other excipients**

Surfactants are sometimes added in the formulation because they reduce the driving force of protein adsorption and/or aggregation at these interfaces. One typical surfactant is Tween 80. Low concentration of non-ionic surfactants is often sufficient to serve this purpose. An excessive amount of surfactants should be avoided because these compounds are liquid at room temperature, and, hence, if present at high concentration they can lower the formulation glass transition temperatures.

Some amino acids can be used to protect proteins during freezing and freeze-drying. To give you an example, it was demonstrated that glycine suppressed the pH drop of sodium phosphate buffer during freezing. Therefore, amino acids may protect proteins from freezing denaturation partly by reducing the rate and extent of buffer salt crystallization.

Another kind of additives can be added, such as tonificiers which make the formulations isotonic with body fluids on reconstitution, preservatives to protect the formulations from microbial contaminations, and antioxidants to improve the stability of freeze-dried products.

## **1.6. Motivation of the thesis**

In attempt to contribute at the research on the lyophilization conducted at Politecnico di Torino, this thesis project is principally focused on the impact of the freezing step on different aspects of lyophilization which include the intra and inter-variability in the batch in terms of nucleation temperature, product structure, mass transfer resistance during primary drying, the sensitivity at the process of an active pharmaceutical ingredient (API) and the influence of parameter uncertainties on the optimization of the process via Design Space.

It is possible to divide the work of this thesis into three main parts.

In the first part the goal is to investigate the intra-variability and the inter-variability of two different freezing methods, shelf-ramped freezing and suspended-vial freezing in relation to the nucleation

temperature, the mean pore size of the dried products, the morphology, and the mass-transfer coefficient  $R_p$ .

In the second part of the work, two different freezing methods, shelf ramped freezing and quench freezing are chosen to study the impact of the freezing protocol on the protein alcohol dehydrogenase, ADH, changing the cooling rate, the concentration of the protein with and without protectants, during freeze-thawing and freeze-drying.

At the end, it was conducted a study on the impact of the uncertainties on a cycle design optimized via dynamic design space considering two different formulations and, for the first one, two different cooling rates.

The results, reported in the next chapters, were obtained by experimental tests conducted partially at Politecnico di Torino and partially at Ghent University.

## List of symbols

$a_v$	Cross-sectional area of the vial, $m^2$
$\frac{dm}{dt}$	Solvent sublimation flux, $Kg\ m^{-2}\ s^{-1}$
$\frac{dq}{dt}$	Heat transfer flow, W
$K_v$	Vial heat transfer coefficient, $W\ m^{-2}\ K^{-1}$
$P_c$	Chamber pressure, Pa
$P_0$	Equilibrium vapour pressure, Pa
$R_p$	Dry product layer resistance to vapour transfer, $m\ s^{-1}$
$R_s$	Resistance of the stopper to vapour transfer, $m\ s^{-1}$
$T_b$	Product temperature at the bottom of the vial, K
$T_c$	Collapse Temperature, K
$T_{eu}$	Eutectic temperature, K
$T_g'$	Glass transition temperature, K
$T_n$	Nucleation temperature, K
$T_s$	Shelf temperature, K

## Abbreviations

API	Active Pharmaceutical Ingredient
DVS	Dynamic Vapour Sorption

## References

- Arakawa T., Prestrelski S.J., Kenney W.C., Carpenter J.F., 2001. "Factors Affecting Short-Term and Long-Term Stabilities of Proteins." *Advanced Drug Delivery Reviews*, **46**(1–3): 307–26.
- Arakawa T. and Timasheff S.N., 1982. "Stabilization of Protein Structure by Sugars." *Biochemistry*, **21**(1):6536–6544.
- Arsiccio, A., 2016. "Sviluppo di un processo continuo per la liofilizzazione di prodotti farmaceutici", Master Thesis work, Polytechnic of Turin.
- Bhatnagar B.S, Bogner R.H, Pikal M.J., 2007. "Protein Stability During Freezing: Separation of Stresses and Mechanisms of Protein Stabilization." *Pharmaceutical Development and Technology*, **12**(1): 505–23.
- Carpenter J.F. and Crowe J.H., 1988. "The Mechanism of Cryoprotection of Proteins by Solutes." *Cryobiology*, **25**(1): 244–55.
- Carpenter J.F. and Crowe J.H. 1988. "Modes of Stabilization of a Protein by Organic Solutes during Desiccation." *Cryobiology*, **25**(1): 459–70.
- Carpenter J.F., Pikal M.J., Chang B.S. and Randolph T.W., 1997. "Rational Design of Stable Lyophilized Protein Formulations: Some Practical Advice." *Pharmaceutical Research*, **14**(1):969-975.
- Carpenter J.F., Prestrelski S.J., Arakawa T., 1993. "Separation of Freezing-and Drying-Induced Denaturation of Lyophilized Proteins Using Stress-Specific Stabilization: I. Enzyme Activity and Calorimetric Studies." *Archives of Biochemistry and Biophysics* **303**(2): 456–64.
- Chang B.S and Patro S.Y., 2004. "Freeze-Drying Process Development for Protein Pharmaceuticals.", in *Lyophilization of Biopharmaceuticals* (Costantino H.R. and Pikal M.J. eds) American Association of Pharmaceutical Scientists, 113-138.
- Cochran T. and Nail S.L., 2009. "Ice Nucleation Temperature Influences Recovery of Activity of a Model Protein after Freeze Drying." *Journal of pharmaceutical sciences*, **98**(9): 3495–3498.
- Kasper J. C. and Friess W., 2011. "The Freezing Step in Lyophilization: Physico-Chemical Fundamentals, Freezing Methods and Consequences on Process Performance and Quality

- Attributes of Biopharmaceuticals.” *European Journal of Pharmaceutics and Biopharmaceutics*, **78**(2): 248–63.
- Khairnar S., Kini R., Harwalkar M., Dr Salunkhe K., Dr Chaudhari S.R., 2013. “A Review on Freeze Drying Process of Pharmaceuticals.” *Intenrational Journal of Reserch in Pharmacy and Science*, **4**(1):76-94.
- Liu J. 2006. “Physical Characterization of Pharmaceutical Formulations in Frozen and Freeze-Dried Solid States: Techniques and Applications in Freeze-Drying Development.” *Pharmaceutical development and technology*, **11**(1): 3–28.
- Liu J. and Zhou X., 2015. “Freeze-Drying of Proteins”, in *Cryopreservation and Freeze-Drying Protocols, Methods in Molecular Biology*, Wolkers W.F. and Oldenhof H., New York, USA.
- De Meyer L, Van Bocksral P.J., Cover J., Vervet C., Remon J.P., De Beer T., 2015. “Evaluation of Spin Freezing versus Conventional Freezing as Part of a Continuous Pharmaceutical Freeze-Drying Concept for Unit Doses.” *International Journal of Pharmaceutics*, **496**(1): 75-85.
- Otero L. and Sanz P.D., 2000. “High-Pressure Shift Freezing . Part 1 . Amount of Ice Instantaneously Formed in the Process.” *Biotechnology Progesse*, **16**(1): 1030–36.
- Patel, S.M., Doen T., Pikal M.J., 2010. “Determination of End Point of Primary Drying in Freeze-Drying Process Control.”, *AAPS PharmSciTech*, **11**(1):73-84.
- Pikal M.J, 2004. “Mechanisms of Protein Stabilization During Freeze-Drying and Storage: The Relative Importance of Thermodynamic Stabilization and Glassy State Relaxation Dynamics.”, in *Freeze Drying / Lyophilization of Pharmaceutical and Biological Products*, Marcel Dekker Inc., New York, USA
- Pikal, M.J., Roy M.L., Shah S. 1984. “Mass and Heat Transfer in Vial Freeze-Drying of Pharmaceuticals: Role of the Vial.” *Journal of Pharmaceutical Science*, **73**(9):1224-1237.
- Pisano R. and Capozzi L.C., 2017. “Prediction of Product Morphology of Lyophilized Drugs in the Case of Vacuum Induced Surface Freezing. *Chemical Engineering Research and Design*, **125**(1):119-129.
- Rey L. and May J.C., 2004. “Glimpses into the Realm of Freeze-Drying: Classical Iusses and New Ventures”, in *Freeze Drying / Lyophilization of Pharmaceutical and Biological Products*, Marcel Dekker Inc., New York, USA.
- Saclier M., Peczalski Ā.M., Andrieu J., 2010. “Effect of Ultrasonically Induced Nucleation on Ice Crystals’ Size and Shape during Freezing in Vials.” *Chemical Engineering Science*, **65**(10): 3064–71.
- Schwegman, J.J, Hardwick L.M, Akers M.J. 2005. “Practical Formulation and Process Development of Freeze-Dried Products., *Pharmaceutical Development and Technology*, **10** (1):151–73.

- Searles J.A, Carpenter J.F., Randolph T.W., 2001. “Annealing to Optimize the Primary Drying Rate, Reduce Freezing-Induced Drying Rate Heterogeneity, and Determine Tg’ in Pharmaceutical Lyophilization.” *Journal of Pharmaceutical Sciences*, **90**(7): 872–887.
- Tang X. and Pikal M.J., 2004. “Design of Freeze-Drying Processes for Pharmaceuticals: Practical Advice.” *Pharmaceutical Research*, **21**(2): 191-200.
- Towns J.K., 1995. “Moisture Content in Proteins: Its Effects and Measurement.”. *Journal Chromatography a*. **705**(1): 115–27.
- Vecchio C., Gazzinga A., 2010. “Freeze-Drying Process: Principle and Practice.” Course notes of *Fabbricazione Industriale dei Medicinali*. Università degli Studi di Milano.
- Wang, W., 2000. “Lyophilization and Development of Solid Protein Pharmaceuticals”.*International Journal of Pharmaceutics*, **203**(1):1-60.
- Zhang X., Inada T., Tezuka A., 2003. “Ultrasonic-Induced Nucleation of Ice in Water Containing Air Bubbles.”, *Ultrasonic Sonochemistry*, **10**(1): 71–76.



# Chapter 2

## 2. Impact of the freezing method on inter and intra-vial variability

### 2.1 Introduction

An important goal of lyophilization is to obtain a homogeneous batch. The selection of the freezing method and of the cooling rate impacts on the variability of the final dried cake structure, not only within the vial, but also from vial to vial. Consequently, the drying time can vary from sample to sample according to the dimension and the shape of the pores.

Because freezing is a critical stage that influences the whole process, in this work two freezing methods, conventional shelf-ramped freezing and suspended-vial freezing, with two different protocols (high cooling rate, HCR and low cooling rate, LCR), were studied to determine the inter and intra-vial variability. In the conventional freezing, the samples were placed in direct contact with the shelf freeze-dryer, in the suspended-vial freezing they were suspended from the shelf through a rising system. As a consequence, the thermal conduction from the shelf to the bottom of the vial was irrelevant in the suspended-vial freezing. Therefore, working with the same operating conditions, the freezing rate was lower in presence of clearance between the shelf and the vials.

Moreover, the stochasticity of nucleation influences the variability of the batch, because samples that nucleate at different temperatures can show different pore size. For this purpose, the nucleation temperature was monitored and experimentally calculated for every vial in order to determine the variability of this parameter. The nucleation temperature distributions curves were built, and, for the HCR protocol, they were linked to the SEM images of some dried samples in order to estimate, always via an experimental way, the pore size distribution curves of the lyophilized products. Moreover, the variability of the product resistance to vapor flow versus thickness of the dried layer was estimated as a function of the intra and inter- mean pores diameter distribution. At last, since the solution used in this work contained mannitol, polymorphs of mannitol were identified by X-ray powder diffractometric analysis to provide a qualitative characterization of the product physical state.

All the experiments shown in this chapter have been carried out at Politecnico di Torino. The suspended configuration has been patented by Politecnico di Torino (Trout B. *et al*, 2017).

### 2.2 Materials and methods

#### 2.2.1 Preparation of the solution

Mannitol-based solutions with a solid content of 5% (w/v) were prepared using water for injection. The solutions were filtered with a filter of 0,2  $\mu\text{m}$  and processed in the DISAT laboratory freeze-dryer (Lyo Beta 25, Teslar, Terrassa, Spain) filling vials (tubing vial 10R, Vidrio Soplado Manuel Perez, Rubi, Spain) with 3 mL of solution. Igloo stoppers (type 13194432/50/ Westar, West Pharmaceutical Services, Terrassa, Spain) were used as closures.

## 2.2.2. Freezing methods: conventional shelf-ramped and suspended-vial freezing

Two freezing methods were investigated: conventional shelf-ramped freezing and suspended-vial freezing. In the case of shelf-ramped freezing, vials were placed on the shelf of the freeze-dryer, while with the second method vials were suspended from the shelf through a rising system made of a Plexiglas track sustained by screw pillars regulated to obtain a gap of 12 mm.

In any batch, 14 suspended vials and 14 non-suspended vials were alternately loaded on the shelves of the freeze-dryer for a total of 56 vials within a batch, as reported in Figure 2.1.



**Figure 2.1** Disposition of vials into the freeze-dryer according to the suspended or non-suspended configuration.

Two freezing protocols were tested: freezing with HCR with which shelf temperature was lowered from 20°C to -55°C at the maximum rate allowed by the equipment, and LCR where shelf temperature was lowered from 20°C to -55°C in 6h.

Under these operating conditions, the freezing rate changed according to the kind of vials disposition. With HCR, suspended vials showed a cooling rate of 0.55 °C/min, while 0.85 °C/min was the cooling rate for non-suspended vials; concerning the protocol LCR, the values were 0.15 °C/min and 0.2 °C/min for suspended and non-suspended vials respectively. These cooling rate values are mean values that were determined calculating the average of the slopes of the experimental product temperature curves when freezing conditions were settled. All cooling profiles as a function of the freezing method and the freezing protocol are reported in Figure 2.2.

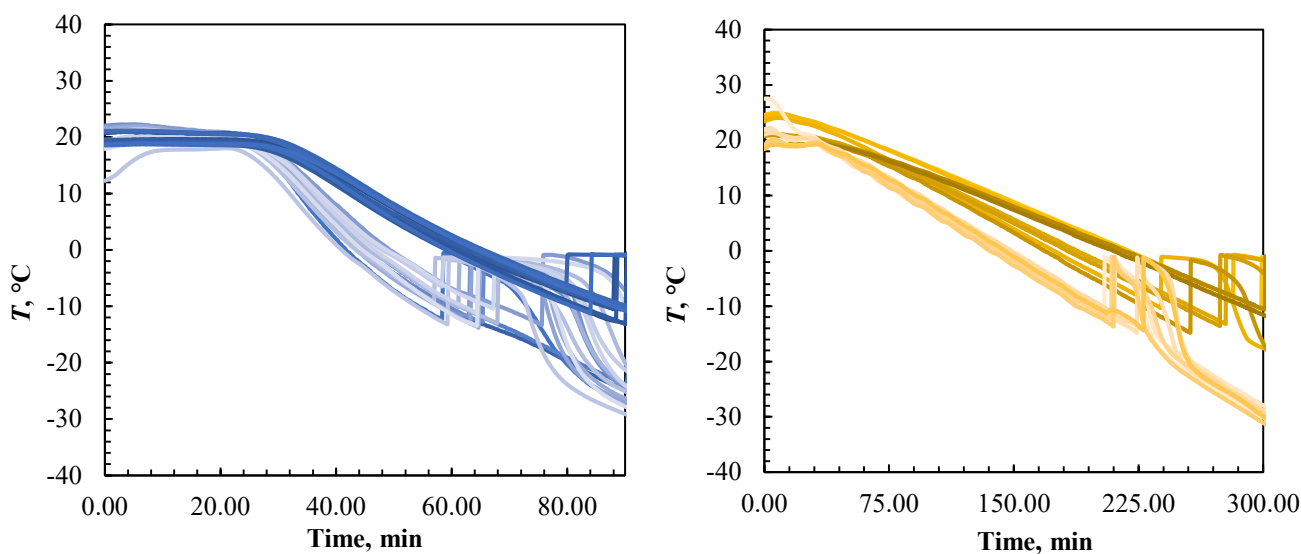


**Figure 2.2** Product temperature profiles recorded with thermocouples for HCR protocol (left) and LCR protocol (right). Dark lines refer to suspended vials monitoring, light lines refer to non-suspended vials.

### 2.2.3. Product characterization

In order to study how the freezing method impacts on the variability of the batch production and on the intra-vial heterogeneity, parameters such as the nucleation temperature, the pores size, the crystallinity of the product and the mass-transfer resistance during primary drying were measured.

#### 2.2.3.1. Nucleation temperature

Since supercooling is stochastic, nucleation takes place in the vials at different temperatures, determining different structures among the vials. The aim is to obtain nucleation temperature distribution curves for the two different arrangements of the vials and, hence, to compare the conventional freezing with the suspended-vial freezing for the two protocols.

A simple and effective method was developed to determine the nucleation temperature of each vial with a reasonable accuracy. It was possible to monitor the product temperature using thermocouples placed in various samples. These thermocouples were connected to an on-line software (Lyomonitor). Moreover, all shelves were monitored via webcams that recorded the freezing process. Through the videos, it was possible to calculate the time at which the nucleation has started. From the temperature profile, measured by thermocouples, known the time on which nucleation of each vial occurred, the nucleation temperatures were obtained.

In order to ignore the nucleation exothermicity profile, it is appropriate to extrapolate from the temperature profile the future trend of the supercooling phase as if nucleation had not occurred. An example is shown in Figure 2.3.

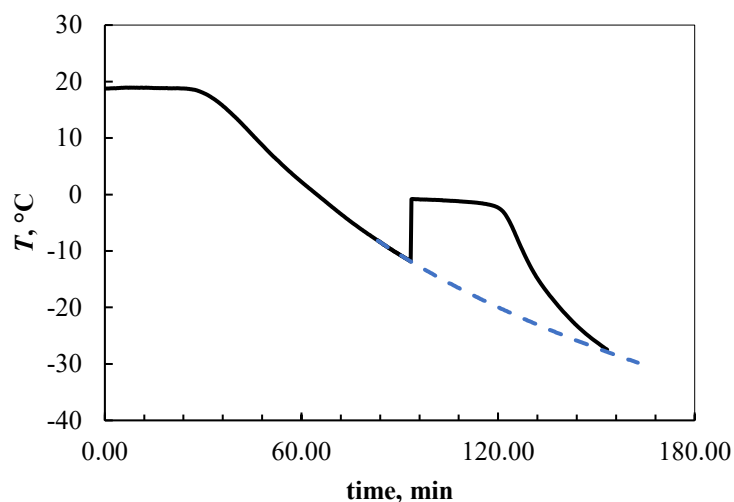


**Figure 2.3** Example of temperature profile measured with thermocouples

The results are collected according to the kind of freezing method and cooling rate to determine the distribution curves. In addition, for each sample, the normalized nucleation temperature ( $T_n - T_m$ ) was calculated;  $T_m$  values were the mean nucleation temperatures correspondent to a specific batch and to a specific configuration (suspended or non-suspended).

### 2.2.3.2. SEM analyses

Some freeze-dried samples with HCR protocol were investigated using Scanning Electronic Microscopy (SEM) to examine the product morphology in relation to the nucleation temperature. 10 samples were selected from the same batch, and respectively 5 suspended vials located on the same shelf and 5 non-suspended vials located on the same shelf, so as to have the widest possible nucleation temperature range.

The visible pores in the SEM images were approximated to the ellipses and the equivalent diameters were calculated. At the last, the mean pore diameters with the standard deviations for each sample were obtained.

SEM images were taken at various positions along the sample (top, centre, bottom) so as to obtain a quantitative estimation of intra-vial heterogeneity.

In order to estimate the mean pore size variability among the batch, a linear function that correlates the mean diameter of the scanned samples to the nucleation temperature was extrapolated for both freezing methods.

### 2.2.3.3. XRD Analysis

The freezing process impacts also on the preferred formation of different polymorphs. The study of the physical state of excipients is important because it can influence the reconstitution time, the storage stability and the protein stability. Both freezing rate and mannitol concentration influence the crystal form of mannitol in the freeze-dried solid when mannitol is present as a single component (Kim *et al.*, 1998). Mannitol shows three different polymorphs:  $\alpha$ ,  $\beta$ ,  $\delta$ . The thermodynamic stable form of mannitol is the  $\beta$  polymorph, while  $\alpha$  and  $\delta$  are metastable.

So, some samples were analyzed and compared with the references spectra for mannitol through a qualitative analysis: the spectra of the samples were compared with the position of  $\alpha$ ,  $\beta$ ,  $\delta$  reference peaks.

XRD measurement were done in the reflection mode, within 5-60° as 2 $\theta$  range; data were acquired at each 0.02° with a time step of 1 s. Analysis of the diffractograms was done using X-Pert Data Analysis program.

#### 2.2.3.4. Measure of mass transfer resistance ( $R_p$ )

During primary drying, the crystalline ice is removed by sublimation. The sublimation rate was influenced by the size and the morphology of ice crystals. The mass transfer resistance to water vapour makes it possible to compare the efficiency of the primary drying step.

The water vapor flow is impeded by three resistances: resistance of the dried-product layer above the frozen product ( $R_p$ ), resistance of the semi stoppered vial ( $R_s$ ), and resistance in transfer from the drying chamber to the condenser ( $R_c$ ). The product resistance ( $R_p$ ) is the most important, so it is used to approximate the global resistance ( $R_t$ ), (Pikal *et.al*, 1983).

It is theoretically possible to calculate the product resistance assuming that the porous cake of thickness  $L_d$ , with porosity  $\varepsilon$ , creates during freeze-drying a collection of capillary tubes of diameter  $d_p$  and tortuosity  $\tau$ . The correlation is the following (Rambhatla et al, 2004):

$$R_p = \frac{3}{2} \frac{\tau^2}{\varepsilon} \frac{L_d}{d_p} \sqrt{\frac{\pi RT}{2M_w}} \quad (2.1)$$

where it can be observed the linear dependence between the mass transfer resistance and the thickness of the dried layer  $L_d$ . As a consequence,  $R_p$  grows during the primary drying.

Moreover,  $R_p$  depends on the ice crystal size formed during freezing. The term  $RT$  refers to the gas constant and absolute temperature, while  $M_w$  is the molecular weight of water.  $\tau$  is frequently taken to be  $\sqrt{2}$ , while the void volume fraction  $\varepsilon$  is been assumed equal to 0.95.

Experimentally, the product resistance to vapor flow can be correlated to the vapor mass flow ( $J_w$ ) by the following equation (Fissore et al., 2011):

$$R_p = \frac{P_o - P_c}{J_w} \quad (2.2)$$

where  $P_o$  represents the equilibrium vapor pressure of ice and  $P_c$  the chamber pressure.

$P_o$  was calculated with the following equations (Fissore et al., 2010) expressing the pressure in Pa and the product temperature ( $T$ ) in K:

$$P_o = \exp\left(\frac{-6140.4}{T} + 28.916\right) \quad (2.3)$$

The product temperature was measured by a thermocouple positioned in a central vial.

Assuming that all heat provided is needed for ice sublimation, it is possible to determine the heat flow as:

$$J_q = \Delta H_s J_w \quad (2.4)$$

where  $\Delta H_s$  is the latent heat of sublimation.

The heat flow was calculated with the following equation through the experimental data:

$$J_q = \frac{\Delta H_s}{A} \frac{\Delta m}{\Delta t} \quad (2.5)$$

where  $A$  is the area of the vial section,  $\Delta m$  is the total mass variation during the primary drying and  $\Delta t$  is the time of the primary drying.

It is also possible to calculate  $J_q$  as:

$$J_q = K_v(T_s - T_b) \quad (2.6)$$

With  $K_v$ , the heat vial transfer coefficient ( $J/m^2 \text{ s K}$ ),  $T_s$  the shelf temperature and  $T_b$  the product temperature at the bottom of the vial.

The end of primary drying was calculated finding the point in which the Pirani pressure starts to sharply decrease indicating that the gas composition is changing from mostly water vapor to nitrogen (Patel et.al, 2010).

Consequently, the product resistance can be evaluated with the equation below:

$$Rp = \frac{P_o - P_c}{J_q} \Delta H_s \quad (2.7)$$

## 2.3. Results and discussions

### 2.3.1. Nucleation temperature distribution

In this section, the distribution curves of nucleation temperature were reported for both suspended and non-suspended vials as a function of the cooling rate.

The batch non-uniformity depends on many factors, such as temperature gradients on the heating shelf, radiation from the wall of the chamber, stochastic subcooling phenomena, variations in the material or in the operating conditions, operator errors; therefore, changes from batch to batch are always present (Barresi *et al.*, 2010).

In order to minimize some of these causes, in particular on operator errors and variations in the material and in the operating conditions, the values of nucleation temperature were normalized ( $T_n - T_m$ ) as specified in the paragraph 2.2.3.1.

With the same freezing protocols, the suspended-vial freezing was characterized by a lower cooling rate than the conventional shelf-ramped freezing due to the different way of heat transmission. In the suspended-vial freezing, the convection is the principal heat transfer mechanism, radiation becomes more significant, but conduction is negligible. On the other hand, the heat transmission for conduction from the shelf to the bottom of the vial is important in the conventional shelf-ramped method. This difference impacted on the time in which samples start to nucleate and at which temperature; the difference in cooling rate was significantly evident when the shelves were cooled as fast as possible, resulting to a cooling rate of  $0.85 \text{ }^\circ\text{C}/\text{min}$  for non-suspended vials and of  $0.5 \text{ }^\circ\text{C}/\text{min}$  for suspended vials, while with the protocol LCR, the difference was less relevant ( $0.2 \text{ }^\circ\text{C}/\text{min}$  for non-suspended vials,  $0.15 \text{ }^\circ\text{C}/\text{min}$  for suspended vials).

The histograms were represented in Figure 2.4 and 2.5 respectively for the HCR and the LCR protocol, while in Table 2.1 and 2.2 all descriptive statistic data were summarized. In Table 2.2 were reported the data of the normalized  $T_n - T_m$  distribution curves. The red lines in the histograms represent the gaussian distributions; the mean values of the distribution,  $\mu$ , and the standard deviations,  $\sigma$ , were reported in Table 2.1 and 2.2.

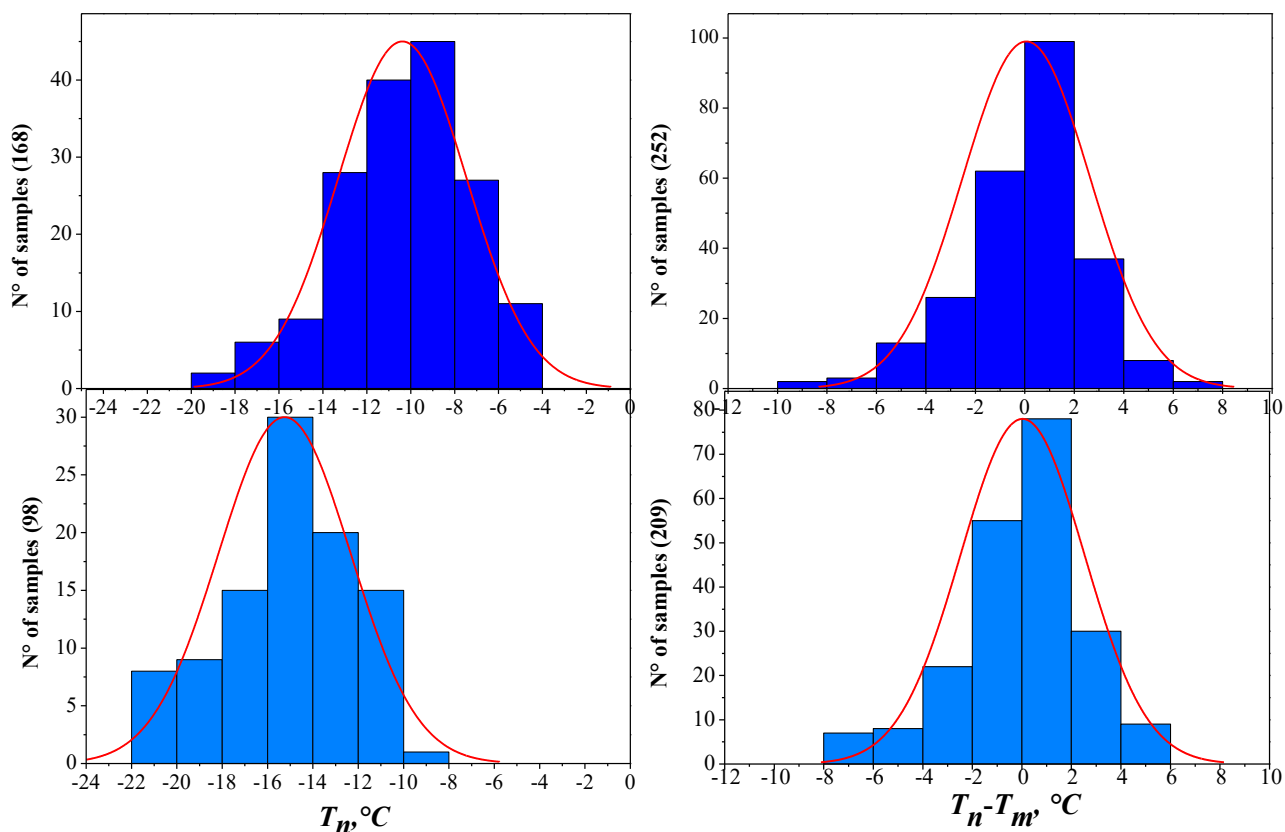


**Figure 2.4** Nucleation distribution curves for the HCR protocol. On the right, the normalized curves ( $T_n - T_m$ ) were reported. Blue histograms refer to non-suspended vials ( $0.85\text{ }^\circ\text{C/min}$ ), cyan bars to suspended vials ( $0.55\text{ }^\circ\text{C/min}$ ).

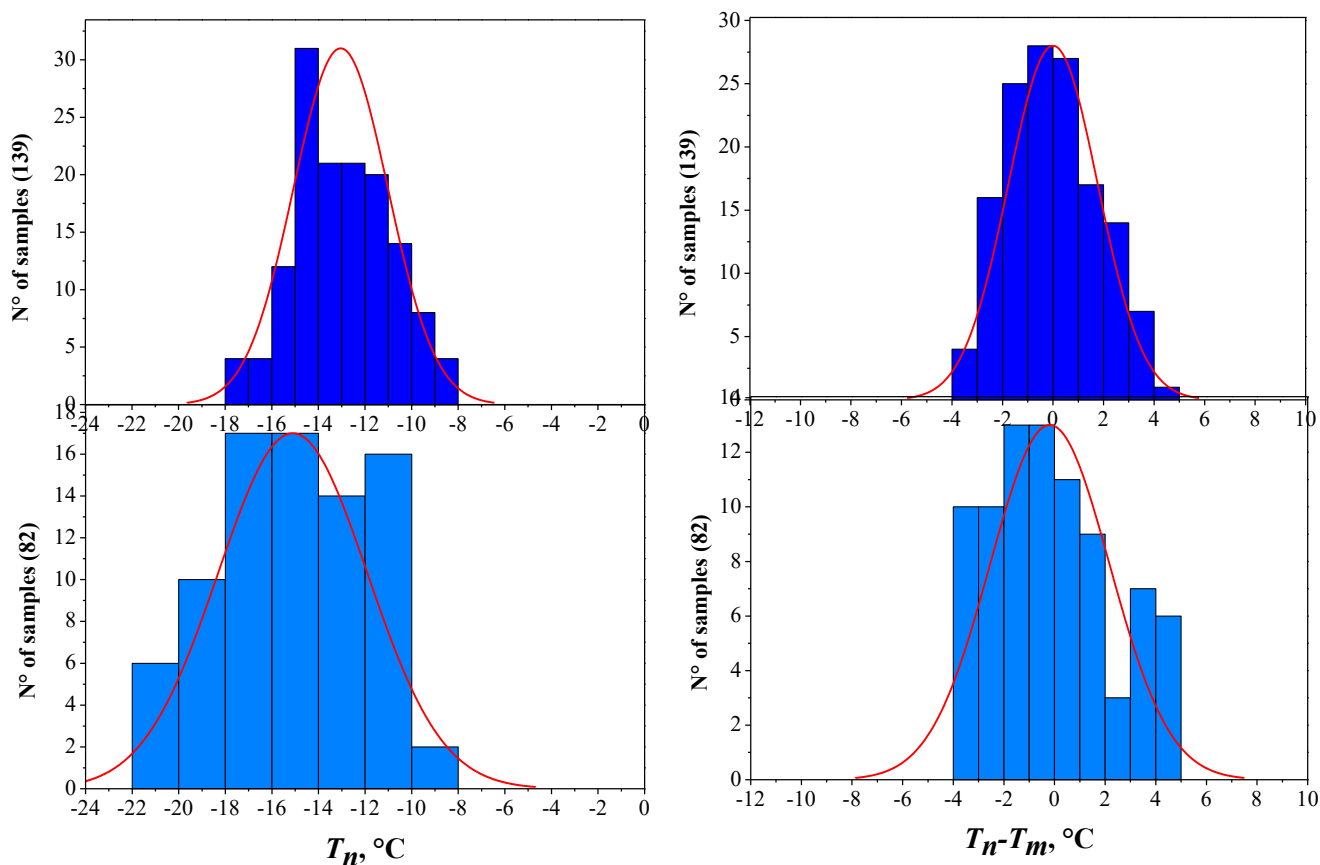


**Figure 2.5** Nucleation distribution curves for the LCR protocol. On the right, the normalized curves ( $T_n - T_m$ ) were reported. Blue histograms refer to non-suspended vials ( $0.2\text{ }^\circ\text{C/min}$ ), cyan bars to suspended vials (CR of  $0.15\text{ }^\circ\text{C/min}$ ).

**Table 2.1** Descriptive statistic data for the nucleation distribution curves.

$T_n$	CR [°C/min]	N° samples	$\mu$ [°C]	$\sigma$ [°C]	Minimum [°C]	Median [°C]	Maximum [°C]	$\Delta T$ [°C]
<b>HCR</b>								
<b>Non_Susp</b>	0.85	168	-10.4	2.9	-19.7	-10.3	-4.1	16
<b>Susp</b>	0.55	98	-15.2	2.9	-22	-14.7	-9.4	13
<b>LCR</b>								
<b>Non_Susp</b>	0.2	139	-13	2	-17.7	-13.2	-8.2	10
<b>Susp</b>	0.15	82	-15.1	3.2	-21.5	-15.4	-9.5	12

**Table 2.2** Descriptive statistic data for the normalized nucleation temperature distribution curves.

$T_n - T_m$	CR [°C/min]	N° samples	$\mu$ [°C]	$\sigma$ [°C]	Minimum [°C]	Median [°C]	Maximum [°C]	$\Delta T$ [°C]
<b>HCR</b>								
<b>Non_Susp</b>	0.85	252	0.1	2.6	-9.5	0.5	7.7	17
<b>Susp</b>	0.55	209	0	2.5	-7.4	0.3	5.9	13
<b>LCR</b>								
<b>Non_Susp</b>	0.2	139	0	1.8	-3.4	-0.1	4.3	8
<b>Susp</b>	0.15	82	-0.2	2.4	-3.9	-0.4	4.8	9

Observing the last column of the Table 2.1, the variability of nucleation temperature (from the maximum to the minimum value of  $T_n$ ), was more or less 13 °C in the suspended vials. Instead, non-suspended vials showed a range of variability of about 16 °C. Similar range values were found if the nucleation temperatures were normalized (Table 2.2). Nevertheless, the standard deviations were the same. With the LCR protocol, since the effective cooling rates between suspended-vial freezing and conventional freezing were comparable, also suspended and non-suspended vials showed a similar range of  $T_n$  (or  $T_n - T_m$ ).

Figure 2.6 shows the values of  $T_m$  as a function of the cooling rate and of the freezing method. The averages of  $T_m$  values for each cooling rate and freezing method were also calculated. It is possible to observe how these mean values decreased with the decrease of the cooling rate for the non-suspended vials. Since the cooling rate gap was small between the HCR protocol and the LCR protocol for suspended freezing, an irrelevant decrease on  $T_m$  values was present.

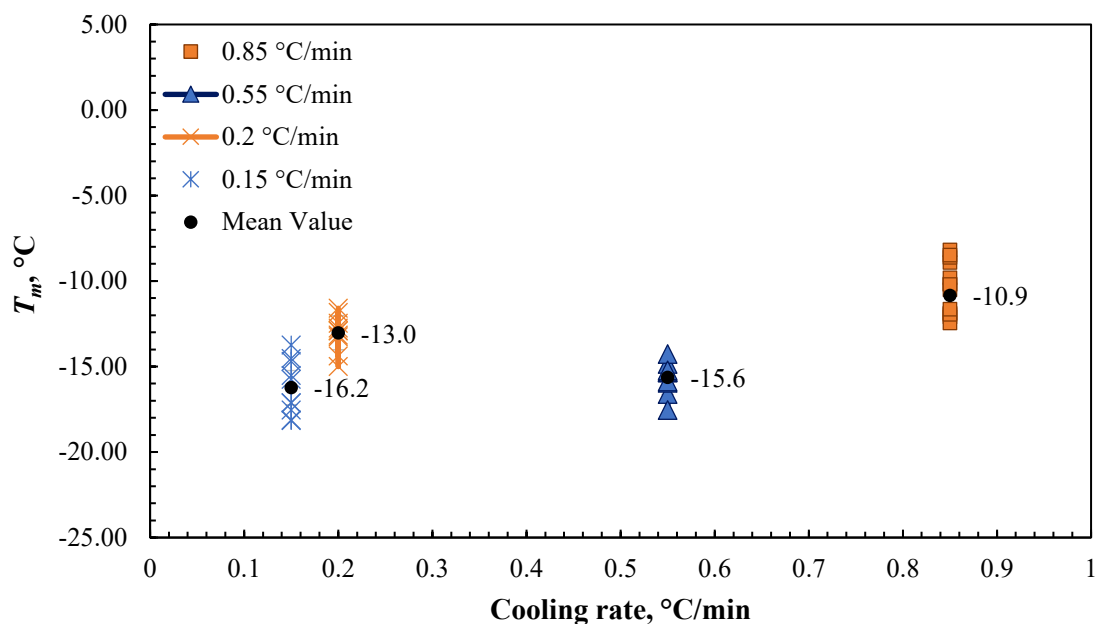


**Figure 2.6**  $T_m$  values as a function of cooling rates and freezing method. The  $T_m$  values of non-suspended freezing are reported in orange, in cyan for suspended-freezing. Black points represent the average of  $T_m$  values for each case.

The range of the distribution curves can be affected by repeatability devices. Although solutions were always filtered, new glass vials were used for each test and the chamber was cleaned every time, the repeatability of the experiments is not obvious. Furthermore, in the industries these curves can suffer more and more about variability because the work is conducted in GMP conditions (dust free).

It is important to observe that the number of the vials impacts on the determination of the distribution curve, and it needs to have a statistically significant number vials to find a thick distribution of the data. For instance, in the case of suspended vials with the LCR protocol, less than 100 samples were used to build the nucleation temperature distribution curves, therefore having less statistic significant results.

### 2.3.2. Characterization of the product morphology

Five suspended vials and five non-suspended vials, subjected to HCR and coming from the same batch, were observed using SEM to determine the intra-vial and inter-vial heterogeneity.

The products were analyzed at different positions along their thickness: at the top, the centre and the bottom.

Figure 2.7 and 2.8 show the SEM images in the top, centre and bottom of the product for the 10 analyzed samples, respectively for non-suspended vials and suspended vials.

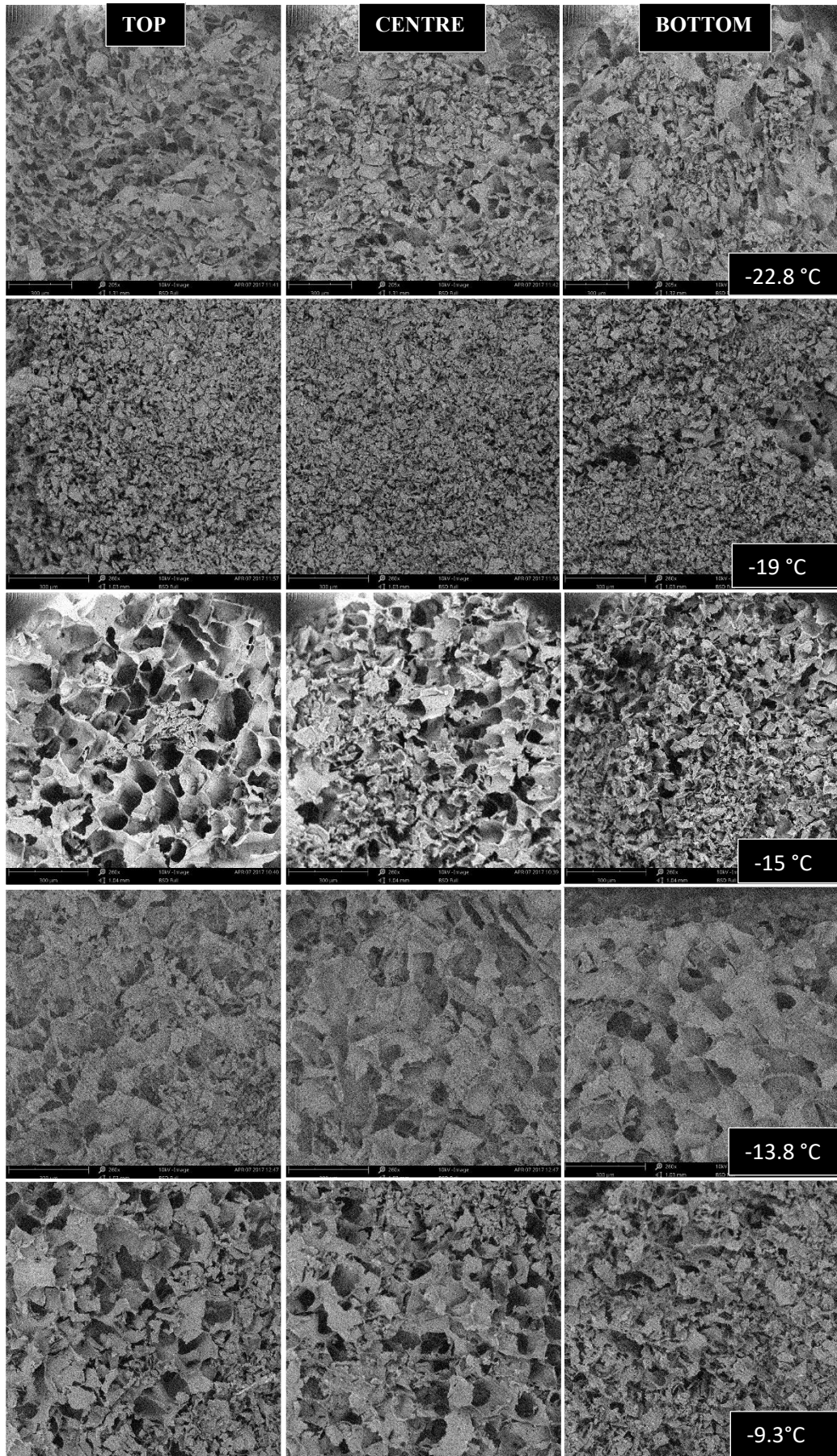


**Figure 2.7** SEM images at the top (left), centre (central) and bottom (right) for non-suspended vials. It is also reported the nucleation temperature of the samples.

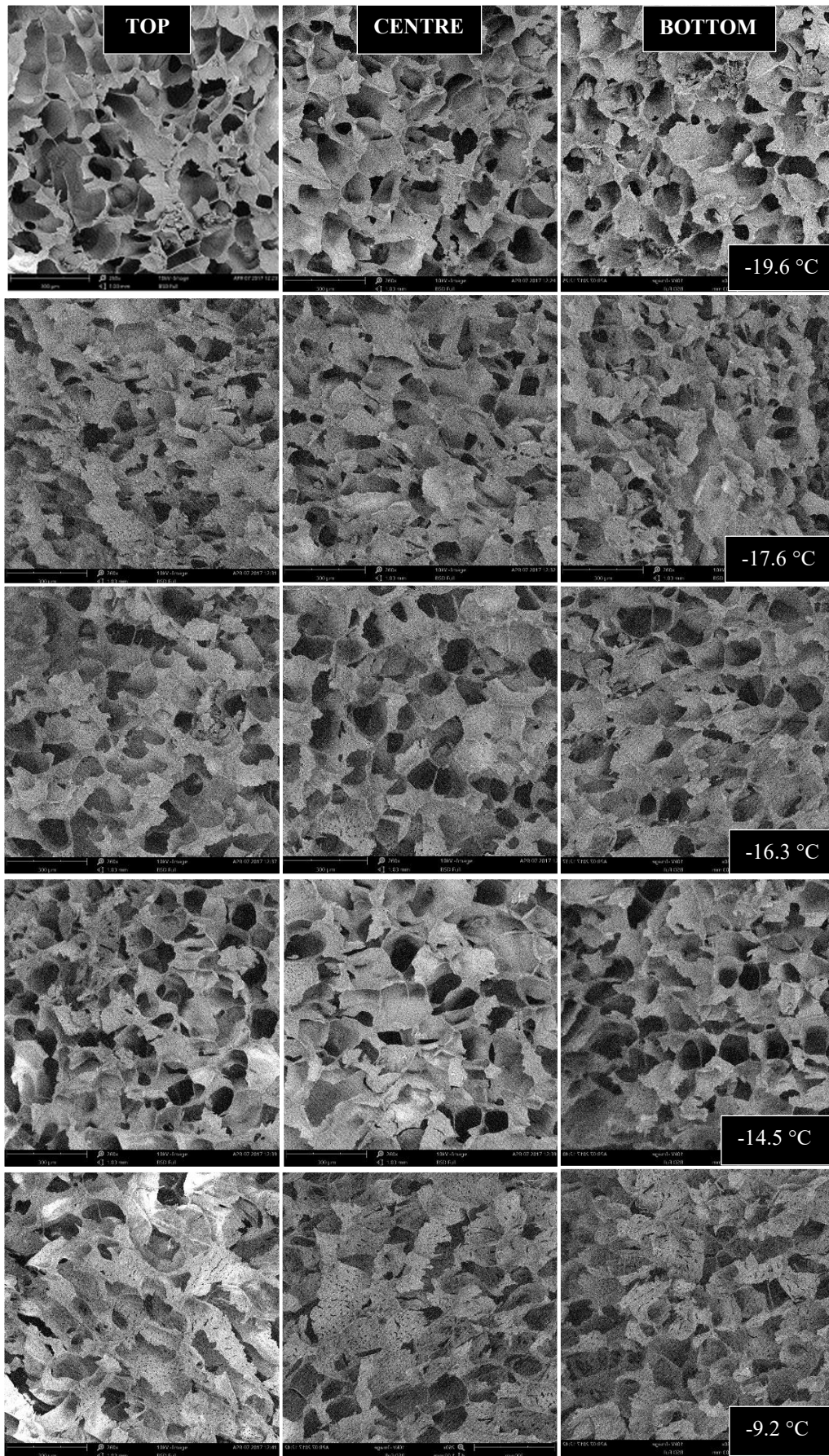


**Figure 2.8** SEM images at the top (left), centre (central) and bottom (right) for suspended vials. It is also reported the nucleation temperature of the samples.

Table 2.3 summarizes the average size ( $D_{eq}$ ) at three different cake positions, its deviations standards, and the nucleation temperature of the samples.

**Table 2.3** The average pore size as observed at different cake positions (top, centre, bottom) in the case of suspended and non-suspended samples (HCR protocol).

	SAMPLE	TOP		CENTER		BOTTOM		$T_n$ [°C]	$D_{eq}$ [μm]	$\sigma$ [mm]
		$D_{eq}$ [μm]	$\sigma$ [μm]	$D_{eq}$ [μm]	$\sigma$ [μm]	$D_{eq}$ [μm]	$\sigma$ [μm]			
Suspended vials	1	87.21	28.62	89.53	26.43	95.01	24.20	-19.6	90.6	26.4
	2	87.88	24.93	88.76	25.39	84.61	20.84	-17.6	87.1	23.7
	3	100.64	28.09	99.32	27.54	101.48	16.89	-16.3	100.5	24.2
	4	101.81	22.93	104.77	23.11	101.48	16.89	-14.5	102.7	21.0
	5	96.89	23.38	101.27	24.61	99.99	19.52	-9.2	99.4	22.5
Non suspended	6	31.38	18.92	24.69	16.69	35.25	23.99	-22.8	30.4	19.9
	7	25.04	21.63	25.36	17.48	23.14	18.21	-19	24.5	19.1
	8	59.16	43.31	48.29	40.26	32.19	24.85	-15	46.5	36.1
	9	28.56	22.56	43.41	25.76	45.15	23.34	-13.8	39.0	23.9
	10	47.34	32.79	46.268	35.057	32.71	19.33	-9.3	42.1	29.1

Figure 2.9 and 2.10 show the mean pore diameter at the top, centre and bottom of the samples, respectively for suspended vials and non-suspended vials.

The value of the mean pore diameter at different heights of the porous cake was almost the same for suspended-vial freezing. On the other hand, it was very different in the case of non-suspended vials.

In addition, it is possible to see that the standard deviation was very high for non-suspended vials: smaller pores coexisted with larger pores. Concerning the suspended vials, the standard deviation was lower and approximately 20±30% of the mean pore diameter.

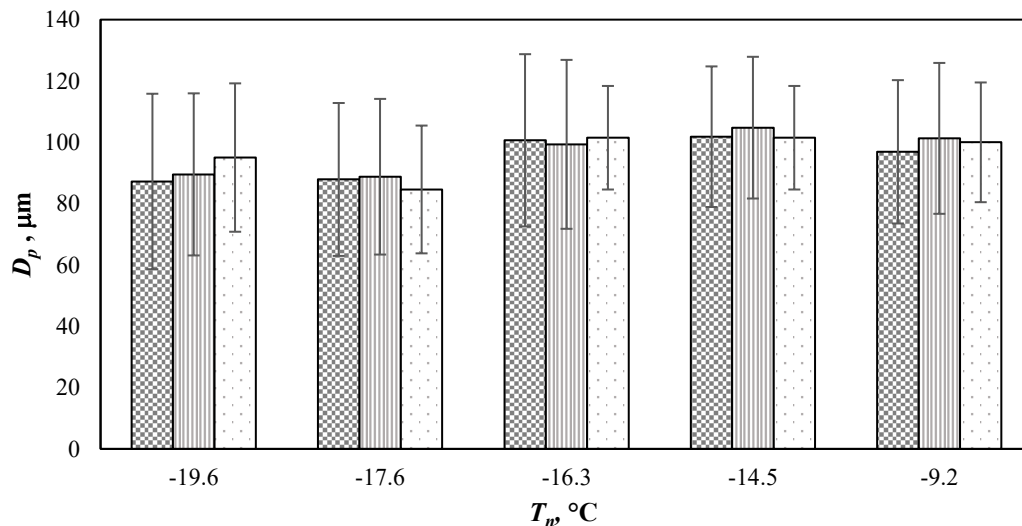


**Figure 2.9** Mean pore diameter at the top (■), centre (■), and bottom (■) of the product for suspended vials with the HCR as a function of the nucleation temperature.

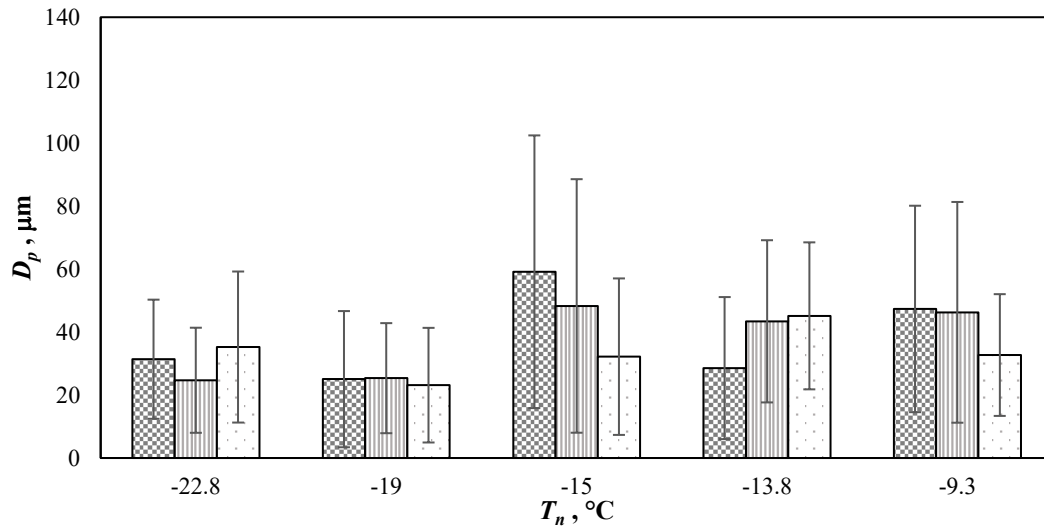


**Figure 2.10** Mean pore diameter at the top (▨), centre (▩), and bottom (▧) of the product for non-suspended vials with the HCR as a function of the nucleation temperature.

Figure 2.11 compares the mean pore diameters of the two freezing methods as a function of the nucleation temperature.

These results indicated that the size of pores was always bigger in the case of suspended-vial freezing than during the shelf-ramped freezing. Bigger pores reduce the mass transfer resistance and, hence, the drying time. Moreover, the presence of a large structure of pores could have a positive impact on the stability of API (Kasper *et al.*, 2011).

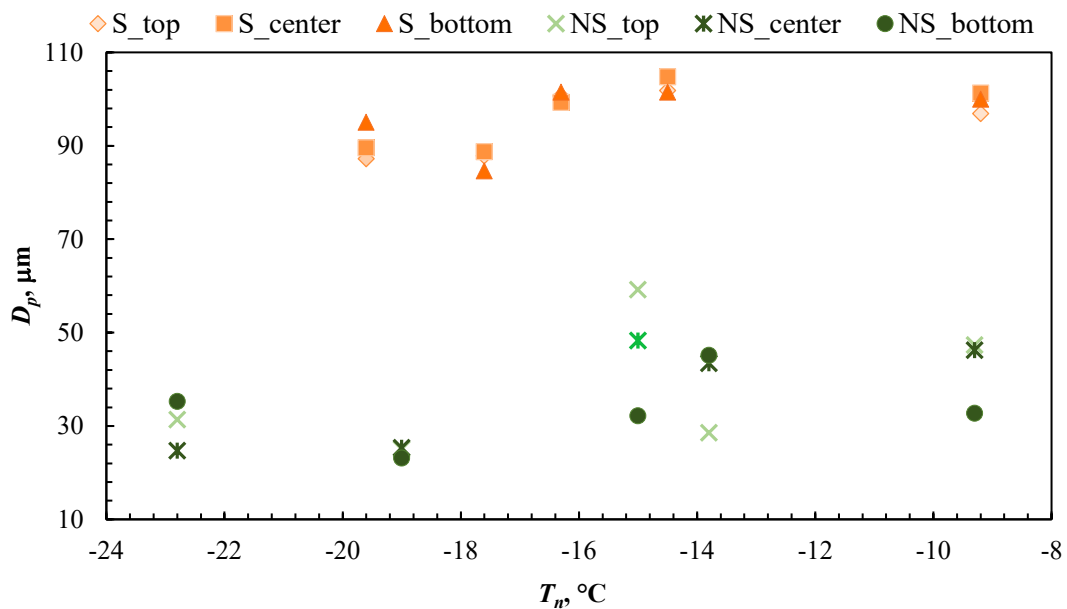


**Figure 2.11** Comparison between the mean pore diameter in the bottom, centre and top as a function of the freezing method and the nucleation temperature of the samples.

In attempt to detect how the mean pore diameter changes from vial to vial, starting from the experimental points, a linear function that correlates the mean pore diameter with the nucleation temperature was

obtained for both freezing methods (Figure 2.12). With this empirical correlation, it was possible to switch from a discrete distribution to a continuous distribution of the pore size.

The nucleation temperature influences the ice crystals size, and lower nucleation temperatures theoretically lead to smaller size of ice crystals, while samples nucleated at higher temperature show greater ice crystals (Liu *et al.*, 2005). Although a linear function is not extremely appropriate to fit the experimental data, it is the easiest function to give a probable distribution of the mean pore in the batch. In fact, the goal is finding a single value of the mean pore diameter and the corresponding standard deviation which are representative of the whole batch.

In the case of suspended vials, the mean diameter of pores changed within a short range of value, between 88  $\mu\text{m}$  and 102  $\mu\text{m}$ . The human error in the calculation of the dimension of pores might be substantial since the samples appeared very similar observing SEM images. Nevertheless, a linear function was still chosen because the consecutive pore size distribution curve gave a mean pore diameter which was similar with the average between the mean smallest pore and the mean biggest pore among the five analyzed samples.

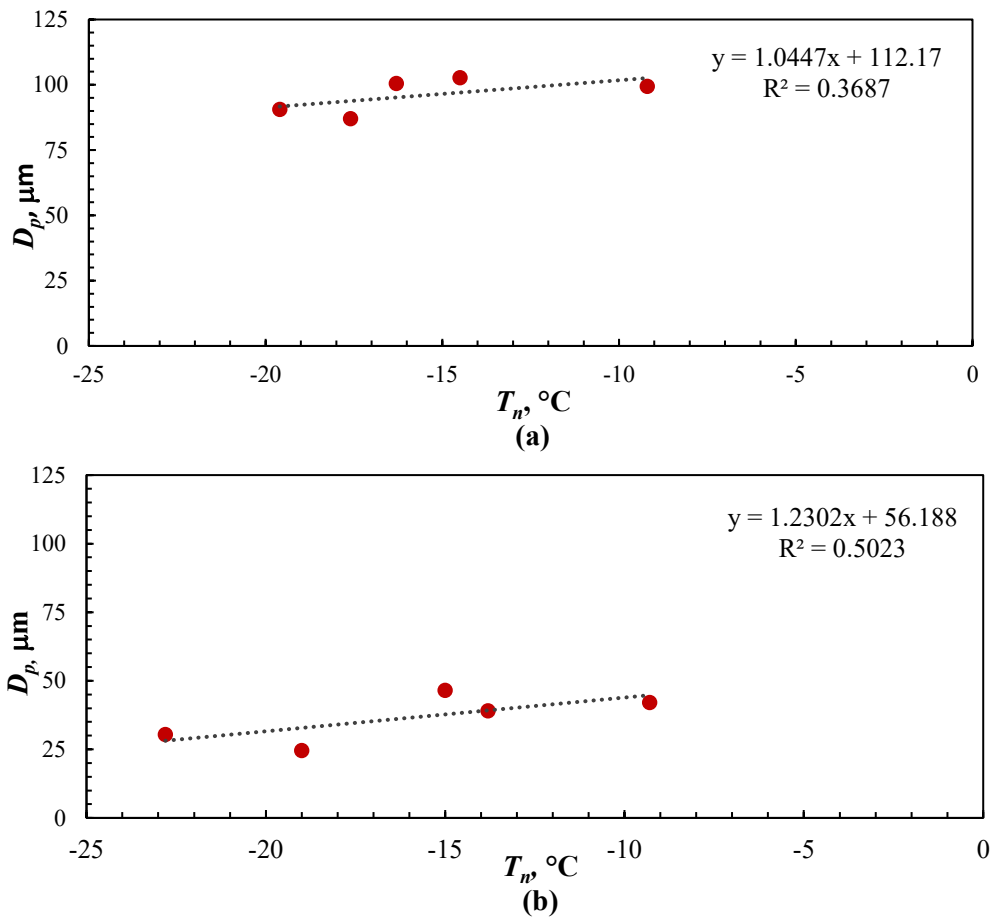


**Figure 2.12** Trends of mean pores size as a function of nucleation temperature for suspended vials (a) and non-suspended vials (b).

Once the nucleation temperature distribution curves and the experimental trends were known, it was possible to use the functions reported in the graphs of Figure 2.12 to obtain the mean pores size distributions which were represented in Figure 2.13, while Table 2.3 summarizes the statistical data correlated to the histograms.

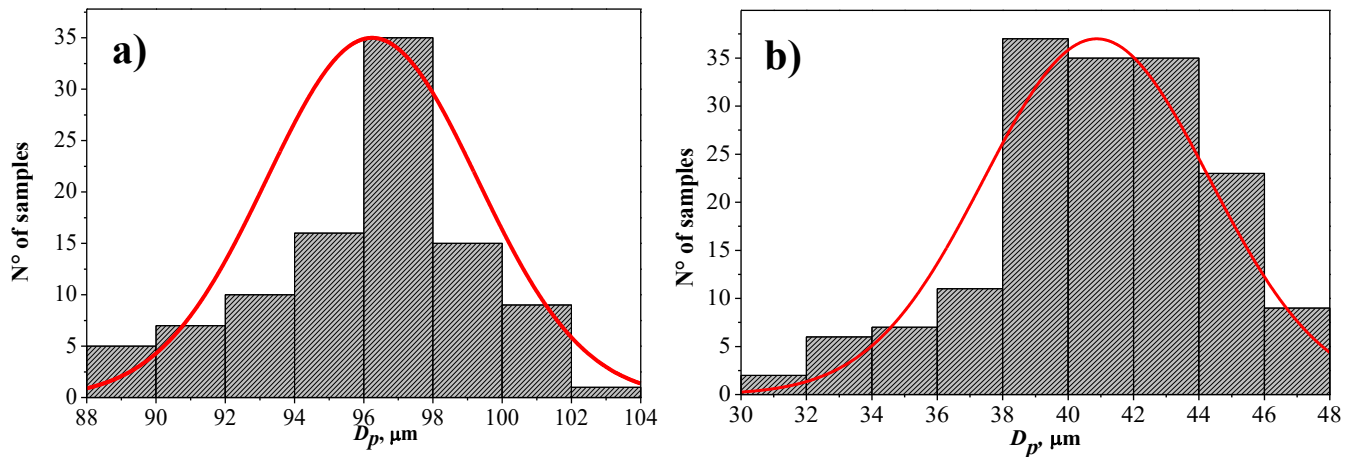


**Figure 2.13** Mean pore diameter distribution for suspended vials (a) and non-suspended vials (b). Red lines refer to the gaussian distributions.

**Table 2.3** Statistical data about pore size distribution curves.

	N total	Μεσν	Στ.Δεσ	Minimum	Median	Maximum	ΔΔπ
<b>Susp_vials</b>	98.0	96.2	3.0	89.2	96.8	102.3	13.2
<b>NonSusp_vials</b>	165.0	40.9	3.4	31.0	41.0	47.1	16.1

### 2.3.3. Variability of mass transfer resistance

This section investigates the uncertainty of the mass transfer coefficient on the basis of results of pore diameters found in the previous sections.

The variability of pore size distribution within the batch and within vials impacts on the sublimation rate. Inter-vial variation in nucleation temperatures causes heterogeneity in drying behavior and affects the porosity of the freeze-dried cake since the dimensions of the pores are a direct reflection of the size and geometry of the ice crystals formed during freezing.

Figure 2.14 shows the experimental value of the product resistance  $R_p$  as a function of the relative dried product thickness for both vials dispositions for the protocol HCR. Product resistance was higher in the case of non-suspended vials than that found in suspended-vial configuration. This result was in accordance with the pore size analysis. In fact, with the non-suspended vials, a greater number of ice crystals resulted in a smaller pore size in the dried cake and, hence, longer primary drying time.

It is evident how the value of  $R_p$  sharply increased at the beginning of the primary drying and, then, continued to increase but more slowly. In general,  $R_p$  for mannitol solution is linear (Pikal *et al.*, 1984). Taking  $Jq$  constant as simplification as in this case, a slight slope was present.

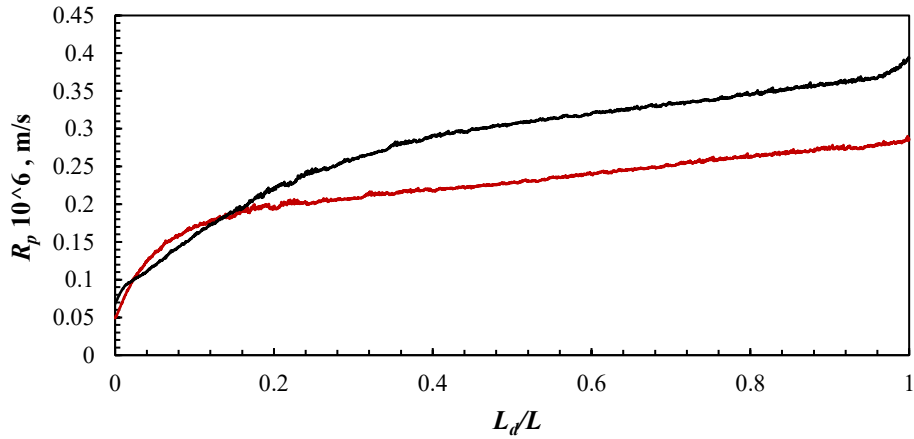


**Figure 2.14** Experimental value of product resistance versus thickness of the dried layer. The black line (-) corresponds to the case of non-suspended vials, the red line (-) represents the case of suspended vials.

The profile of the product resistance, as calculated using Equation 2.1, was reported in Figure 2.15. In this case, the pore diameters were taken constant along the thickness of the dried product, with a diameter of 97  $\mu\text{m}$  for suspended vials, and 41  $\mu\text{m}$  for non-suspended vials. These values correspond to the mean pores diameters achieved by the pores size distribution curves (Table 2.4).

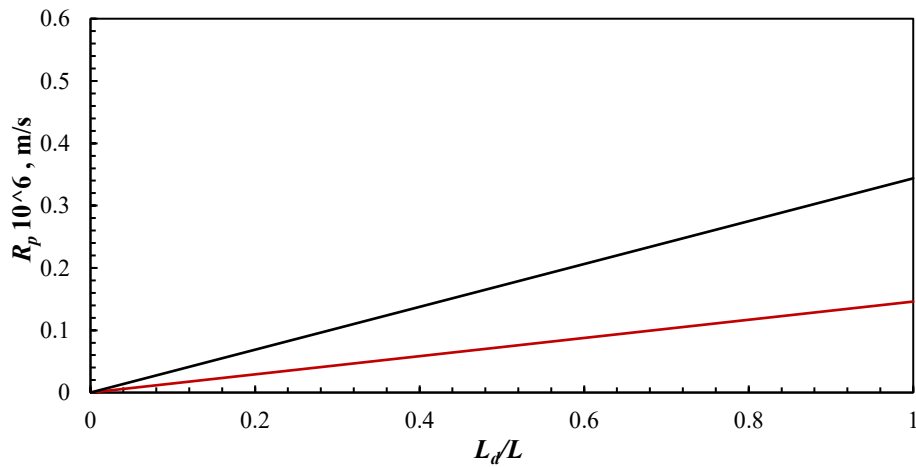


**Figure 2.15** Theoretic value of product resistance as a function of the dried product thickness. The black line (-) corresponds to the case of non-suspended vials, the red line (-) represents the case of suspended vials.

$R_p$  variability within the batch, were calculated according to Eq. 2.1 in which the value of the mean pore diameter,  $d_p$ , was corrected respectively adding and subtracting the standard deviation value originated by the empirical pore size distribution, and without changing the other parameters.

Figure 2.16 shows the variability range of  $R_p$  both for non-suspended vials and suspended vials. As can be seen, there was a significant difference in the two cases. This trend indicated that suspended vials, that showed a greater uniformity in pore size as confirmed by SEM images, have a slower variability of  $R_p$  within the batch comparing to the non-suspended vials.

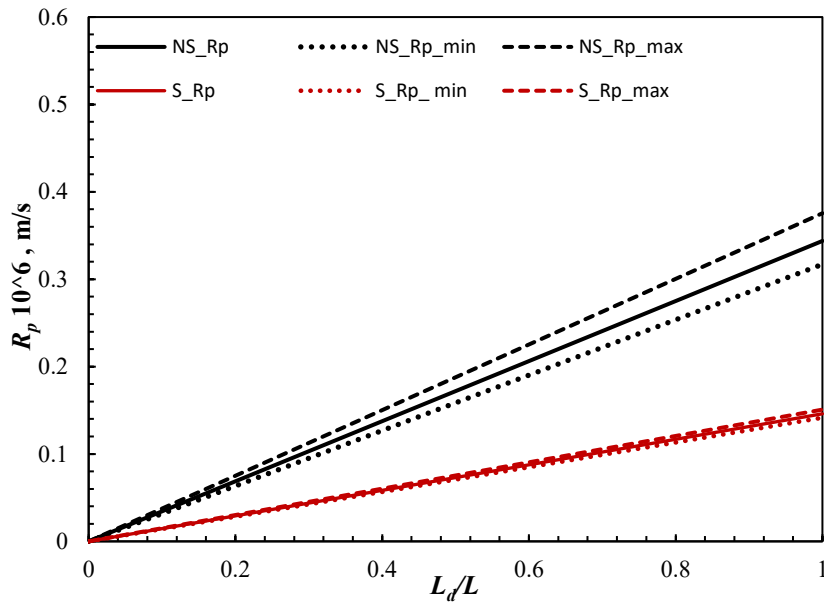


**Figure 2.16** Inter-variability of  $R_p$  as a function of the dried product thickness. As summarized in the legend, red lines refer to the suspended configuration, black lines refer to the non-suspended configuration.

Since non-suspended vials showed higher variability of the pore size in the dried cake, instead of using a unique mean diameter, it is interesting to calculate what are the mean values of the diameters in the three sections of the cake (top, centre and bottom) that are representative of the whole batch. So, with the same previous procedure, three linear functions, correlating the pore size to the nucleation temperature, were calculated in the top, centre and bottom of the dried cake; then, the mean diameters and the standard deviations were extrapolated by the consequent distribution curves.

Setting the top at 1 mm, the centre at 5 mm and the bottom at 9 mm of the dried cake,  $R_p$  and its variability were determined in that points. In this case,  $R_p$  was less linear and the variability was not constant but increased during the primary drying (Figure 2.17).

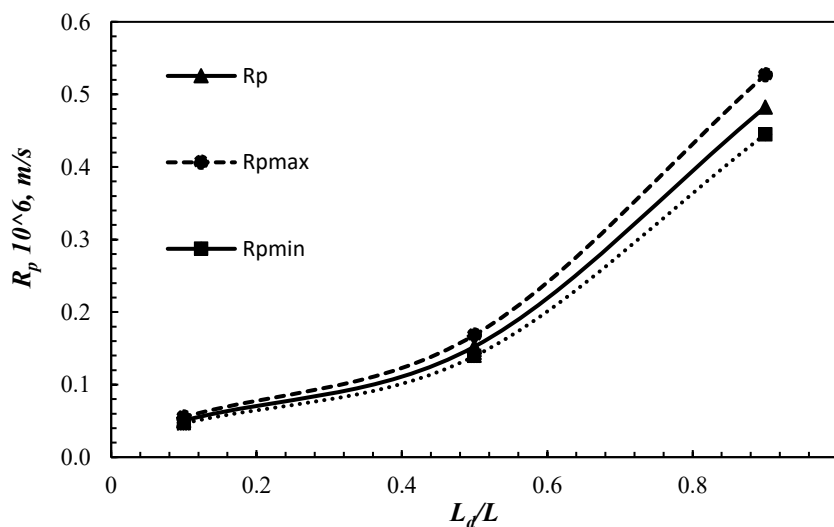


**Figure 2.17** Inter-variability of  $R_p$  in case of non-suspended vials with variable  $D_p$  among the layer of the dried cake.

Moreover, for each vial analysed by SEM, it was possible to calculate  $R_p$  in two different ways: maintaining constant the diameter, calculated as the average among the mean values at the top, centre and bottom, or calculating  $R_p$  in three points using the diameter corresponding to the different layers. An example of  $R_p$  as a function of variable  $D_p$  was reported in Figure 2.18 for two samples with a similar nucleation temperature: a suspended sample characterized by a  $T_n$  of  $-14.5^\circ\text{C}$  and a non-suspended sample with a  $T_n$  of  $-15^\circ\text{C}$ .

It is interesting to note that, for the suspended vial, the intra-variability of  $R_p$  appeared almost constant. Conversely, since there was a greater heterogeneity among the dried layer of non-suspended vials, the variability increased a lot with the increase of the thickness of the dried product. The other dried samples showed the same trends and so, they were not reported.

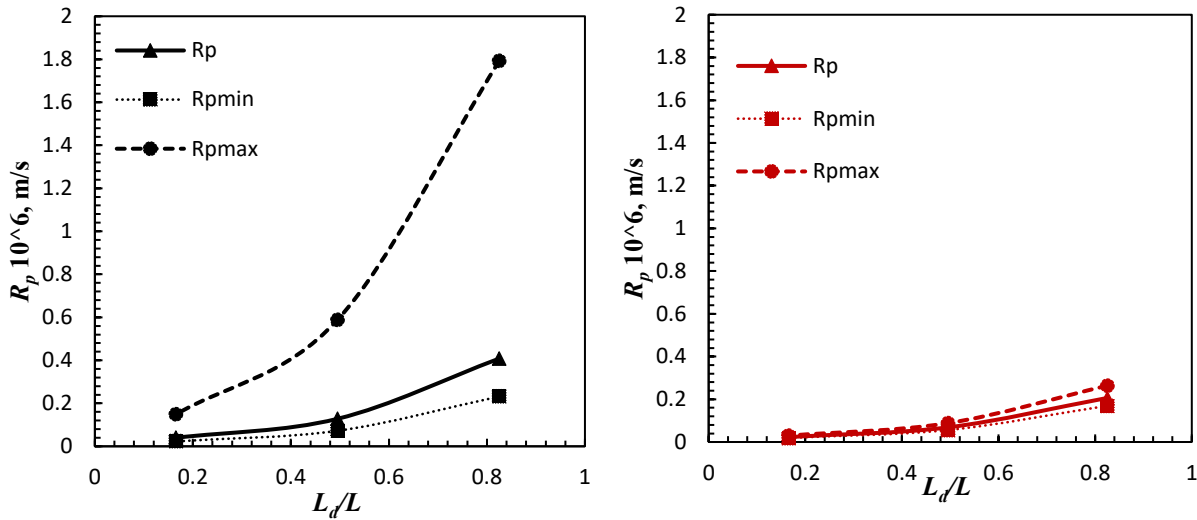


**Figure 2.19** Comparison of the intra-variability of  $R_p$  in case of variable  $D_p$  along the thickness. Figure on the left reports the profile for a non-suspended vial nucleated at  $-15^\circ\text{C}$ , while on the right the profile corresponds to a suspended vial nucleated at  $-14.5^\circ\text{C}$ .

In Figure 2.20 the profiles of  $R_p$  as function of  $T_n$  were plotted for both sample configuration. These figures confirmed what already found by the morphology analysis as a function of the nucleation temperature. In fact, for non-suspended vials, the variability of  $R_p$  is higher and increased with the decrease of the nucleation temperature, because of the smaller dimension of the pores. For suspended vials the range of variability of  $R_p$  was smaller, and some profiles matched even if  $T_n$  changed.

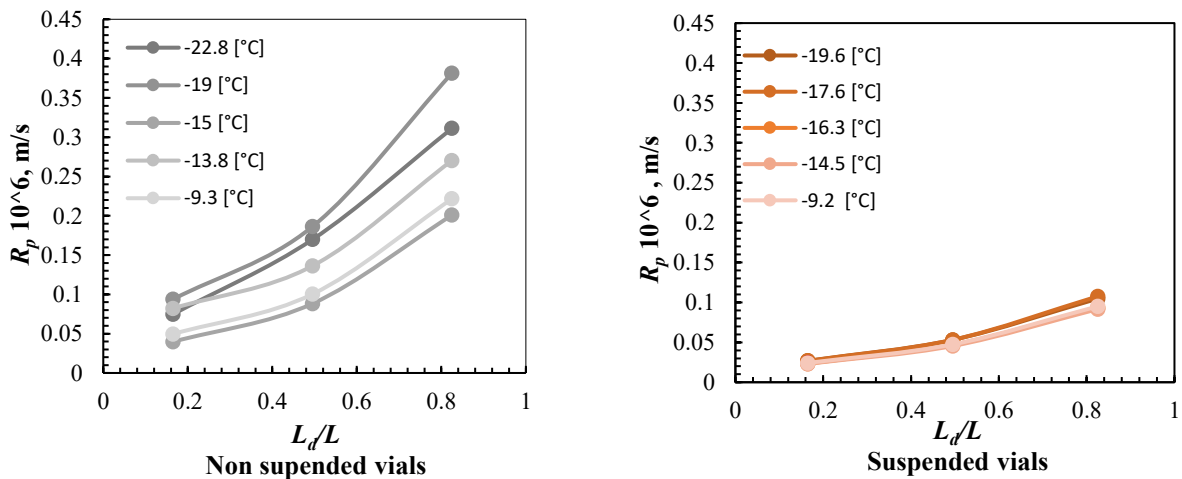


**Figure 2.20**  $R_p$  profile as a function of  $T_n$  for non-suspended vials (left) and suspended vials (right).

### 2.3.4. Characterization of Mannitol formulation

Four lyophilized samples with the non-suspended configuration and six ones with suspended configuration were analyzed with X-ray Powder Diffractometry (XRD) to carry out a qualitative determination of mannitol crystalline forms.

The spectra of these samples were compared with the references peaks  $\alpha, \beta, \delta$ , of mannitol showed in Figure 2.21.

In Figure 2.22 and 2.23, the spectra of suspended vials and non-suspended vials with the specific peaks of the three polymorphs of mannitol were reported.

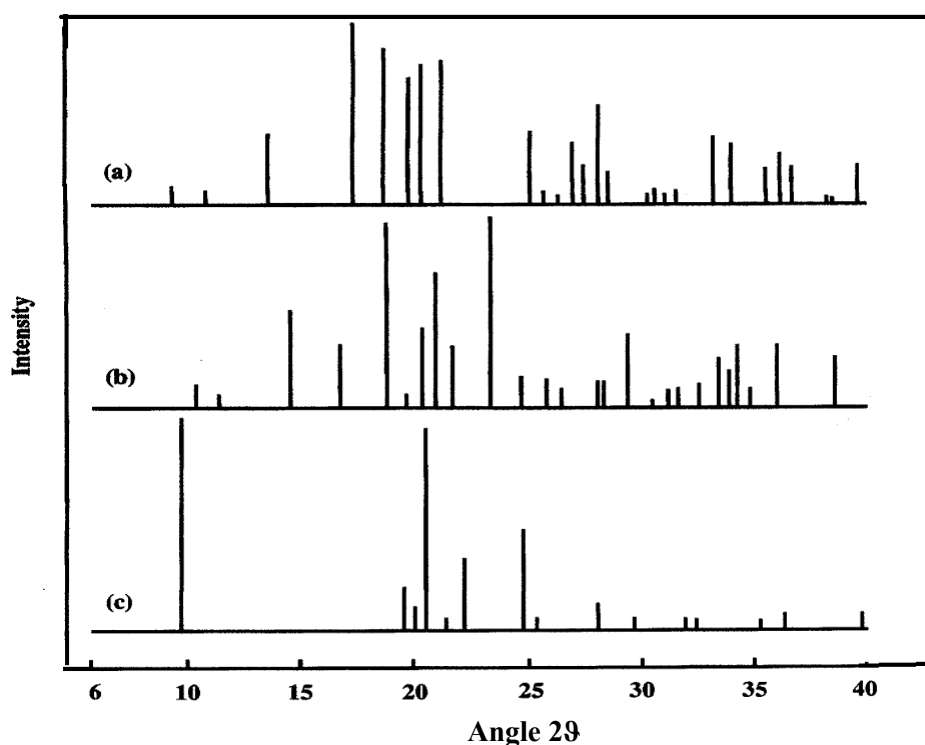


**Figure 2.21** X-ray diffraction patterns of polymorphic forms of mannitol; (a)  $\alpha$  form (b)  $\beta$  form, (c)  $\delta$  form. (From Yoshinari *et al.*, 2002 with modifications).

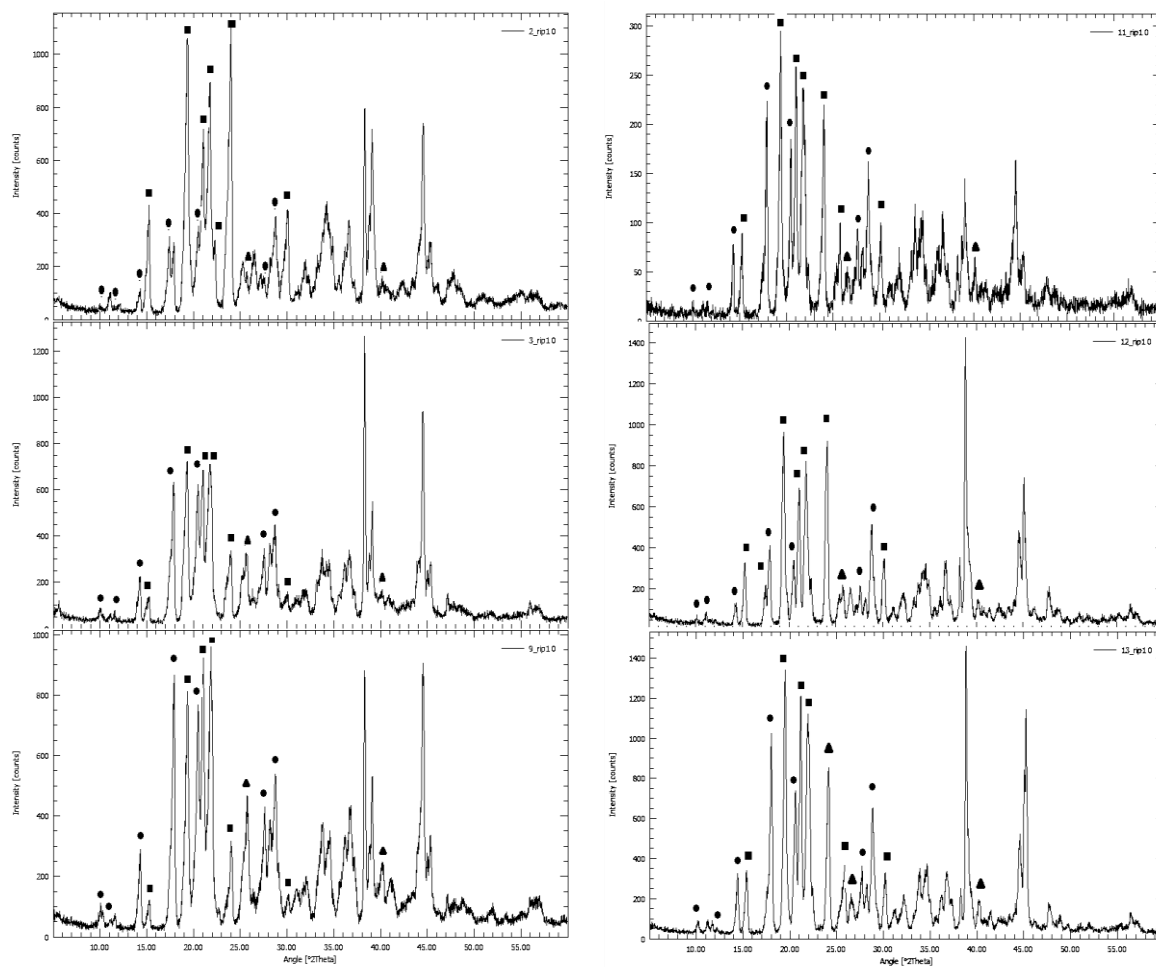


**Figure 2.22** X-ray diffraction spectra of six different product of suspended freeze-drying. ● indicates the  $\alpha$  peaks,▲ the  $\delta$  peaks, and ■ the  $\beta$  peaks. Peaks at 2theta of 38.30 and 44.54 correspond to Al.

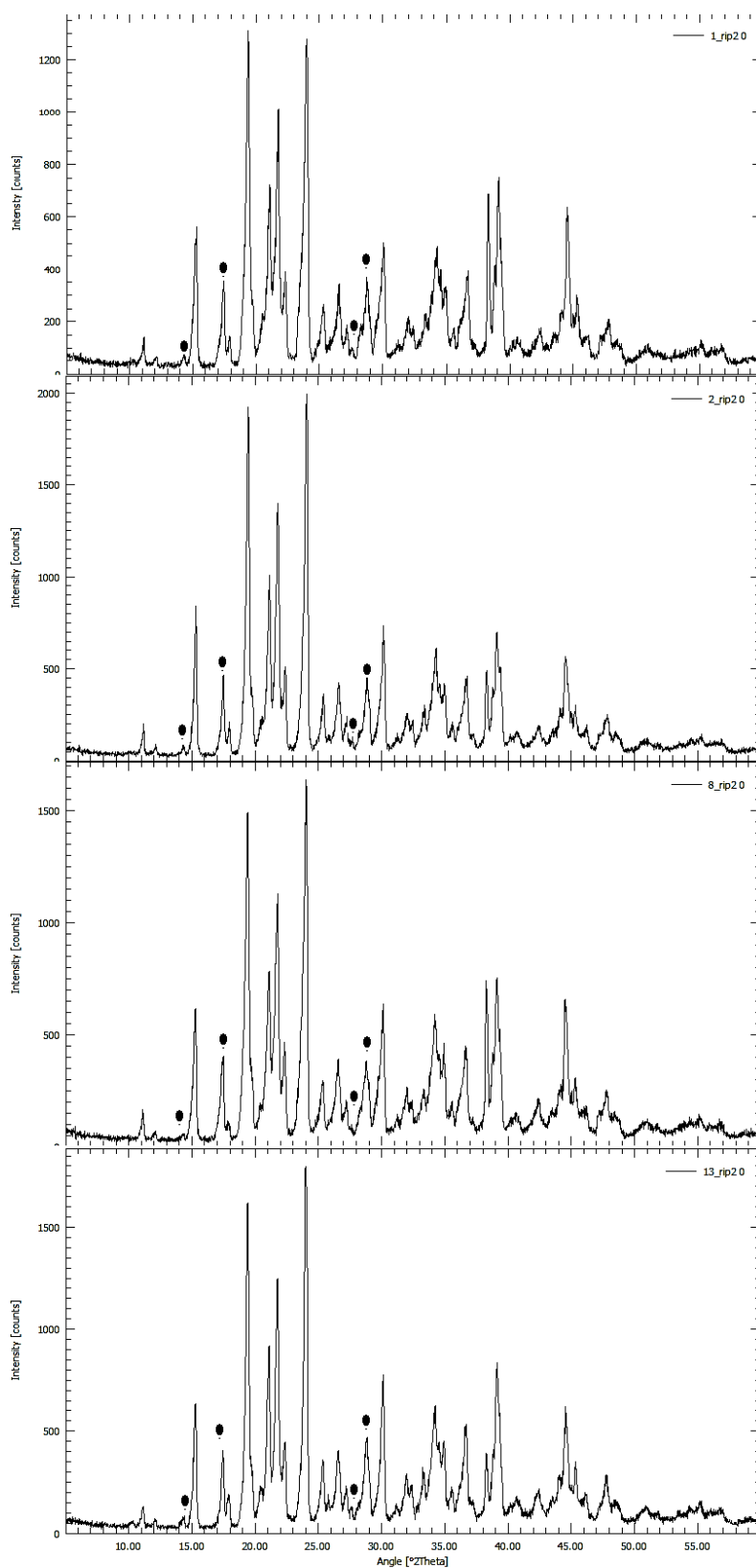


**Figure 2.23** X-ray diffraction spectra of four different product of non-suspended freeze-drying. ● indicates the  $\alpha$  peaks. The remaining peaks correspond to  $\beta$  polymorph of mannitol, except for peaks at 2theta of 38.30 and 44.54 that correspond to Al.

As shown in Figure 2.23, all non-suspended vials seemed to have similar spectra characterized by the prevalence of  $\beta$  polymorph with traces of  $\alpha$ . Instead, suspended vials spectra were more different from each other. Anyway, these latter were characterized by the presence of  $\beta$  and  $\alpha$  polymorphs with traces of  $\delta$ .

## 2.4. Conclusions

The study on the heterogeneity of the batch has revealed interesting results about the impact of the freezing methods and the cooling rates on the intra and inter-vial variability.

Suspended-vial freezing and shelf-ramped freezing were chosen as models, and the experiments were conducted with two different freezing recipes (HCR and LCR). In the first part of the experiments, the nucleation temperature distribution curves were determined. As first results, the suspended-vial freezing showed a narrower range of the nucleation temperature variation when the HCR protocol was applied, but working with the other protocol, the range was similar because the two methods showed very similar freezing rates. The variability of the nucleation temperature is an important factor because can determine the different dimension of ice crystals and, hence, can impact on the variability of the mass transfer resistance of vapor flow during the primary drying. Moreover, also the freezing methods itself can impact on the final structure of the dried samples according to the kind of the heat transfer mechanism that were prevalent during freezing.

After this part, the subsequent results only regarded the HCR protocol. A future work could be to repeat these experiments for the other protocol.

The most interesting result was found analyzing SEM images of some dried samples of the two vials configuration and correlating these images to the nucleation temperature that was known for every vial. Observing these images, it is immediate to see that non-suspended vials showed a big variability, not only in the cake of each vial, but also among vials. On the other hand, SEM images of suspended vials showed bigger and similar pores independently from the nucleation temperature and the depth of thickness of the dried cake. Moreover, exploiting the nucleation distribution curves and the value of the mean pore size linked to the nucleation temperature, it was possible to extrapolate a function to determine the mean pore size distribution curves.

Furthermore, the mass transfer resistance  $R_p$  and its variability were theoretically determined; the variability was found as a direct consequence of the inter-variability of the pore size represented by the standard deviations found with the Gaussian curves. The results showed that,  $R_p$  was lower for the suspended vials, and so the primary drying time was reduced with this configuration, also the inter-variability was smaller. These results were confirmed by the variability of  $R_p$  as a function of the nucleation temperature as illustrated in Figure 2.20.

At last, investigating the physical structures of some lyophilized products, it can be seen that, in the case of conventional freezing, X-ray diffraction spectra indicated similar crystalline forms principally characterized by the presence of the stable form of mannitol  $\beta$  with traces of  $\alpha$ , while a presence of the  $\alpha$  and  $\beta$  polymorphs with some traces of  $\delta$  polymorph were found in suspended vials.

This study, therefore, suggests that the suspended-vial freezing is in general preferable to the conventional freezing, since it allows to work with fast operating conditions reaching good product quality in terms of intra-vial and inter-vial homogeneity.

## List of symbols

$A$	Area of the vials section, $\text{m}^2$
$D_p$	Diameter of the pore
$\Delta H_s$	Heat of sublimation, $\text{J mol}^{-1}$
$\Delta t$	Duration of primary drying
$J_w$	Sublimation flow, $\text{Kg s}^{-1}\text{m}^{-2}$
$J_q$	Heat flux transferred to the product, $\text{W m}^{-2}$
$L$	Total product thickness, $\text{m}$
$L_d$	Dried product thickness, $\text{m}$
$m$	Mass of water molecule, $\text{kg}$
$M_w$	Molar mass of water, $\text{kg mol}^{-1}$
$P_0$	Equilibrium vapor pressure of ice, $\text{Pa}$
$P_c$	Total pressure in the drying chamber, $\text{Pa}$
$R_p$	Mass transfer resistance to vapor flow in the dried layer, $\text{m s}^{-1}$
$R_s$	Mass transfer resistance to vapor flow in the stopper, $\text{m s}^{-1}$
$R_c$	Mass transfer resistance to vapor flow from the drying chamber to the condenser, $\text{m s}^{-1}$
$R_t$	Global mass transfer resistance to vapor flow, $\text{m s}^{-1}$
$R$	Gas constant, $\text{J mol}^{-1}\text{K}^{-1}$
$T$	Absolute temperature, $\text{K}$
$T_n$	Temperature of nucleation, $\text{K}$

## Greek symbols

$\varepsilon$	Porosity of the dried layer
$\sigma$	Standard deviation

$\tau$  Tortuosity of the channel in the dried layer

## Subscripts

eq Equivalent value

max Maximum value

min Minimum value

## Abbreviations

CR Cooling Rate

HCR High Cooling Rate

LCR Low Cooling Rate

SEM Scanning Electronic Microscopy

XRD X-ray Powder Diffractometry

## References

Barresi A., Pisano R., Rasetto V., Fissore D., Marchisio D.L., 2010. "Model-Based Monitoring and Control of Industrial Freeze-Drying Processes: Effect of Batch Nonuniformity." *Drying Technology*, **28**(1):577–590.

Fissore D., Pisano R., Barresi A., 2010. "On the Methods Based on the Pressure Rise Test for Monitoring a Freeze-Drying Process." *Drying Technology*, **29**(1):73-90.

Fissore D., Pisano R., Barresi A., 2011. "Advanced Approach to Build the Design Space for the Primary Drying of a Pharmaceutical Freeze-Drying Process." *Journal of Pharmaceutical Sciences* **100**(11): 4922–33.

Kasper J. C. and Friess W., 2011. "The Freezing Step in Lyophilization: Physico-Chemical Fundamentals, Freezing Methods and Consequences on Process Performance and Quality Attributes of Biopharmaceuticals." *European Journal of Pharmaceutics and Biopharmaceutics*, **78**(2): 248–63.

Kim A.I., Akers M.J., Nail. S.L.,1998. "The Physical State of Mannitol after Freeze-Drying: Effects of Mannitol Concentration, Freezing Rate, and a Noncrystallizing Cosolute." *Journal of Pharmaceutical Sciences*,**87**(8):931–935.

Liu J., Viverette T., Virgin M., Anderson M., Paresh D., 2005. "A Study of the Impact of Freezing on the Lyophilization of a Concentrated Formulation with a High Fill Depth." *Pharmaceutical Development and Technology*, **10**(2): 261-72.

Patel, S.M., Doen T., Pikal M.J., 2010. "Determination of End Point of Primary Drying in Freeze-Drying Process Control." *PharmSciTech*, **11**(1):73-84.

Pikal, M.J., Roy M.L., Shah S. 1984. "Mass and Heat Transfer in Vial Freeze-Drying of Pharmaceuticals: Role of the Vial." *Journal of Pharmaceutical Science*, **73**(9):1224-1237.

Yoshinari T., Forbes R.T., York P., 2002. "Moisture induced polymorphic transition of mannitol and its morphological transformation." *International Journal of Pharmaceutics*, **247**(1): 69–77.

Rambhatla S., Ramot R., Bhugra C., Pikal M.J., 2004. "Heat and Mass Transfer Scale-up Issues during Freeze Drying: II. Control and Characterization of the Degree of Supercooling." *AAPS PharmSciTech*, **5**(4):1-9.

Trout, B., Pisano, R., Capozzi, L.C., 2017. "Continuous freeze-drying methods and related products", US Provisional Application No.: 62/500,466.

Wang, W., 2000. "Lyophilization and Development of Solid Protein Pharmaceuticals." *International Journal of Pharmaceutics*, **203**(1):1-60.



# Chapter 3

## 3. Impact of the freezing method on ADH activity recovery

### 3.1 Introduction

In this section alcohol dehydrogenase (ADH) was selected as a model protein to study the impact of the cooling rate, the freezing method, the nucleation temperature, the concentration and the formulation on the recovered activity of the protein after freeze-thawing and freeze-drying. For this purpose, several tests were performed using the equipment provided by the Department of Pharmaceutical Analysis at the University of Ghent.

Two freezing methods were chosen to evaluate the impact of the cooling rate on ADH: the shelf-ramped freezing with a cooling rate of 1 °C/min and 0.1 °C/min and the quench freezing in liquid nitrogen. ADH was tested with and without a protector. The protectants used in this work were PEG and sucrose. PEG is generally a good cryoprotectant, while sucrose is a lyoprotectant (Pikal,2004; Liu,2015). As the concentration of the protein influences the activity recovery, the solutions were prepared with two different final concentrations of the enzyme (0.1 mg/ml and 0.01 mg/ml). Moreover, the nucleation temperature was monitored during some trials to find if exists a correlation between the activity of the protein and the dimension of the ice crystals and, hence, of the pores of the dried cake.

### 3.2 Materials and methods

#### 3.2.1 Preparation of the solutions

According to the kind of the test, solutions with a concentration of 0.1 mg/mL of ADH were prepared (i) without additives, (ii) with 2.5 % (w/v) of PEG, and (iii) 2.5 % (w/v) of sucrose. Alcohol dehydrogenase from *Saccharomyces Cerevisiae* was provided by Sigma-Aldrich in lyophilized powder. The aqueous solutions were filtered with a filter of 1.2 µm before adding the enzyme to avoid the loss of some protein molecules. In case of a final concentration of 0.01 mg/ml the enzyme solutions were appropriately diluted with water (or with the placebo solution) to reach the desired value of concentration. The diluted enzyme solutions were transferred into glass vials of 10 ml, filling the samples with 3 ml of the solutions.

#### 3.2.2 Inactivation tests: freeze-thawing and freeze-drying of ADH solutions

The impact of the cooling rate on the activity of ADH, after freeze-thawing and freeze-drying, was evaluated following three freezing protocols. These freezing protocols are: shelf-ramped freezing with a cooling rate of (1) 0.1 °C/min and (2) 1°C/min, and quench freezing in liquid nitrogen for 90 seconds with and without a storage time of 15 hours at -55°C. Moreover, during some experiments, the nucleation temperature for each vial was estimated using the experimental procedure explained in Chapter 2. Figure 3.1 represents how the nucleation temperature was monitored with the use of a webcam. In Table 3.1 the freezing protocols for the freeze-thawing tests were summarized. After storage, the frozen samples were thawed by soaking in a water bath at 15°C.

**Table 3.1** Freezing protocols during freeze-thawing tests.

Cooling rate	0.1°C/min	1°C/min
<i>Stabilization</i>	20 °C for 30'	20°C for 30'
<i>Freezing</i>	From 20°C to -55°C in 12h30'	From 20°C to -55°C in 1h15'
<i>Storing</i>	-55 °C for 13h40'	-55°C for 13h40'

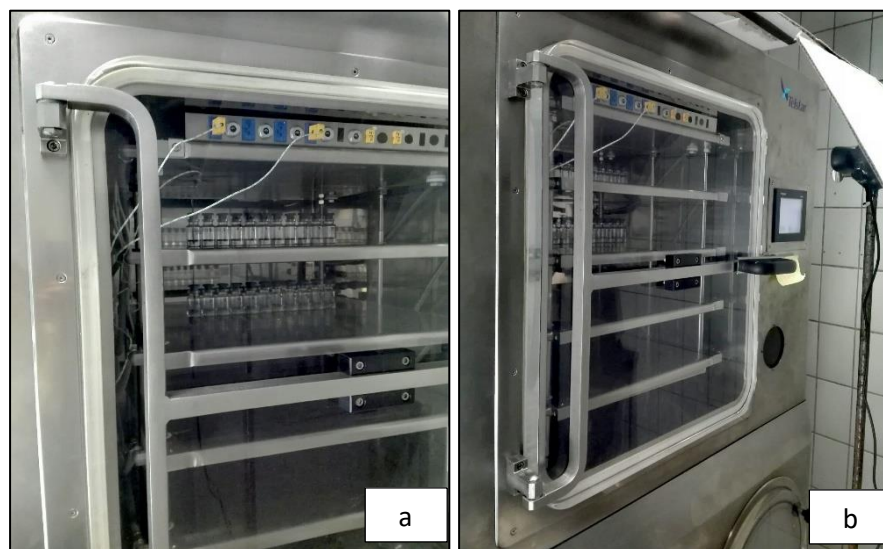


**Figure 3.1** Disposition of the vials and installation of two thermocouples to measure the temperature during freezing (a); disposition of the webcam to recover the nucleation step (b).

Table 3.2 reports the freeze-drying protocols. After freeze-drying, the vials were filled with 3 mL of pure water for the reconstitution in attempt to measure the residual activity of the protein.

**Table 3.2** Freeze-drying protocols

Cooling rate	0.1 °C/min	1°C/min	Quench
<i>Freezing</i>	From 3°C to -40°C in 7h 10'	From 3°C to -40°C in 43'	In liquid nitrogen for 1 min and 20s.
<i>Storing</i>	-40 °C for 1h	-40 °C for 7h 27'	-40 °C for 6h 45'
<i>Primary drying</i>	-32°C at 10 Pa for 42 h	-32°C at 10 Pa for 42 h	-32°C at 10 Pa for 42 h
<i>Secondary Drying</i>	From -32°C to 20°C in 9h	From -32°C to 20°C in 9h	From -32°C to 20°C in 9h
<i>Secondary Drying</i>	20 °C at 10 Pa for 12 h	20 °C at 10 Pa for 12 h	20 °C at 10 Pa for 12 h

To determine the impact of the nucleation temperature on the recovery activity after freeze-drying the formulation ADH 0.01 mg/ml with sucrose 2.5%w/v was selected to perform the experiments according to the protocols described in Table 3.3.

**Table 3.3** Freeze-drying protocols to determine the impact of  $T_n$  on the formulation ADH (0.01 mg/ml) + sucrose (2.5%w/v)

Cooling rate	0.1 °C/min	1°C/min
<i>Freezing</i>	From 20°C to -40°C in 1h	From 20°C to -40°C in 10h
<i>Storing</i>	-40 °C for 1h	-40 °C for 1h
<i>Primary drying</i>	-28°C at 10 Pa for 42 h	-28°C at 10 Pa for 38 h
<i>Secondary Drying</i>	From -28°C to 20°C in 8h	From -28°C to 20°C in 8h
<i>Secondary Drying</i>	20 °C at 10 Pa for 12 h	20 °C at 10 Pa for 12 h

### 3.2.3 Measurement of enzymatic recovered activity

The magnitude of the protein-stabilizing effects was determined as the relative enzyme activity that remained after freeze-thawing or freeze-drying to that before freezing as calculated in Eq.3.1.

$$\text{Recovered activity (\%)} = \left( 1 - \frac{\text{Activity } ADH_{ref.} - \text{Activity } ADH_{sample}}{\text{Activity } ADH_{ref.}} \right) * 100 \quad (3.1)$$

ADH activity was measured using the protocol provided by Sigma Aldrich with some modifications.

The assay was confirmed with some preliminary tests with which the activity of ADH without any protectants, with 2.5 % (w/v) of sucrose and with 2.5 % (w/v) of PEG were analyzed.

The protocol was based on the reduction of NAD by ethanol to NADH, which results in an increase in absorbance at 340 nm caused by the increase of the concentration of NADH.

Alcohol dehydrogenase (ADH) is an enzyme that oxidizes ethanol to aldehyde according to the following reaction. Hereby is  $\beta$ -nicotinamide adenine dinucleotide phosphate ( $NAD^+$ ) used as a co-substrate and converted to its reduced form NADH. One unit of ADH will convert 1  $\mu$ mol of ethanol to acetaldehyde per minute at pH 8.8 at 25 °C.



### 3.2.3.1 Test equipment positive control

#### *Preparation of the reaction mixture*

The reaction mixture consisted of 50 mM of sodium pyrophosphate (pH 8.8) 90  $\mu$ l, 35 % (v/v) ethanol 21  $\mu$ l, and 15 mM  $\beta$ -NAH solution 100  $\mu$ l which were inserted in a 96 well plate. The reaction was started by the addition of 18  $\mu$ l of properly cold diluted enzyme solution with a final concentration of 1.25  $\mu$ g/ml of ADH.

Enzyme diluent was prepared by dissolving 0.1 % (w/v) of bovine serum albumin (BSA) in 10 mM sodium phosphate buffer, pH 7.5.

To prepare sodium phosphate buffer with the final pH of 7.5, 10 mM of sodium phosphate, monobasic dihydrate and 10 mM of sodium phosphate dibasic were prepared. The pH of the dibasic solution was adjusted adding the monobasic solution to achieve the pH value of 7.5 (25  $^{\circ}$ C).

The measurements at the plate reader were conducted ensuring slight deviations of the temperature ( $\pm$  0.5 $^{\circ}$ C) from the set point fixed at 24 $^{\circ}$ C during the reaction.

#### *ADH formulations*

Three kinds of formulation were tested:

- 1) 0.1 mg/ml ADH in pure water
- 2) 0.1 mg/ml ADH + 2.5% (w/v) of sucrose
- 3) 0.1 mg/ml ADH + 2.5 % (w/v) of PEG

#### *Activity measure*

After the addition of enzyme preparation, the increase in absorbance at 340 nm was measured immediately by a spectrometer following the absorbance increase during the first 6 minutes and collecting data per 10 seconds.

The activity was calculated according to formula 3.2:

$$\frac{\text{Units}}{\text{ml enzyme}} = \frac{(\Delta A_{340} / \text{min Test} - \Delta A_{340} / \text{min Blank})}{6.22 * 0.018} * 0.229 * (df) \quad (3.2)$$

where 0.229 is the total volume (ml) of the assay,  $df$  is the dilution factor, 6.22 is the millimolar extinction coefficient of  $\beta$ -NADH at 340 nm, and 0.018 is the volume (ml) of Enzyme Solution used.

In order to normalize the values, the units per mg of solid protein were calculated as follows:

$$\frac{\text{Units}}{\text{mg solid}} = \frac{\text{units/ml enzyme}}{\text{mg solid/ml enzyme}} \quad (3.3)$$

where the mg solid/ml enzyme is the first prepared solution with a concentration approximatively of 0.1 mg/ml or 0.01mg/ml.

A blank solution was tested to evaluate the quality of the measurement. In this case, 18  $\mu$ l of 50 mM sodium pyrophosphate was added instead of ADH diluted solution. In this case, the absorbance did not increase during the time because the reaction did not occur.

## Results

As an example, the graphs relative to the absorbance measurement in case of ADH solution without any protectors were reported in Figure 3.2.

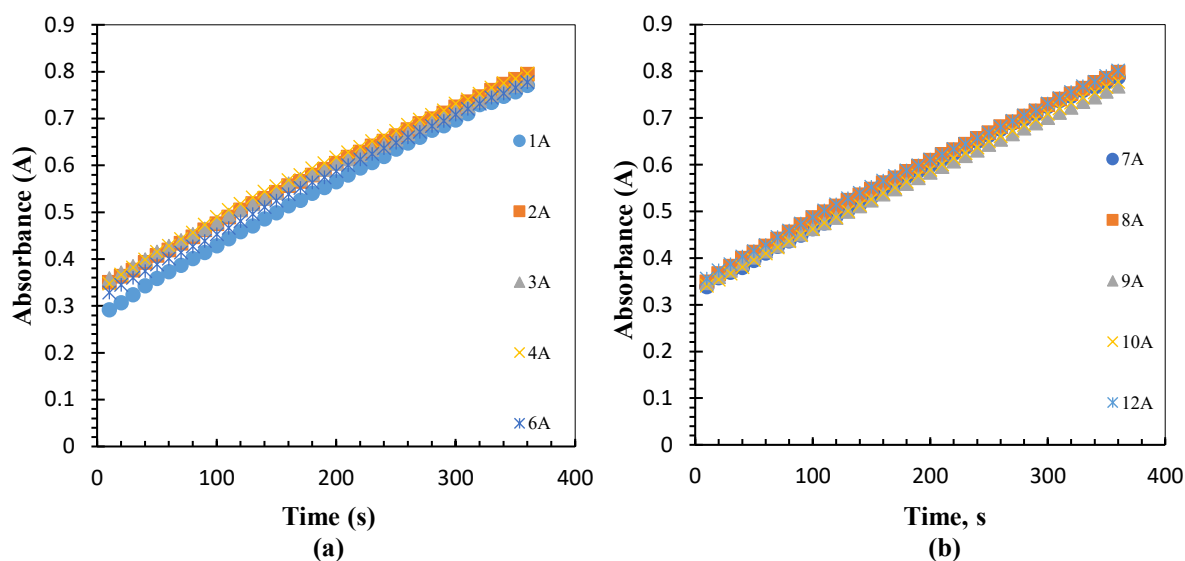


**Figure 3.2** Measure of absorbance at 340 nm during the first 6 minutes of reaction in case of ADH solution (0.1 mg/ml) without any protectants. Graph (a) shows the results of the first 6 columns of the 96 well plate row A, graph (b) shows the last 6 columns.

In Table 3.4 the units/mg of ADH activity for the three tested solutions with the respective standard deviations among the 12 values for each formulation are present.

**Table 3.4** ADH activity results for the test equipment positive control in case of 0.1 mg/ml of ADH without any protector, with 2.5% w/v of sucrose, with 2.5% w/v of PEG.

	ACTIVITY Units/mg solid	ST-DEV
ADH	124.29	3.98
ADH+SUCROSE	112.94	5.59
ADH+PEG	121.75	4.19

## 3.3 Results and discussions

### 3.3.1 After Freezing-thawing

Figure 3.3 shows the value of the activity of ADH after freeze-thawing as a function of the degree of supercooling with a cooling rate of 1°C/min. ADH was tested only in pure water without any additives and with a concentration of 0.1 mg/ml.

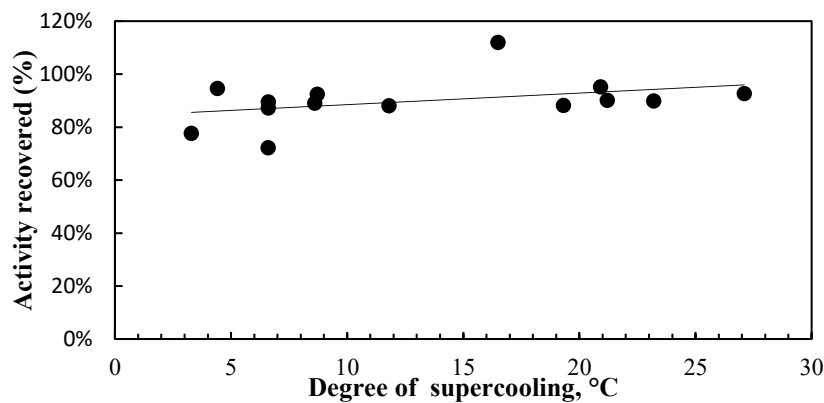


**Figure 3.3** Recovered Activity versus supercooling (°C) for cooling rate of 1°C/min after freeze-thawing of 0.1 mg/ml of ADH without protectors.

The mean value of the residual activity (%) of ADH after freeze-thawing amounted to  $90.6 \pm 2.6$ .

The protein seemed to maintain its activity after freeze-thawing without cryoprotectants. This is probably due to the fact that the partial unfolding of the protein is largely reversible upon freeze-thawing. In general, protein adsorption to the container surfaces or to the ice/freeze-concentrate interfacial area impacts on the changing of the secondary or tertiary protein structures (Pikal, 2004). The denaturation of the protein is largely reversible upon thawing as already confirmed in literature according to which ADH is a molecule freeze-tolerant (Racker, 1950 and Imamura et al. 2014).

In this case, there was not a correlation between the activity recovered after freeze-thawing and the degree of supercooling

Another test was conducted changing the cooling rate at 0.1°C/min and testing in the same batch two different concentrations: 0.1 mg/ml and 0.01 mg/ml of ADH prepared from the same solution, in order to analyze the effect of the concentration. The results were reported in Figure 3.4.

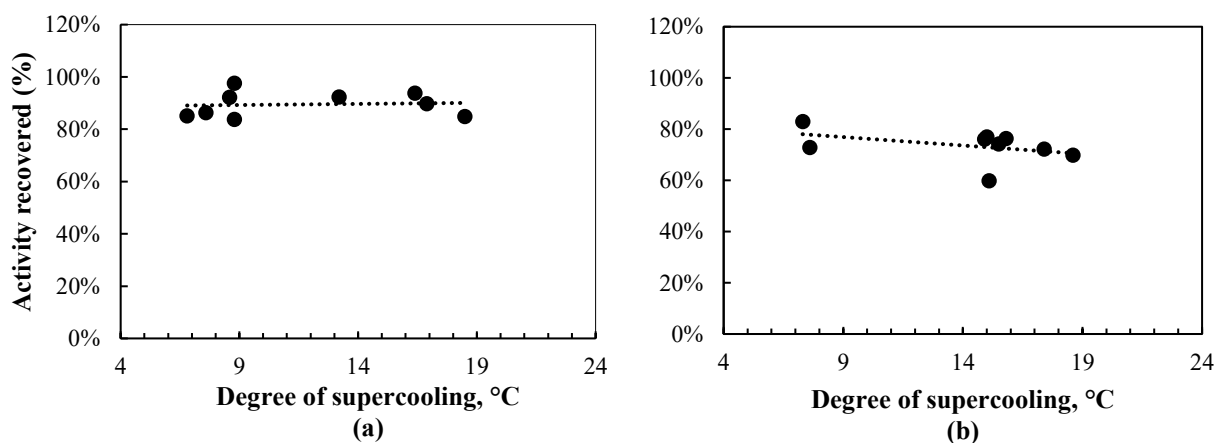


**Figure 3.4** Activity recovered versus supercooling (°C) for cooling rate of 0.1°C/min after freeze-thawing of 0.1 mg/ml of ADH without protectors (a) and 0.01 mg/ml of ADH (b).

Comparing the mean activity recovered after freeze-thawing at 0.1°C/min and 1°C/min with the highest concentration of the enzyme, the samples showed a similar value respectively of 89 % ( $\pm 5\%$ ) and 90%

( $\pm 3\%$ ), meaning that the formulation with a concentration of 0.1 mg/ml is not susceptible to freezing and thawing stresses in the range between 0.1 and 1 °C/min. But, decreasing the concentration, the mean recovered activity is lower with a value of 74% ( $\pm 6\%$ ). This result could demonstrate the fact that the protein itself preserves its activity if it is in higher concentration (Wang,200).

Moreover, it is possible to observe a slight decrease in activity with the increase of the degree of supercooling in presence of a lower amount of the protein. However, the slope of the line is really slight, and the number of the data is inconsistent to conclude that there was a correlation between the two parameters. In fact, it is more correct thinking that there is no correlation between nucleation temperature and the recovered activity after freeze-thawing for ADH formulations without protectants because of the absence of an interface. The repetition of the test with the cooling rate of 1°C/min confirmed our hypothesis, see in Figure 3.5.

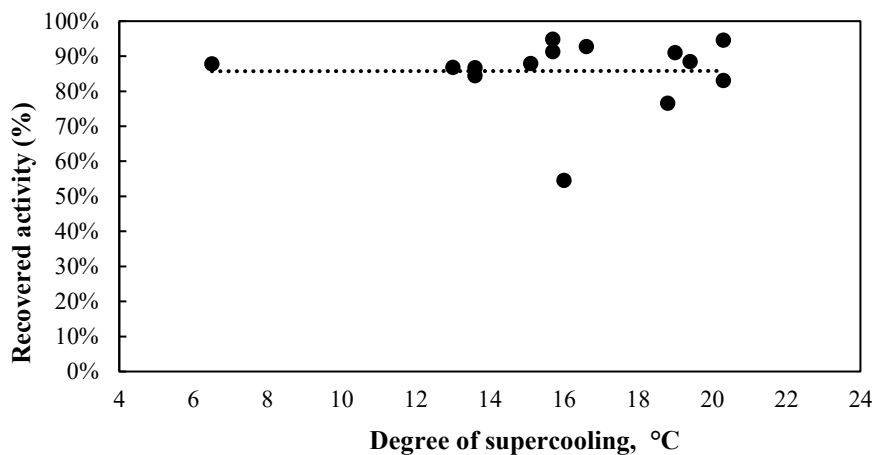


**Figure 3.5** Activity recovered versus supercooling (°C) for cooling rate of 1°C/min after freeze-thawing of 0.01 mg/ml of ADH.

Cao and his colleagues (Cao et.al,2002) also found that the activity recovery of ADH with a low concentration of 0.025 mg/ml in buffer solution at pH 7 was higher in the range of 0.1-1°C/min without showing any impact of the cooling rate, except if the cooling rate is higher than 20 °C/min since a decrease of activity occurred (see Figure 3.6).

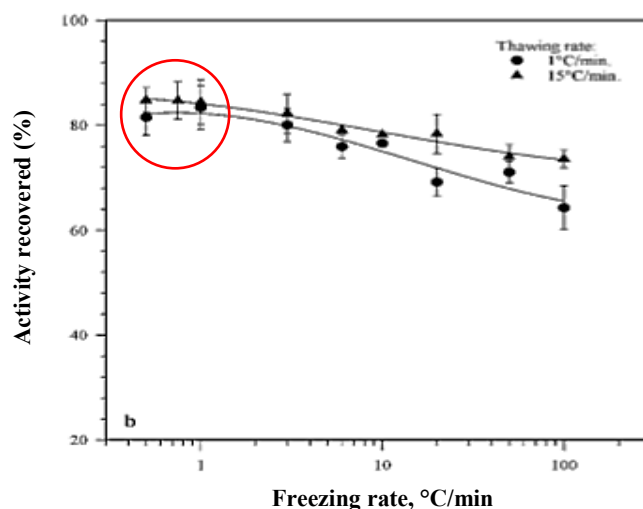


**Figure 3.6** Effect of cooling rate of activity recovery of ADH (potassium phosphate buffer, seeding temperature - 1°C, freezing to -30°C). (From Cao et. Al., 2002 with some modifications)

The effect of the interface was then investigated by including sucrose in the formulation with a concentration of ADH of 0.01 mg/ml and the results were reported in Figure 3.7.

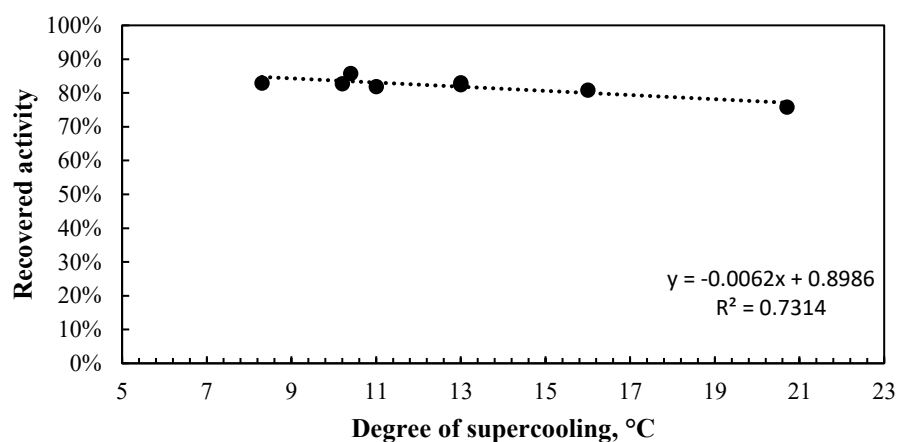


**Figure 3.7.** Activity recovered versus supercooling (°C) for cooling rate of 1°C/min after freeze-thawing of 0.01 mg/ml of ADH with 2.5%(w/v) of sucrose.

The activity recovered after freeze-thawing is high and a slight decrease is evident. The presence of sucrose creates interface of ice/ sugar molecules. The interaction between the sugar molecules interfaces and the protein can create hydrogen bonds that could probably impact on the reversibility of the denaturation after thawing. In this case, different nucleation temperature, and so, different specific surface, has an impact on recovery. Through a linear regression analysis, this data seemed to be statistically consistent, but it should be necessary repeat different times the trial to have a significant statistic result.

The same analysis was carry out by freezing the samples in liquid nitrogen and then thawing them. In order to evaluate the impact of storing at a cold temperature on the activity of ADH, some samples were immediately thawed in a bath water and other samples were stored at -55°C for 15 h before thawing.

As shown in table 3.5, the storage time after quench-freezing did not impact on the recovery activity of the enzyme. Anyway, the protein seemed to show a large resistance to the freezing stresses performed during quench freezing for both concentrations of 0.1 mg/ml and 0.01 mg/ml.

**Table 3.5** Recovery activity after quench freeze-thawing with and without storage at -55°C for 15 hours with 0.1 mg/ml of ADH without protectors.

Without Storage	Recovery Activity	St-Dev
Sample 1	87%	4%
Sample 2	79%	5%
Sample 3	80%	2%
Sample 4	79%	3%
<b>With Storage 15h</b>		
Sample 1	81%	3%

Sample 2	87%	4%
Sample 3	81%	6%
Sample 4	85%	3%
<b>Mean</b>	<b>82%</b>	
<b>St-Dev</b>	<b>3%</b>	

**Table 3.6** Recovery activity after quench freeze-thawing with 0.01 mg/ml of ADH without protectors.

Sample	Recovered activity (%)	St-Dev (%)
1	95%	3%
2	83%	7%
3	88%	2%
4	87%	4%
5	83%	4%
<b>Mean</b>	<b>87%</b>	
<b>St-Dev</b>	<b>4%</b>	

### 3.3.2. After Freeze-drying

Figure 3.8-3.11 show the effect of the formulation and the freezing method on the activity recovery after freeze-drying. In these tests, three samples for each formulation were freeze-dried and then analyzed at the plate-reader after reconstitution.

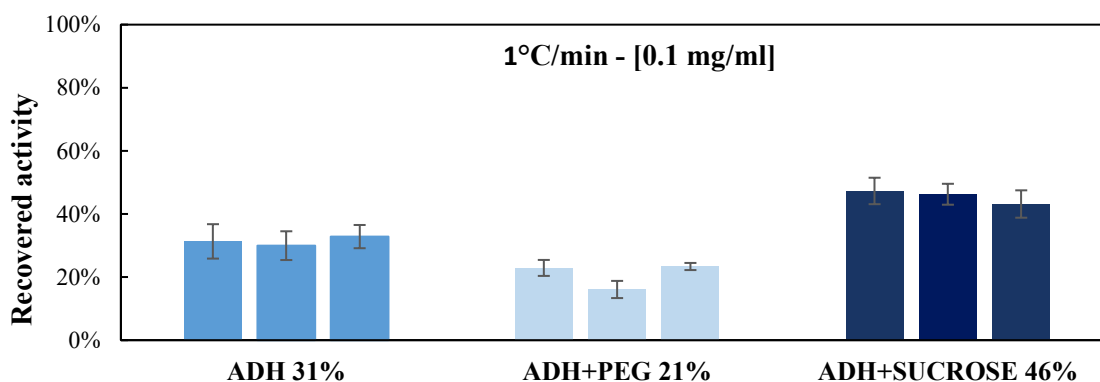


**Figure 3.9** Recovered activity of ADH after freeze-drying with a cooling rate of 1 °C/min and concentration of 0.1 mg/ml. On the x axis the mean value of the recovered activity is reported for all formulations.

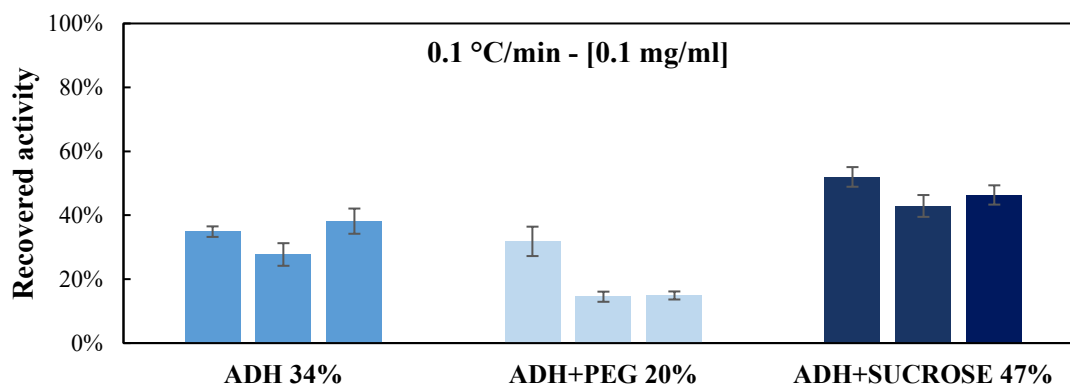


**Figure 3.8** Recovered activity of ADH after freeze-drying with a cooling rate of 0.1°C/min and concentration of ADH of 0.1 mg/ml. On the x axis the mean value of the recovered activity is reported for all formulations.

Observing these histograms, it is possible to conclude that ADH lost part of its activity during freeze-drying. Without any protectants, ADH approximately lost the 10÷20% of the activity during freezing and other 60% during drying.

In all cases, there is a loss, but sucrose seemed to be a better lyoprotectant for ADH than PEG. In fact, formulation with PEG showed a lower recovery activity than that found in ADH formulation without excipients. Probably, as it was observed with lactate dehydrogenase (LDH) and phosphofructokinase (PFK), PEG did not stabilize the dried enzyme because its crystallization during freeze-drying and its large size prevent the formation of hydrogen bonds to substitute water molecules during the dehydration (Carpenter et al., 1993, Izutsu et al., 1994).

In accordance with the results after thawing, also in this case, there is no correlation between activity recovery and cooling rate in the range of 0.1-1°C/min.

The same trend was reported in Figure 3.10 and 3.11 for the concentration of 0.01 mg/ml.

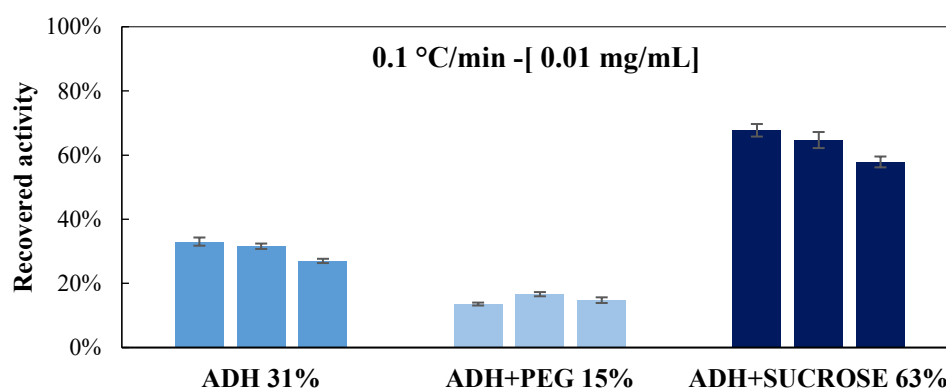


**Figure 3.10** Recovered activity of ADH after freeze-drying with a cooling rate of 1 °/min and concentration of 0.01 mg/ml. On the x-axis the mean value of the recovered activity is reported for all formulations.

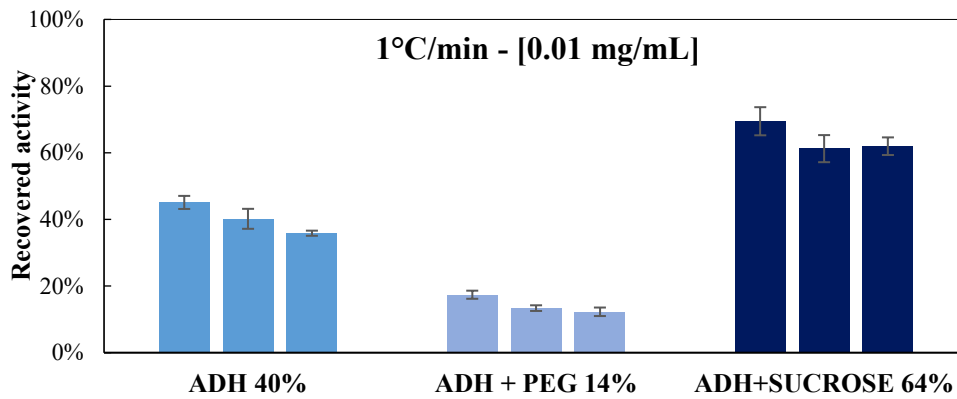


**Figure 3.11** Recovered activity of ADH after freeze-drying with a cooling rate of 0.1 °/min and concentration of 0.1 mg/ml. On the x-axis the mean value of the recovered activity is reported for all formulations.

In the case of freezing in liquid nitrogen before drying, it is possible to compare the effect of the concentration on the recovery activity after drying because the two concentrations with the respective three formulations were tested in the same experiments, starting from the same initial solution. In this case, it is possible to see how the impact of the formulation was always the same, but for a concentration of 0.1 mg/ml the recovered activity after the freeze-drying was higher than the case with the lower concentration.

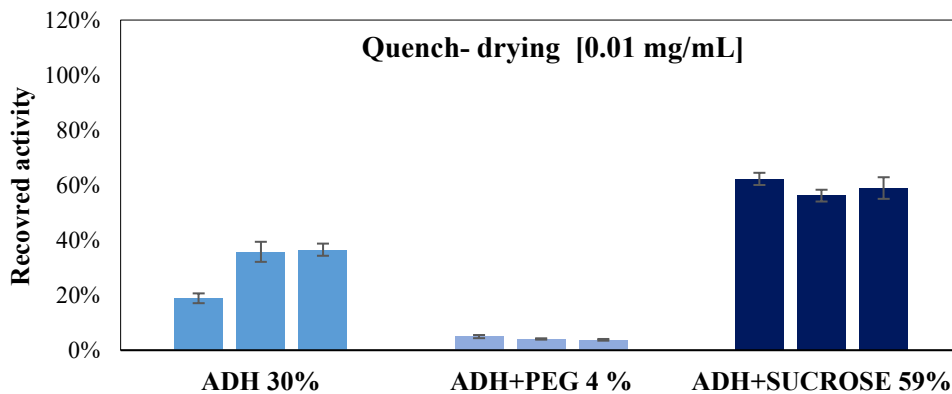


**Figure 3.12** Recovered activity of ADH for the three tested formulations after quench-drying with a concentration of 0.01 mg/ml. On the x-axis, the mean value of the recovered activity is reported for all formulations.

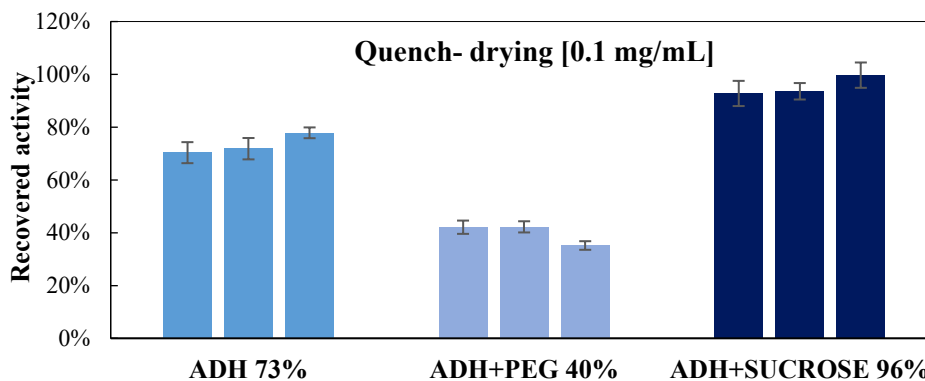


**Figure 3.13** Recovered activity of ADH for the three tested formulations after quench-drying with a concentration of 0.1 mg/ml. On the x-axis, the mean value of the recovered activity is reported for all formulations.

As for last experiments, the formulation with 0.01 mg/ml of ADH and 2.5%(v/w) of sucrose was chosen to conduct some freeze-drying tests to evaluate the impact of the nucleation temperature after drying as a function of the cooling rate. The connection between the nucleation temperature and the protein activity is correlated to the surface specific area (SSA) of the product that depends on morphology of ice crystals and, hence, it is a reflection of the supercooling phenomenon (Rambhatla *et.al*, 2004). In the case of 1°C/min, the results were represented in Figure 3.14, 3.15 and 3.16. According to these experimental results, the activity of the protein seemed to be influenced by the nucleation temperature, and by the cooling rate. The linear regression of the data demonstrated that this trend is statistically repeatable.

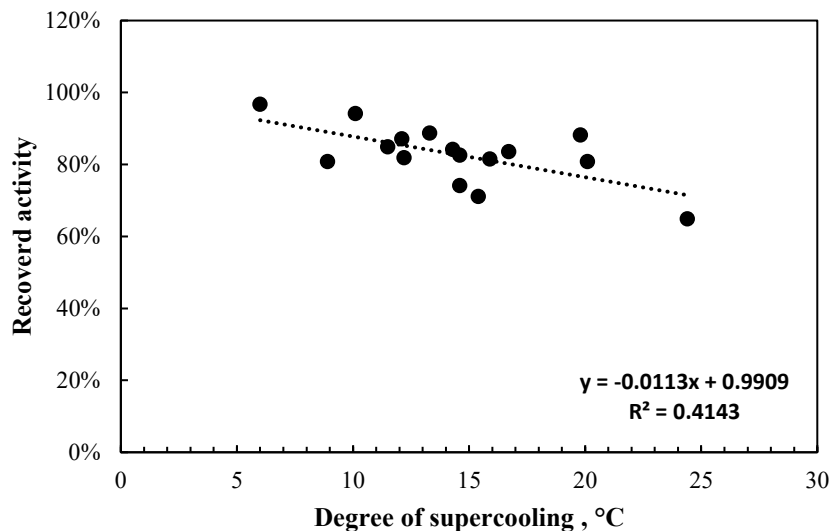


**Figure 3.14** Activity recovered versus supercooling (°C) for cooling rate of 1°C/min after freeze-drying of 0.01 mg/ml of ADH with sucrose 2.5%(w/v). Test 1.

The test was repeated another time to have a positive response to this result (Figure 3.15). In Figure 3.16 all samples were reported in the same graph. In the lower left, the two tests were separately reported with two different colors, while in the main graph the line red is the linear trend that counts all points.

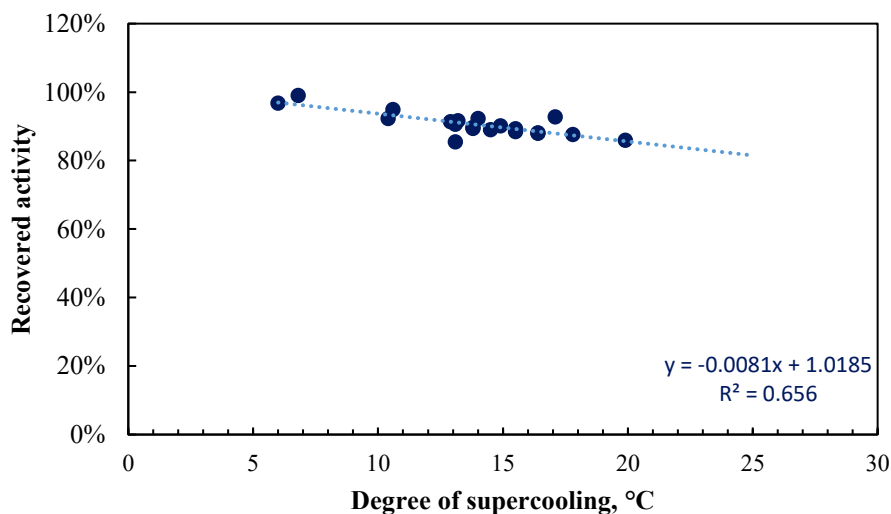


**Figure 3.15** Activity recovered versus supercooling (°C) for cooling rate of 1°C/min after freeze-drying of 0.01 mg/ml of ADH with 2.5%(w/v) of sucrose. Test 2.

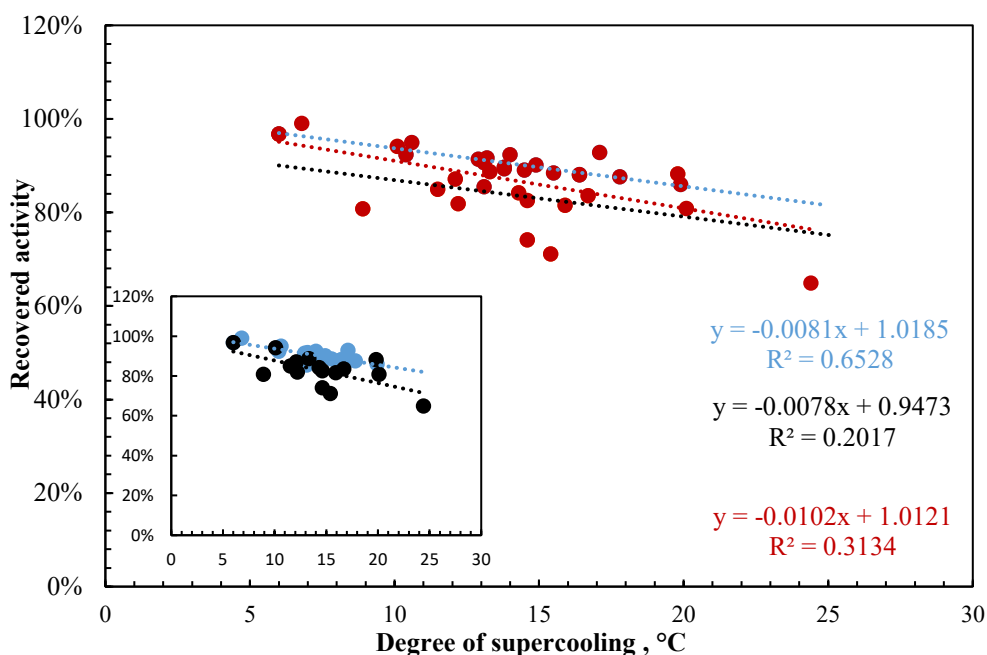


**Figure 3.16** Activity recovered versus supercooling ( $^{\circ}\text{C}$ ) for cooling rate of  $1^{\circ}\text{C}/\text{min}$  after freeze-drying of  $0.01\text{ mg/ml}$  of ADH with  $2.5\%(\text{w/v})$  of sucrose (Gathering data from Test1 and Test2). Test 1 and Test 2 are separately reported in black and blue, respectively.

The same formulation was tested during freeze-drying with the cooling rate of  $0.1^{\circ}\text{C}/\text{min}$ . It is possible to see in Figure 3.17 that with lower cooling rate there was not a trend. This is due to the fact that with low cooling rate samples of the same batch showed more uniformity in the structure of the pores as demonstrated in Chapter 2. Moreover, it could be due to a critic threshold of the pore size: if the pores are bigger than a critic dimension, ADH can preserve its activity. For this reason, the nucleation temperature had not an impact on the recovery activity of ADH for a cooling rate of  $0.1^{\circ}\text{C}/\text{min}$ . Nevertheless, the range of supercooling of this experiment is from  $9^{\circ}\text{C}$  to  $16^{\circ}\text{C}$  and it is lower than the case of  $1^{\circ}\text{C}/\text{min}$  (from  $6^{\circ}\text{C}$  to  $24^{\circ}\text{C}$ ) and the variability among the samples is unexpectedly bigger than the previous tests. Anyway, only an experiment was conducted with this protocol and it is not enough to find a result that is statistically significant.

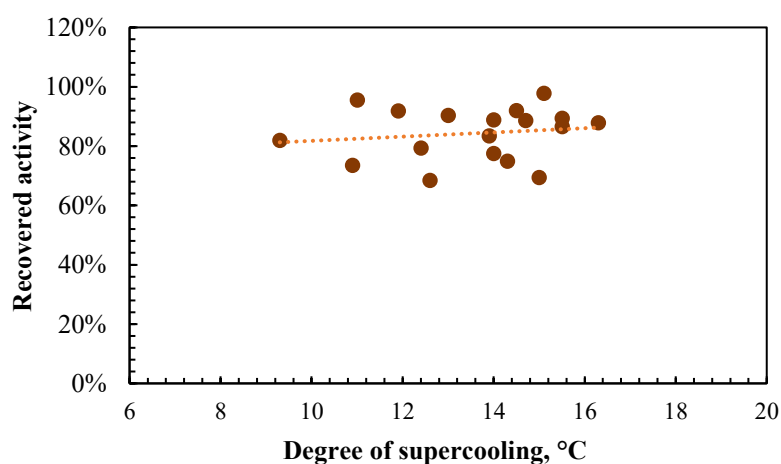


**Figure 3.17** Activity recovered versus supercooling ( $^{\circ}\text{C}$ ) for cooling rate of  $0.1^{\circ}\text{C}/\text{min}$  after freeze-drying of  $0.01\text{ mg/ml}$  of ADH sucrose  $2.5\%(\text{w/v})$ .

### 3.4. Conclusions

Before summarizing the results of this experimental work, it is important to take into account some observations about the experimental error. In fact, although the standard deviations were limited during the measurement of the activity of ADH at the plate reader, the protein (Tamiya et al., 1985) and the reagent NAD are sensitive in aqueous solution and the total duration of the activity test could impact in a relevant way on the results. For these reasons, the relevance of the trials is confined by the experiment of a specific batch and the results were reported and commented according to these devices. Moreover, also the operator error and the calibration and sensitivity of the laboratory equipment have to be included as error factors.

However, analyzing these results, it is possible to summarise some notes about the preservation of the alcohol dehydrogenase after freeze-thawing and freeze-drying.

By the first set of experiments, it is evident that ADH is freeze-tolerant because preserved almost its activity after freeze-thawing in absence of any kind of protection. Moreover, working with a higher concentration of protein is a better way to preserve more activity since protein itself is able to act as a stabilizer. Nevertheless, there was no impact of freezing methods and so, of cooling rate and nucleation temperature during freeze-thawing. Since ADH did not suffer from ice interaction, the dimension of ice crystal, as consequence of the freezing method and the cooling rate, was not a cause of the deactivation of the protein. This behavior was probably due to the absence of an interface that could irreversibly compromise the denaturation of the protein. In fact, the denaturation of the protein is reversible after thawing, confirming some published studies about ADH.

Contrary to the study of Cao et al., according to which the use of a freezing rate higher than 20°C/min could decrease the activity of ADH in water solution without additives, in this thesis work the quench freezing (that means higher cooling rate) did not show any difference in the recovery of activity from the previous freezing method. Future works could carry on these studies analyzing the effect of another freezing method, as for example the spin freezing, that works with high values of cooling rate.

In relation to the formulation, three formulations were tested after freeze-drying. It was discovered that PEG was not able to protect ADH during drying. In fact, the recovered activity is lower than the case with ADH alone. Instead, there is a good recovery if in the formulation the sucrose is included in accordance with what Shimizu and his colleagues recently found (Shimizu et al., 2017).

In order to stabilize if there is a correlation between nucleation temperature and the enzymatic activity, some tests with freeze-drying were conducted only working with the ADH + sucrose formulation. The nucleation temperature could impact on the protein activity since  $T_n$  is correlated to the SSA of the dried product and, hence, the protein could lose its activity if the sample is characterized by a lower nucleation temperature because of the increase of SSA. The formulation with the lower concentration of enzyme was selected because the protein seems to be more sensitive in lower concentrations and sucrose was chosen as protectant because promoted the recovery of the activity but, at the same time, it influenced the activity for the presence of an interface during drying. In fact, it was found that after drying, working with 1°C/min there was a decrease in activity with the decrease of nucleation temperature. This kind of results was found with other proteins as LDH (Cochran and Nail, 2009) and recently confirmed by Fang *et al.*, (2017).

Instead, for 0.1°C/min the nucleation temperature seemed to not impact the activity because of the more uniformity of the cake structure and the bigger dimension of pores.

Because of the stochastic nature of the nucleation temperature, and the several reasons of uncertainty during these tests, these results are to be taken into account, but they are only preliminary, and it would be good to repeat several times these experiments to confirm these behaviors.

## Abbreviations

ADH	Alcohol Dehydrogenase
LDH	Lactate Dehydrogenase
PFK	Phosphofructokinase
<i>df</i>	dilution factor

## References

- Cao E., Chen Y., Cui Z., Foster P.R., 2003. "Effect of Freezing and Thawing Rates on Denaturation of Proteins in Aqueous Solutions." *Biotechnology and Bioengineering*, **82** (6): 684-690.
- Carpenter J.F., Prestrelski S.J., Arakawa T., 1993. "Separation of Freezing-and Drying-Induced Denaturation of Lyophilized Proteins Using Stress-Specific Stabilization: I. Enzyme Activity and Calorimetric Studies." *Archives of Biochemistry and Biophysics*, **303**(2): 456-64.
- Cochran T. and Nail S.L., 2009. "Ice Nucleation Temperature Influences Recovery of Activity of a Model Protein after Freeze Drying." *Journal of pharmaceutical sciences*, **98**(9): 3495-3498.
- Fang R., Tanaka K., Mudhivarthi V., Bogner R.H., Pikal M.J., 2017. "Effect of Controlled Ice Nucleation on Stability of Lactate Dehydrogenase during Freeze-Drying." *Journal of Pharmaceutical Sciences*, **107**(3):824-830.
- Imamura K., Murai K., Korehisa T., Shimizu N., Yamahira R., Matsuura T., Tada H., Imanaka H., Ishida N., Nakanishi K., 2014. "Characteristics of Sugar Surfactants in Stabilizing Proteins During Freeze-Thawing and Freeze-Drying." *Journal of pharmaceutical sciences*, **103**(6): 1628-37.
- Izutsu k., Yoshioka S., Terao T., 1994. "Stabilizing Effect of Amphiphilic Excipients on the Freeze-thawing and Freeze-drying of Lactate Dehydrogenase." *Biotechnology and bioengineering*, **43**(11): 1102-7.
- Liu J. and Zhou X., 2015. "Freeze-Drying of Proteins", in *Cryopreservation and Freeze-Drying Protocols, Methods in Molecular Biology*, Wolkers W.F. and Oldenhof H., New York, USA.
- Tamiya T., Nobuo O., Ryoza S., Toshifumi A., Takayuki A., Juichiro M.J. 1985. "Freeze Denaturation of Enzymes and Its Prevention with Additives." *Cryobiology* **22**(1): 446-56.
- Pikal M.J., 2004. "Mechanisms of Protein Stabilization During Freeze-Drying and Storage: The Relative Importance of Thermodynamic Stabilization and Glassy State Relaxation Dynamics.", in *Freeze Drying / Lyophilization of Pharmaceutical and Biological Products*, Marcel Dekker Inc., New York, USA
- Racker, E. "Crystalline Alcohol Dehydrogenase from Bakers'Yeast." 1950. *Journal of Bioogical Chemistry*, **184**(1):313-320.

Shimizu T., Korehisa T., Imanaka H., Ishida N., 2017. "Characteristics of Proteinaceous Additives in Stabilizing Enzymes during Freeze-Thawing and - Drying." *Bioscience, Biotechnology, and Biochemistry* **81**(4): 687-697.

# Chapter 4

## 4. Impact of freezing on cycle design: optimization via dynamic Design Space.

### 4.1. Introduction

As primary drying is the longest step of the lyophilization process, the optimization of the total cycle is often focused on the reduction of primary drying time but without compromising the product qualities. Adapting the process parameters, shelf temperature  $T_s$  and chamber pressure  $P_c$ , in a dynamic way during primary drying, it is possible to optimize the freeze-drying cycle (Giordano *et al.*, 2011; Pisano *et al.*, 2013).

The implementation of a dynamic profile of  $T_s$  and  $P_c$  is necessary since some parameters change during primary drying. For instance, the thickness of the dried product layer,  $L_d$ , increases during primary drying, producing an increase of the mass transfer resistance  $R_p$ . Therefore, the heat transfer from the shelf to the product should be gradually lowered to avoid an increase in the sublimation front,  $T_i$ , that has to be maintained below the product collapse temperature  $T_c$ . The reduction of the heat transfer can be achieved changing  $P_c$  and  $T_s$  during primary drying, allowing to run the process in lower time comparing to a conservative cycle with fixed settings (Mortier *et al.*, 2016).

With this purpose, a mechanistic primary drying model, developed at Ghent University (Mortier *et al.*, 2016), was used to determine the dynamic Design Space. A definition of the Design Space is present in ICH Q8 Pharmaceutical Development Guideline; in few words, it shows the interaction between the input parameters and the process parameters and it configures the cycle in attempt to run the step as time efficient as possible, hereby respecting some limitations due to the equipment power, the sublimation efficiency and the specific Critical Quality Attributes (CQAs) for the dried product, such as the dried cake appearance.

Moreover, the model includes the uncertainty of some input variables and other parameters, and realizes computational calculations as a function of the Risk of Failure (RoF), which is defined as the possibility that one or more vials collapse during primary drying (Van Bockstal *et al.*, 2017). The uncertainty of the input parameters is included in the model formulation to take into account that some of them change from vial to vial.

Among the factors characterized by the uncertainty and considered in the model (i.e. the heat and mass transfer coefficients, the thickness of the dried layer, the geometric parameters of the vials, the filling volume, and the deviations of  $T_s$  and  $P_c$ ), a special attention was given to the determination of the uncertainty for the mass transfer resistance  $R_p$ , because it is directly correlated to the morphology of the dried samples, thus, to the freezing method and the cooling rate. So, a mechanistic model, developed by Capozzi and Pisano, (2017), that correlates the influence of freezing on  $R_p$ , was used to determine this parameter and its variability.

Furthermore, also the formulation impacts on the choice of the setting parameters. In fact, during primary drying the product temperature at the sublimation front,  $T_i$ , has to be kept below the collapse temperature,  $T_c$ , that is specific for each formulation.

So, two case studies were developed considering different case of Risk of Failure (1%, 50%, 99%). In the first case, mannitol (4 %w/v) and sucrose (1 %w/v) solution in buffer salt was chosen as model-

solution in order to detect the role of the uncertainties and the role of the cooling rate on the optimization of the cycle via the dynamic Design Space. In the second case, a second formulation, studied in Chapter 3, and that contains alcohol dehydrogenase and sucrose as protectant, was chosen to validate the predictions of the model for different RoFs.

## 4.2. Material and Methods

### 4.2.1. Preparation of the solutions and freezing protocols

Two solutions were chosen: 1% (w/v) of sucrose, 4% (w/v) of mannitol in 0.05 M of buffer sodium phosphate (pH 7.4) as first solution, and 2.5 % (w/v) of sucrose, 0.01 mg/ml of alcohol dehydrogenase (ADH) as second solution.

The buffer was prepared mixing 1,65 g of dibasic sodium phosphate ( $\text{Na}_2\text{HPO}_4$ ) and 0.53 g of monobasic sodium phosphate dihydrate ( $\text{NaH}_2\text{PO}_4 \cdot 2 \text{H}_2\text{O}$ ) in 300 ml of water for injection to obtain a 0.05 M of aqueous solution. This buffer solution was used to prepare the final formulation adding mannitol and sucrose. Then, the pH was measured to verify that the target 7.4 was not changed. The solution was filtered with a 0.2  $\mu\text{m}$  filter.

The second solution was filtered before adding the enzyme.

For the validation of the model, each test was performed in the freeze-dryer (LyoBeta 25, Tesla, Spain) with a total of 100 glass vials filled with 3 ml of the studied formulation and placed directly on the shelf using a square arrangement.

For the validation of the second case study, only 10 vials contained the protein. Two vials, one at the edge and one at the centre of the square arrangement, contained the thermocouples to monitor the product temperature; the other 8 vials were casually positioned in the square. This adjustment did not influence the validation of the tests because the low presence of the protein does not impact on the thermal properties of the formulation.

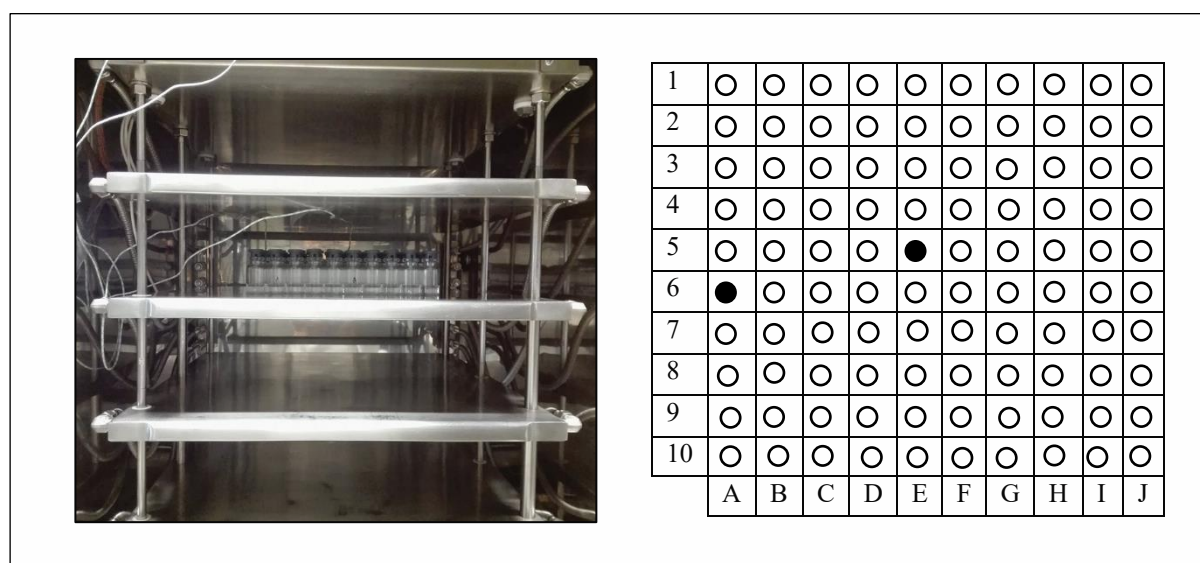


**Figure 4.1** On the left, disposition of 100 vials using a square arrangement (10x10). On the right, the scheme reports in black, the position of the thermocouples to monitor the product temperature for the outer (6-A) and the inner (5-E) vial.

In Table 4.1 the freezing protocols for both case studies were reported. In the first case, two freezing protocols were analyzed: high cooling rate (HCR) and low cooling rate (LCR); with the second formulation it was worked with a fixed rate of 1°C/min during freezing.

**Table 4.1** Freezing protocols during the validation cycles of the dynamic Design Space

	<b>1<sup>st</sup> case study 1°C/min -HCR</b>	<b>1<sup>st</sup> case study 0.1°C/min -LCR</b>	<b>2<sup>nd</sup> case study 1°C/min</b>
<i>Freezing</i>	From 20°C until -55°C in 1h15'	From 20°C until -55°C in 12h30'	From 20°C until -40°C in 1h
<i>Storing</i>	-55°C for 1h	-55°C for 1h	-55°C for 1h

#### 4.2.2. Measure of the critical temperature ( $T_{cr}$ )

In order to avoid the collapse, to have fast reconstitution of the dried product, but also for aesthetic purposes, the product temperature at the sublimation front,  $T_i$ , should not exceed the collapse temperature,  $T_c$ , during primary drying (Koganti *et al.*, 2011).

In general, since the glass transition temperature,  $T_g'$ , is slightly lower than  $T_c$ ,  $T_g'$  was used as input parameter to indicate in the model the critical product temperature,  $T_{cr}$ , introducing, in this way, a safety margin.

For the first formulation, the mid-point collapse temperature ( $T_{c-50}$ ) was used as  $T_{cr}$ , taking the value from literature (Flores Brun, 2017). This temperature was calculated as the average between the onset of collapse temperature ( $T_{oc}$ ) and the full collapse temperature ( $T_{fc}$ ) measured using the Freeze-Drying Microscope “BX51”(FDM) at the Politecnico di Torino (Flores Brun, 2017).

Instead, the glass transition temperature,  $T_g'$ , was used as critical temperature for the second case study. It was measured using the Modulate Differential Scanning Calorimetry (MDSC) Q2000 (TA instruments, Zellik, Belgium) provided by Ghent University. The sample was initially cooled until -90°C and it was maintained at that temperature for 5 min; then, the temperature was increased until 0°C with a heating rate of 2°C/min. The experiment was carried out in triplicate. The  $T_g'$  value was determined by analysis of the thermograms with TA Instruments Universal Analysis 2000.

It is important to take into account the method used to measure the critical temperature. Indeed, as demonstrated by Pikal *et al.*, the collapse temperature observed in a product being freeze-dried in a vial should be 1-3°C higher than the collapse temperature measured by the Freeze-Drying Microscope. Moreover, the collapse temperature can depend on the measurement methodology, the variation of the sublimation rate, and the variation of the surface area of the dried product (Pikal *et al.*, 1990).

Also Flores Brun, in her recent work, confirmed that  $T_{c-50}$ , originated by FDM analysis, was always higher than  $T_g'$  measured via DSC.

So, especially in the second case study, in which the measurement of the critical temperature was determined via the thermal analysis, the process conditions were very conservative. Whereas if the process is well optimized, an increase of 1°C in the product temperature could result in at least a 13% reduction in primary drying time (Pikal, 1985).

#### 4.2.3. Model formulation for primary drying

The mechanistic primary drying model is based on mass and energy equations which approximatively describe the sublimation process during primary drying. As mentioned before, the model is constructed

verifying that the product temperature at the sublimation front,  $T_i$ , is always lower than the critical product temperature  $T_{cr}$  (input parameter of the model) during the entire primary drying and modeling the process parameters  $P_c$  and  $T_s$  to have a maximum sublimation efficiency (optimization of the cycle). Moreover, the model checks during the simulation that the “choked flow” phenomenon is not present (Van Bockstal et al., 2017).

The model is based on some simplifications: it considers that the sublimation front is planar, and that the transferred energy was only used for ice sublimation, thus, the system is in a steady-state. Also, the computational load is confined by a limited calculation grid for  $P_c$  and  $T_s$ . The limits for  $P_c$  were set at 10 Pa and 14 Pa, while the range for  $T_s$  changes during the process as a function of the maximum temperature ramp of 1°C/min that the freeze-dryer can support (Van Bockstal et al., 2017). In this way, the calculation time is reduced.

The model calculates the evolution of the thickness of the dried layer  $L_d$  as a function of the time for a set of input parameters. The following series of equations were used to calculate the temperature at the sublimation front  $T_i$  (K) and the difference of temperature through the ice layer  $\Delta T$  (Mortier *et. al*, 2016).

$$e^{9.550426 - \frac{5723.256}{T_i} + 3.53068 \ln(T_i) - 0.00728332 T_i} = - \frac{(-A_p \Delta H_{sub} P_c - A_v K_v R_p M T_i + A_v K_v R_p M \Delta T)}{A_p \Delta H_{sub}} \quad (4.1)$$

$$\Delta T = \frac{889200 \frac{(L_T - L_d)(P_i - P_c)}{R_p} - 0.0102(L_T - L_d)(T_s - T_i)}{1 - 0.0102(L_T - L_d)} \quad (4.2)$$

Where  $A_p$  and  $A_v$  are the product and the vial area (m<sup>2</sup>),  $\Delta H_{sub}$  is the latent sublimation heat of ice (J/mol),  $P_i$  the water vapour partial pressure at the sublimation interface (Pa),  $P_c$  the chamber pressure (Pa),  $K_v$  the vial heat transfer coefficient (W/m<sup>2</sup> K),  $M$  the molecular weight of water (Kg/mol),  $T_s$  the shelf temperature,  $R_p$  the dried product resistance (m/s), and  $L_T$  the total thickness of the product layer (m).

For each time step  $\Delta t$ , the model calculates the sublimation rate  $\dot{m}_{sub}$  (kg/s) as:

$$\dot{m}_{sub,t+1} = \dot{m}_{sub,t} + \dot{m}_{sub} \Delta t \quad (4.3)$$

Where the sublimation rate is calculated following this equation:

$$\dot{m}_{sub} = A_p \frac{(P_t - P_c)}{R_p} \quad (4.4)$$

Moreover, the evolution of the thickness of the dried layer is given by:

$$L_d = \frac{\dot{m}_{sub}}{\rho_{ice} \xi A_p} \quad (4.5)$$

With  $m_{sub}$  the mass of ice removed by sublimation (kg),  $\rho_{ice}$  the density of ice (kg/m<sup>3</sup>) and  $\xi$  the volume fraction of ice.

If the uncertainties are not included as input parameters, the model calculates the shelf temperature and the chamber pressure profiles as follows. At each time step, a grid ( $T_s$ - $P_c$ ) is created. For each grid point, that means for each combination of  $T_s$  and  $P_c$ , the sublimation rate is calculated and the two limits conditions ( $T_i < T_{cr}$  and the choked flow criteria) are verified. If at least one of the two limit conditions is not verified, for that grid point, the sublimation rate is set equal to zero. In the end, the combination  $T_s$ - $P_c$  at which corresponded the maximum sublimation rate (optimization of the process) is selected. The simulation goes on with a new time step until  $L_d$  reaches  $L_T$ .

In Table 4.2 a resume of the values of the model parameters, used in this work, is shown.

**Table 4.2** Values of the model parameters used in the simulations.

Parameter		1 <sup>st</sup> case study CR 1°C/min	1 <sup>st</sup> case study CR 0.1 °C/min	2 <sup>nd</sup> case study	
Inner radius of 10Rvial	$r_{v,i}$	0.011	0.011	0.011	m
Outer radius of 10R vial	$r_{v,o}$	0.012	0.012	0.012	m
Radius of the vial neck	$r_{v,n}$	0.0063	0.0063	0.0063	m
Radius of the duct of the dryer	$r_d$	0.08	0.08	0.08	m
$K_v$ -coefficient	$\alpha$	11.18	11.18	11.18	J/(m <sup>2</sup> sK)
$K_v$ -coefficient	$\beta$	1.435	1.435	1.435	J/(m <sup>2</sup> sKPa)
$K_v$ -coefficient	$\gamma$	0.04088	0.04088	0.04088	1/Pa
$R_p$ -coefficient	$R_{p,o}$				m/s
$R_p$ -coefficient	$A_{Rp}$				1/s
$R_p$ -coefficient	$B_{Rp}$				1/m
Critical product temperature	$T_{cr}$	-34.8	-34.8	-35.2	°C
Filling volume	$V$	3	3	3	mL
Density of ice	$\rho_{ice}$	919.4	919.4	919.4	Kg/m <sup>3</sup>
Volume fractio of ice	$\xi$	0.97	0.97	0.97	-
Ratio of the specific heat of water	$k$	1.33	1.33	1.33	-
Molecular weight of water	$M$	0.018015	0.018015	0.018015	Kg/mol

#### 4.2.4. Uncertainty analysis

The model Uncertainty can arise from (Mortier et al., 2016):

- 1) The mechanistic model contains a degree of uncertainty because it is based on assumptions and simplifications of the reality.
- 2) The numerical errors included in the calculations.
- 3) The parameters used in the mechanistic model are often an estimation (literature-based or experimentally determined) and their uncertainty originated from various sources.

To evaluate the impact of the uncertainty on the determination of the Design Space, the model uses the ‘‘Sobol sampling technique’’ that creates a set of input variables and process parameters combinations,

which have a lower and upper limit or are characterized by a range of variability from the mean value. Then, the model estimates the uncertainty of the model predictions in term of Risk of Failure (RoF).

The uncertainty of 8 factors are included in the model and, as  $L_d$  is an output and input variable, the propagation of the error on the estimation of the thickness of the dried layer as a function of the primary drying time was included in the uncertainty analysis. Table 4.3 summarizes these 8 factors (Van Bockstal *et al.*, 2017).

**Table 4.3** Uncertainty level for the input variables on the uncertainty analysis.

Factor	Uncertainty level	Reason of inclusion in uncertainty level analysis
$L_d$	-	Error propagation
$R_p$	16-20%	Based on experimental data
$K_v$	5%	Based on experimental data (Van Bockstal <i>et.al</i> , 2017)
$r_{v,i}$	0.0001 m	Process variable with inherent error
$r_{v,o}$	0.0001 m	Process variable with inherent error
$T_s$	2.5-10°C	Based on experimental data (Van Bockstal <i>et. al</i> , 2017).
$P_c$	1 Pa	Process variable with inherent error (Van Bockstal <i>et. al</i> , 2017)
$V$	1%	Process variable with inherent error

For  $R_p$ ,  $K_v$  and  $V$  a relative uncertainty is defined. In this work, the uncertainty of  $R_p$  was determined (for the first case study) with the help of a mathematical model (Pisano and Capozzi, 2017).

For  $T_s$ ,  $P_c$ ,  $r_{v,i}$ ,  $r_{v,o}$  the uncertainty is defined as an absolute value. The supplier of 10R vials (Schott, Müllheim, Germany) provided the uncertainty on the inner ( $r_{v,i}$ ) and the outer ratio ( $r_{v,o}$ ). For  $T_s$  two levels of uncertainty are considered; if  $T_s$  is constant, the uncertainty level is 2.5°C, while if it changes with a ramp temperature, the uncertainty changes from 2.5 to 10°C due to the thermal inertia of the shelves. For  $P_c$ , the uncertainty arises from experiments conducted by Van Bockstal *et al.*, (2017).

#### 4.2.4.1. Determination of the Risk of Failure acceptance level

The 8 factors were varied together between their lower and upper limits obtaining 1000 different combinations. So, at each time step, and for each point of the grid  $T_s$ - $P_c$ , 1000 simulations were run obtaining 1000 different values for  $T_i$  (for that grid point). Then, the  $T_i$  values were ordered from the lower to the higher value and (for each grid point)  $T_i$  was fixed at the value corresponding to the “ $\alpha$  %” upper percentile (of the ordered distributions of the 1000  $T_i$  values). After this, the sublimation rate was calculated in each grid point and it was set to 0 if the limits ( $T_i < T_{cr}$  and/or the choked flow criteria) were not respected. Then, for each time step, the combination  $P_c$ - $T_s$  with the maximum sublimation rate was chosen (Mortier *et al.*, 2016).

In this way, there is a probability of  $1-\alpha$  that the true temperature overcomes the  $T_i$  calculated by the model, and the Risk of Failure associated is  $1-\alpha$  %.

For instance, if  $T_i$  is fixed to the 99% upper percentile, the Risk of Failure is 1%. At the opposite, 99% RoF corresponds to the choice of the 1% upper percentile of  $T_i$  (in each grid point).

According to this methodology, if the Risk of Failure acceptance level is higher (i.e. 99% RoF), the Design Space is less conservative, which means higher sublimation rate and shorter primary drying time. Instead, with a more conservative value of RoF, it is obvious that  $T_s$  and  $P_c$  are more conservative, and the process time increases. In Figure 4.2 the procedure of the uncertainty analysis is illustrated.

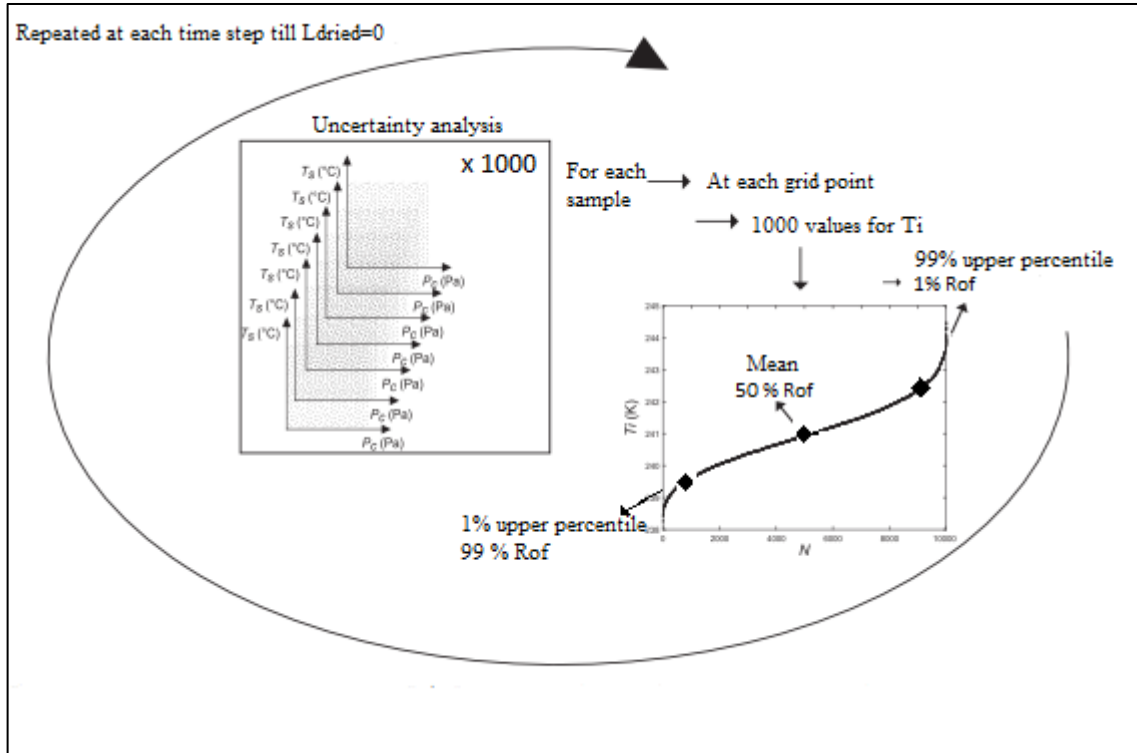


**Figure 4.2** Explanation of the uncertainty analysis on the dynamic Design Space. For each of the 1000 combinations of the input matrix,  $T_i$  is calculated and ordered from low to high value. The 1%, 50%, 99% upper percentile are indicated which respectively correspond to a risk of failure of 99%, 50%, 1% (From Mortier et al., 2016 with modifications).

#### 4.2.4.2. Determination of the mass transfer coefficient and its uncertainty.

For the first case study, a mechanistic model developed at the Politecnico di Torino (Pisano and Capozzi, 2017) was used to predict the morphology of the product along the dried cake and its inter-variability that depends on the nucleation distribution curve. Then, for each class of the mean pore diameter  $D_p$  of the distribution, the model determines  $R_p$  and its uncertainty as a function of the dried layer. The input parameters of the model are taken from a previous work (Flores Brun, 2017).

Once the profile is known,  $R_p$  was fitting as a function of  $L_d$  according to this equation:

$$R_p = R_{p,0} \frac{A_{R_p} L_{dried}}{1 + B L_{dried}} \quad (4.6)$$

With  $R_{p,0}$  (m/s),  $A_{Rp}$  (1/s) and  $B_{Rp}$  (1/m) the constants determined by the fitting that are inserted as input parameters of the mechanistic primary drying model. The global uncertainty of  $R_p$  was also determined to calculate the mean of the uncertainties at a different position of the thickness of the dried product.

For the second study,  $R_p$  was experimentally determined.

Considering the heat used for the sublimation process equal to the heat entering the frozen layer, it is possible to calculate  $R_p$  through Eq. 4.7 (Fissore *et al.*, 2011):

$$K_v(T_s - T_b) = \Delta H_{sub} \frac{1}{R_p} (P_{w,i} - P_{w,c}) \quad (4.7)$$

Where,  $T_s$  (K) is the shelf temperature monitored during the process,  $T_b$  (K) is the product temperature at the bottom of the vial measured with a thermocouple,  $\Delta H_{sub}$  the ice sublimation rate,  $P_{w,i}$  the water pressure at the sublimation front,  $P_{w,c}$  the water vapour pressure in the drying chamber (equal to the chamber pressure  $P_c$ ), and  $K_v$  the heat vial transfer coefficient.  $K_v$  was experimentally determined and taken by literature (Van Bockstal, 2017), while  $P_i$  was calculated using Eq. 4.8 (Fissore *et al.*, 2010).

$$P_0 = \exp\left(\frac{-6140.4}{T} + 28.916\right) \quad (4.8)$$

A nonlinear regression was used to fit the experimental data as a function of  $L_d$  (Eq. 4.6) and to determine the  $R_p$  coefficients ( $R_{p,0}$ ,  $A_{Rp}$  and  $B_{Rp}$ ).

According to the experimental results of Van Bockstal *et al.*, (2017) and the value of the mean uncertainty found via the mathematical model for the first case study, here, the mean uncertainty of  $R_p$  was fixed at 20%.

### 4.3. Results and discussion

#### 4.3.1. Freeze-drying of the mannitol-based formulation

In the first case study, the predictions of the processing parameters with a RoF of 1%, 50%, 99% were simulated for both protocols (HCR and LCR). Moreover, other two simulations without including the uncertainties were performed. In order to validate the model predictions, it was run the cycle HCR without uncertainty. It was not possible to verify the predictions that included the Risks of Failure because of the limited power of the condenser to decrease the shelf temperature below -28°C.

In Figure 4.3,  $R_p$  profile and its uncertainty level were plotted for the protocol HCR and LCR. As mentioned before,  $R_p$  was calculated through the predicted product morphology with the help of a mathematical model (Pisano and Capozzi, 2017).

The mean uncertainty level was 20% for the HCR protocol and 16,5 % for the LCR protocol. The lower uncertainty of the latter is due to the more uniform structure of the product.

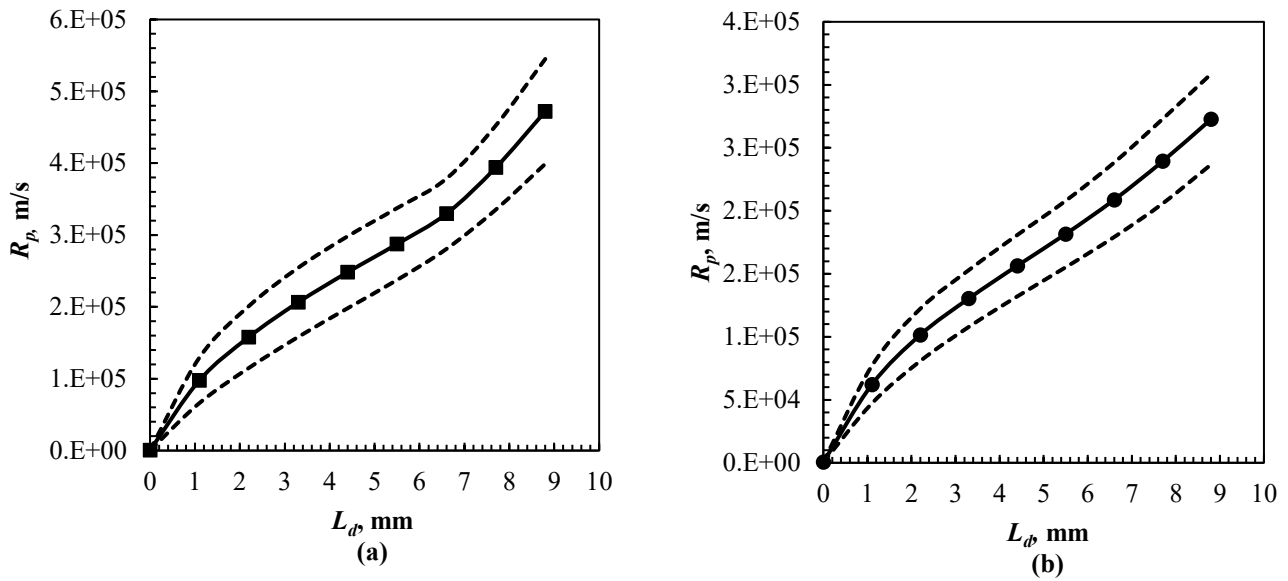


**Figure 4.3**  $R_p$  in function of  $L_d$  for HCR (a) and LCR (b) protocol. The dashed lines represent the upper and the lower limit of  $R_p$ .

Figure 4.4 illustrates the evolution of the frozen layer thickness  $L_f$  during primary drying as calculated by the model for the two freezing protocols and considering three different values of RoF.

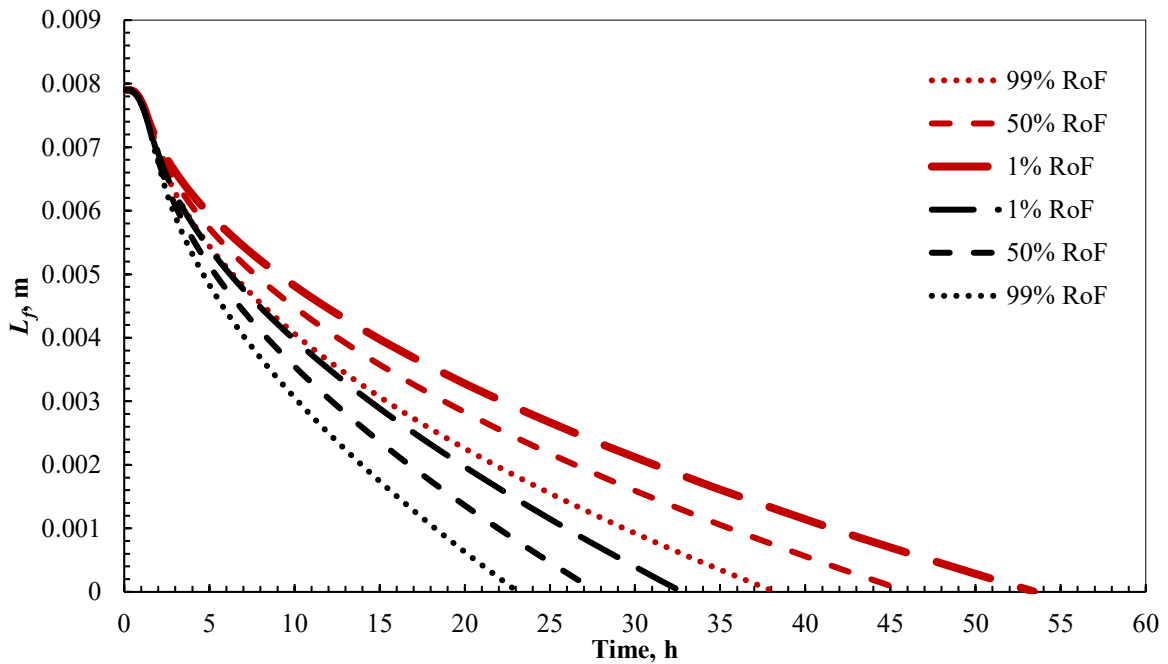


**Figure 4.4** Evolution of  $L_f$  during primary drying for various values of RoF (1%, 50%, 99%) for HCR protocols (red lines) and LCR protocols (black lines). The stroke of the lines is different as a function of the RoF as reported in the legend.

The most interesting results is obtained comparing the two protocols. All simulations referred to edge-vials because these vials undergo more aggressive process conditions, mainly due to radiation from chamber walls and the freeze-dryer door. As the values of  $R_p$  and its uncertainty were lower in the case of LCR protocol, the predictions showed a primary drying endpoint for the edge-vials that was shorter

(at maximum 32h with 1% RoF) than working with the HCR cycle with which the time can increase almost two times more.

The optimal values of  $T_s$  for different RoFs as a function of time were represented for both protocols in Figure 4.5; chamber pressure remained constant during the whole process at a value equal to 10 Pa.

As shown in Figure 4.5, the optimal shelf temperature has its higher values at the beginning of primary drying and then decreased during the process. Anyway, a higher RoF is associated with a higher  $T_s$  profile and therefore, the primary drying time became shorter.

The black line represents the prediction of  $T_s$  if the uncertainties of the 8 factors reported in Table 4.3 were not considered by the primary drying model. The results showed that the worst situation was represented by this configuration, because it seemed similar to the predictions with the higher Risk of Failure. Theoretically, if the uncertainty was not taken into account, the model works with the mean value of the input variables and the process parameters, and hence, the predictions should be closer to the 50% RoF and not to the 99% RoF. This behavior could be explained, in part, considering that the matrix of 1000 samples in which the model combines the uncertainties is random and could give a conservative combination of these parameters. In the previous works, Mortier *et al.* worked with a matrix of 10,000 samples (Mortier *et al.*, 2016; Van Bockstal *et al.*, 2017). The number of the combinations improves the reliability of the model, but the computational cost time increases a lot. Moreover, the input variables were determined experimentally or by the help of some models and they could be an under or over estimations of their real values.

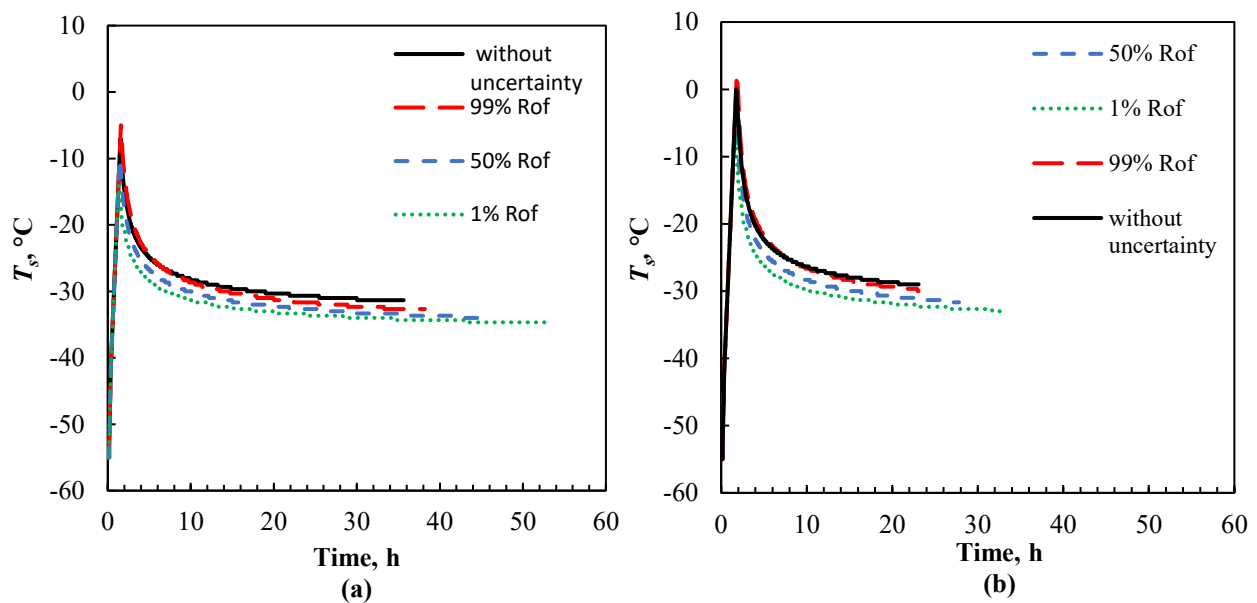


**Figure 4.5** Optimal values for  $T_s$  in function of time for RoF of 1%, 50% and 99% with the protocol HCR (a) and LCR (b).

Only the validation of the HCR protocol without considering uncertainty of input parameters was possible. In Figure 4.6 the product temperature profiles ( $T_i$ ) were plotted as a function of time. The product temperature was monitored inserting a thermocouple at the bottom of a central vial and of an edge-vial. The horizontal line represents the critical product temperature that, in this case, was supposed to be equal to  $T_{c-50}$  (-34.8 °C). The product temperature for the edge-vial monitored with the thermocouple overcame  $T_{cr}$ , so it could be concluded that the prediction was confirmed.

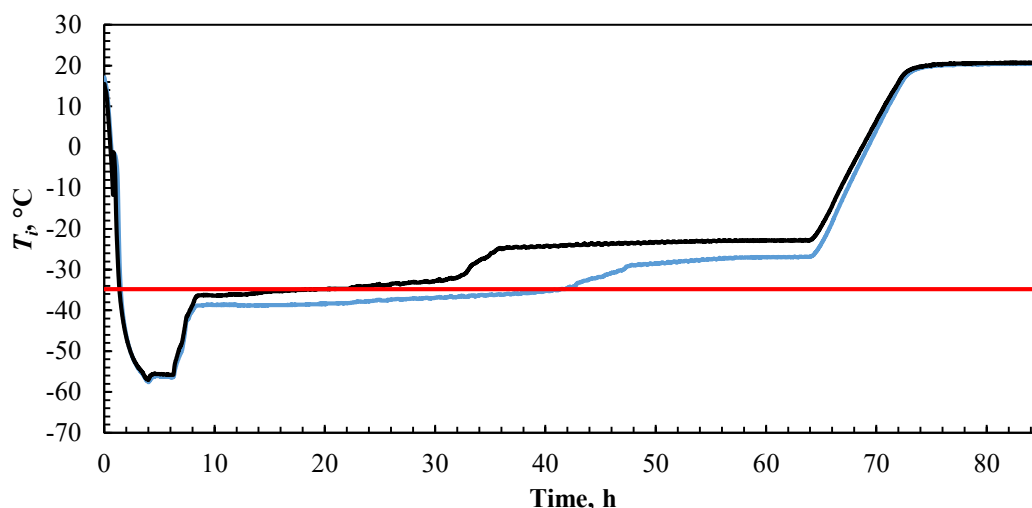


**Figure 4.6** Prediction of the product temperature for (blue) central vial and (black) edge vials in the case of HCR protocol without including the parameters uncertainty. The horizontal red line is the critical product temperature ( $-34.8^{\circ}\text{C}$ ).

In this cycle, the shelf temperature started to swing around  $-28^{\circ}\text{C}$  as shown in Figure 4.7. For this reason, it was chosen to not verify the predictions which included a level of uncertainty because they induce to work with lower shelf temperatures than  $-28^{\circ}\text{C}$  during primary drying, as observed in Figure 4.5.

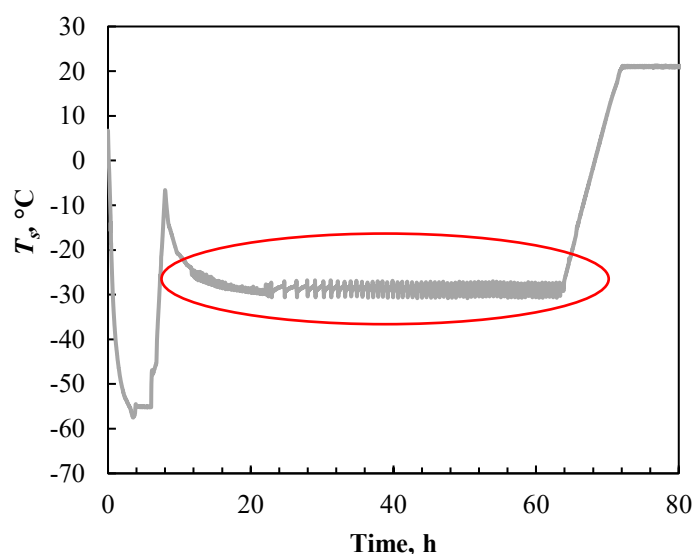


**Figure 4.7** Oscillation around  $-28^{\circ}\text{C}$  of the shelf temperature during the validation of HCR protocol without uncertainty.

It is important to remind that the temperature measurement did not coincide with the temperature at the sublimation front, but it slightly deviates from that value (Pikal *et al.*, 1990). Nevertheless, no macroscopic collapse was observed in the final dried samples. Moreover, in a recent research it was reported that in some cases the macroscopic collapse of the structure did not occur even if the temperature at the sublimation rate could overcome the collapse temperature (Rey and May, 2011). Also the presence of mannitol in the solution makes difficult the possibility of a macroscopic collapse.

### 4.3.2. Freeze-drying of the sucrose-based formulation

A formulation constituted by ADH and sucrose was studied and its  $R_p$  was experimentally calculated. Figure 4.8 shows the profile of  $R_p$ , as a function of  $L_d$ , and the fitting of the experimental data with a nonlinear regression.

The dynamic Design Space was calculated verifying the RoF, 1%, 50% and 99%, and the case that does not include the uncertainty analysis. Figure 4.9 and 4.10 show the evolution of  $L_d$  and  $T_s$  during primary drying. The plot of  $P_c$  was not reported because  $P_c$  decreased in 15 minutes until the value of 10Pa and stayed constant at this level during all primary drying in each prediction.

Also, in this case, if a high value of RoF was included, the primary drying time is shorter as shown in Figure 4.9 and 4.10. Without including the uncertainty, the prediction was positioned between 50% and 99% RoF.

All simulations referred to edge-vials because these vials undergo more aggressive process conditions, mainly due to radiation from chamber walls and the freeze-dryer door, whereas the real primary drying end point was found experimentally by observing the Pirani/Baratron ratio.

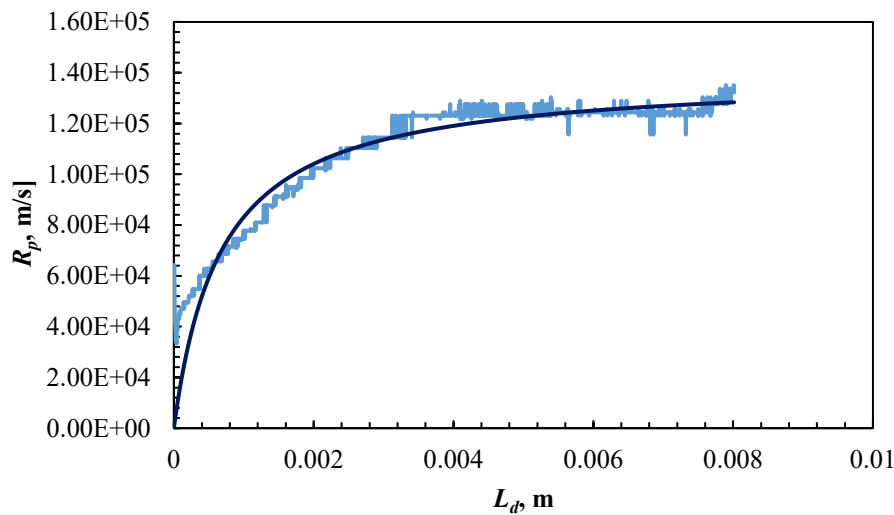


**Figure 4.8**  $R_p$  as a function of the product thickness layer. The blue line represents the fitted profile of  $R_p$  according to Eq.4.6, the cyan line represents the experimental data.

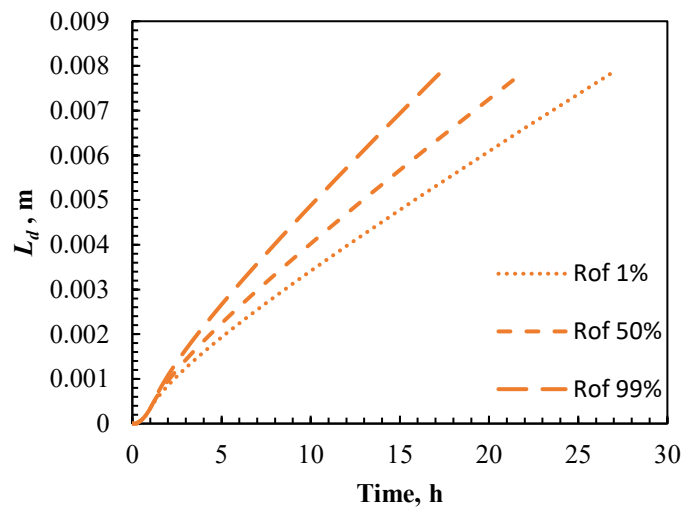


**Figure 4.9** Evolution of  $L_d$  during primary drying for a RoF of 1%, 50%, 99% for the sucrose-based formulation

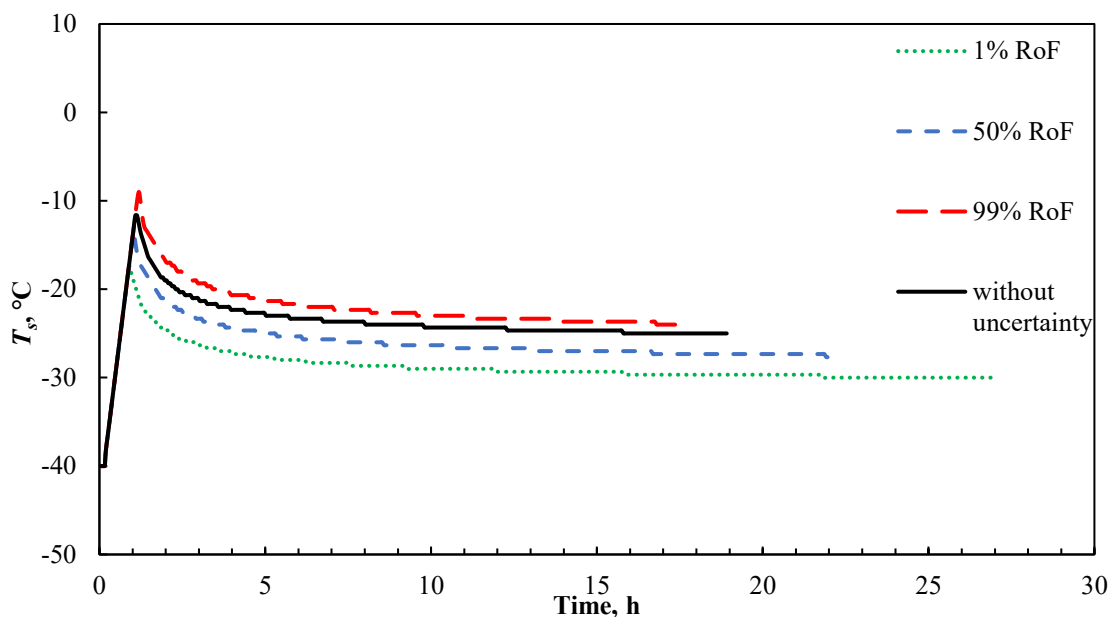


**Figure 4.10** Optimal values for  $T_s$  as a function of time for 1%, 50% ,99% RoF and without RoF.

In Figure 4.11 the experimental runs using the process conditions as obtained from the Design Space with 99% and 50% RoF are shown. With the higher risk of failure,  $T_i$  was closer to  $T_{cr}$  than the case with 50% RoF. Moreover, once  $T_s$  reached its maximum, the product temperature at the edge-vial overcame a little bit the critical product temperature in the case of 99% RoF. Anyway, the macroscopic collapse did not occur.

It should be remarked that the critical product temperature was taken equal to the glass transition temperature  $T_g'$  calculated by MDSC analysis and, as explained in section 4.2.2, this value is very conservative, because the critical temperature measured in a vial can be in general few degrees higher of the  $T_{cr}$  measured by an instrument (Pikal et al., 1990). Thus, it was expected to not observe the exceeding of  $T_c$  and, hence, macroscopic collapse.

A consideration on the  $T_{cr}$  used here fore calculating the design space is necessary in order to understand why we did not observe collapse. The glass transition temperature measured by MDSC was  $-35.2^\circ\text{C}$  for the formulation ADH (0.01 mg/ml) + 2.5% (w/v) of sucrose. Greco *et al.*, (2013), reported that the glass transition temperature of sucrose measured with DSC was  $-34^\circ\text{C}$ , while using the optical coherence tomography freeze-drying microscope (OCT-FDM),  $T_{c-50}$ , as the average between the onset of collapse and the full collapse temperature was  $-30^\circ\text{C}$ . Another measurement of  $T_g'$  of sucrose solution with DSC analysis found in the literature reported a value of  $-32^\circ\text{C}$  (Van Bockstal *et al.*, 2017; Chang *et al.*, 1992). So,  $T_{cr}$  set here is much lower than the actual critical temperature that determines the collapse.

This behavior underlines how the uncertainty of  $T_{cr}$  influenced a lot the simulation that can deviate from the reality. The model itself introduces a safety margin since  $T_{cr}$ , setting equal to  $T_g'$ , that is in general few degrees slower than the collapse temperature, was not included as uncertainty parameter to not consider higher values than the mean value of  $T_{cr}$ .

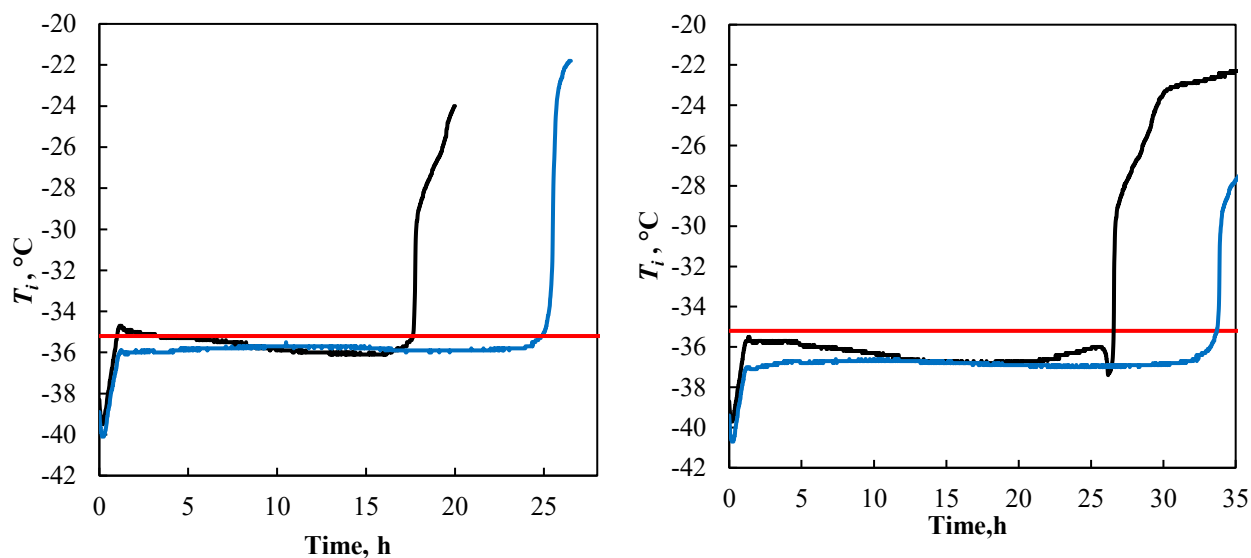


**Figure 4.11** Prediction of the product temperature for (blue) central vial and (black) edge-vials for 99% RoF (left) and 50% RoF (right). The horizontal red lines represent the critical product temperature ( $-35.2^{\circ}\text{C}$ ).

Finally, we studied the effect of RoF on drying time using (a) fixed  $T_s$  and  $P_c$ , and using the process conditions determined by the design space with (b) 50% RoF and (c) 99% RoF. For case (a) the freeze-drying cycle was the same used for the freeze-drying experiments with ADH and sucrose with a freezing rate of  $1^{\circ}\text{C}/\text{min}$  (see Table 3.3 in Chapter 3).

Using the process conditions (a), the primary drying ended after 39.5 h, in the case (b) primary drying endpoint was of 33.5h and in the case (c) 25h. So, there was a reduction of the primary drying time of 15% and 37%. These data are summarized in Table 4.4.

This result confirmed the utility of applying a dynamic Design Space to optimize the cycle in terms of time and energy consumptions.

**Table 4.4** Experimentally primary drying time in case of dynamic Design Space with 50% and 99 % RoF and fixed settings  $P_c$  and  $T_s$ .

Cycle	Primary Drying Time [h]	Reduction primary drying time (%)
(a) Fixed $T_s$ and $P_c$	39.5	-
(b) Dynamic design space with 50% RoF	33.5	15%
(c) Dynamic design space with 99% RoF	25	37%

Moreover, the enzymatic activity of ADH was measured for the three cycles without observing relevant changes in the recovery activity, also due to the presence of sucrose as protectant.

#### 4.4. Conclusions

In this section a mechanistic model developed at Ghent University (Van Bockstal *et. al*, 2017) was used to determine the dynamic Design Space with the inclusion of the uncertainty of input parameters, such as the heat and mass transfer coefficient, the inherent errors of the vials dimension, the uncertainty of the setting parameters  $P_c$  and  $T_s$ , and the filling volume. The model was used to predict the primary drying cycle of two different formulations (two case studies) considering 3 different Risks of Failure (1%, 50%, 99% RoF), based on the probability that one or more vials could collapse during primary drying. Moreover, for the first case study, the impact of the cooling rate on the cycle design was studied.

Simulations revealed that the inclusion of an uncertainty level impacted on the primary drying time and on the quality of the final products. If the uncertainties were not included in the model, the probability of failure was higher than 50% and closer to 99% RoF. In general terms, it is obvious that working with a higher risk of failure involves higher sublimation rate, decreasing the primary drying time but the probability of cake collapse is higher.

Comparing the predictions of HCR and LCR protocols, it was confirmed that the freezing method impacted on the optimization of the cycle also via Design Space. In fact, the prediction of the primary drying time is lower working with the LCR protocol due to the bigger dimension of pores that reduced the mass transfer resistance  $R_p$ .

Regarding the second case study, two validations of the model predictions (50% and 99% RoF) were made. With these experiments, it was possible to underline that the uncertainty of the critical temperature  $T_{cr}$  was important because it is, in general, an underestimation of the real collapse temperature making the predictions too conservative. Moreover, with this second case study, the experimental primary drying time with the fixed values of  $P_c$  and  $T_s$  was compared with the validations of the two dynamic design cycles. The result showed that the dynamic Design Space allowed to optimize the cycle in terms of time (and energy) guaranteed and gave information on the risk that one vial within the batch did not meet the quality attributes.

#### List of symbols

$A_p$	Inner vial area, m <sup>2</sup>
$AR_p$	$R_p$ coefficient of Eq.4.6, s <sup>-1</sup>
$A_v$	Outer vial area, m <sup>2</sup>
$BR_p$	$R_p$ coefficient of Eq. 4.6, m <sup>-1</sup>
$D_p$	Size of ice crystal/pore, m
$J_w$	Sublimation flux, Kg s <sup>-1</sup> m <sup>-2</sup>
$k$	Ratio of the specific heat for water

$K_v$	Heat transfer coefficient, $\text{Jm}^{-2}\text{s}^{-1}\text{k}^{-1}$
$L_d$	Thickness of the dried layer, m
$M$	Molecular weight of water, $\text{kg mol}^{-1}$
$m_{sub}$	Mass of sublimated ice, kg
$\dot{m}_{sub}$	Sublimation rate, $\text{Kg s}^{-1}$
$P_c$	Chamber pressure, Pa
$P_i$	Vapor pressure at the sublimation front, Pa
$P_{w,c}$	Water vapor partial pressure in the chamber, Pa
$R_p$	Product resistance to vapor flow, $\text{ms}^{-1}$
$R_{po}$	$R_p$ coefficient of Eq. 4.6, $\text{m s}^{-1}$
$r_{v,i}$	Inner radius of vial, m
$r_{v,n}$	Radius of vial neck
$r_{v,o}$	Outer radius of vial, m
$T_{c-50}$	Mid-point collapse, $^{\circ}\text{C}$
$T_{cr}$	Critical product temperature, $^{\circ}\text{C}$
$T_g'$	Glass transition temperature, $^{\circ}\text{C}$
$T_{fc}$	Full collapse temperature, $^{\circ}\text{C}$
$T_i$	Temperature at the sublimation front, $^{\circ}\text{C}$
$T_{oc}$	Onset collapse temperature, $^{\circ}\text{C}$
$T_s$	Shelf temperature, $^{\circ}\text{C}$
$V$	Filling volume, $\text{m}^3$
$\Delta H_{sub}$	Latent sublimation heat, $\text{J mol}^{-1}$
$\Delta T$	Temperature across the ice layer, K

## Greek symbols

$\alpha$	$K_v$ coefficient, $J\ m^{-2}s^{-1}k^{-1}$
$\beta$	$K_v$ coefficient, $J\ m^{-2}s^{-1}k^{-1}Pa^{-1}$
$\gamma$	$K_v$ coefficient, $Pa^{-1}$
$\zeta$	Volume fraction of ice
$\rho_{ice}$	Ice density, $kg\ m^{-3}$

## Abbreviations

ADH	Alcohol Dhydrogenase
CQA	Critical Quality Attributes
DSC	Differential Scanning Calorimetry
FDM	Freeze-Drying Microscope
HCR	High Cooling Rate
LCR	Low Cooling Rate
MDSC	Modulate Differential Scanning Calorimetry
OCT- FDM	Optical Coherence Tomography Freeze-Drying Microscope

## References

- Chang B.S, and Randal C.S., 1992. "Use of Subambient Thermal Analysis to Optimize Protein Lyophilization." *Cryobiology*, **29**(1):632-656.
- Fissore, D., Pisano, R., Barresi, A. A., 2010. "On the Methods Based on the Pressure Rise Test for Monitoring a Freeze-Drying Process", *Drying Technology*, **29**(1):73-90.

- Fissore, D., Pisano, R., & Barresi, A. A., 2011. “Advanced approach to build the design space for the primary drying of a pharmaceutical freeze-drying process.” *Journal of Pharmaceutical Sciences*, **100**(11), 4922–4933.
- Flores Brun E., 2017. “Development of Freeze-Drying Cycles and Evaluation of Uncertainty on Heat and Mass Transfer.” Master Thesis work, Politecnico di Torino.
- Giordano, A., Barresi, A. A., & Fissore, D., 2011. “On the use of mathematical models to build the design space for the primary drying phase of a pharmaceutical lyophilization process.” *Journal of Pharmaceutical Sciences*, **100**(1), 311–324.
- Greco K., Mujat M., Kinney K.L.G., Hammer D.X., Ferguson R.D., Iftimia N., Mulhall P., Sharma P., Kessler W.J., Pikal M.J., 2013. “Accurate Prediction of Collapse Temperature Using Optical Coherence Tomography-Based Freeze-Drying Microscopy.” *Journal of Pharmaceutical Sciences*, **102**(6): 1773–85.
- Koganti V.R., Shalaev E.Y., Berry M.R., Osterberg T., Youssef M., Hiebert D.N., Kanka F.A., Nolan M., Barrett R., Scalzo G., Fitzpatrick G., Fitzgibbon N., Luthra S., Zhang L., 2011. “Investigation of Design Space for Freeze-Drying: Use of Modeling for Primary Drying Segment of a Freeze-Drying Cycle.” *AAPS PharmSciTech*, **12**(3): 854–61.
- Mortier, S. T. F. C., Van Bockstal, P. J., Corver, J., Nopens, I., Gernaey, K. V., & De Beer, T., 2016. “Uncertainty analysis as essential step in the establishment of the dynamic Design Space of primary drying during freeze-drying.” *European Journal of Pharmaceutics and Biopharmaceutics*, **103**(1), 71–83.
- Rey, L., & May, J. C., 2011. Freeze-drying/ lyophilization of pharmaceutical and biological products, *Second Edition, Revised and Expanded*. Drugs and the Pharmaceutical Sciences. Taylor & Francis.
- Pikal M.J., 1985. “Use of laboratory data in freeze drying process design: Heat and mass transfer coefficients and the computer simulation of freeze drying.” *Journal of Pharmaceutical Science and Technology*, **39** (3): 115–138.
- Pikal M.J and Shah S., 1990. “The Collapse Temperature in Freeze Drying: Dependence on Measurement Methodology and Rate of Water Removal from the Glassy Phase.” *International Journal of Pharmaceutics*, **62**(1): 165–86.
- Pisano, R., & Capozzi, L. C., 2017. “Prediction of product morphology of lyophilized drugs in the case of Vacuum Induced Surface Freezing.” *Chemical Engineering Research and Design*, **125**(1), 119–129.
- Pisano, R., Fissore, D., Barresi, A. A., Brayard, P., Chouvinc, P., & Woinet, B., 2013. “Quality by design: optimization of a freeze-drying cycle via design space in case of heterogeneous drying behavior and influence of the freezing protocol.” *Pharmaceutical Development and Technology*, **18**(1), 280–295.

Van Bockstal, P. J., Mortier, S. T. F. C., Corver, J., Nopens, I., Gernaey, K. V., & De Beer, T., 2017. "Quantitative risk assessment via uncertainty analysis in combination with error propagation for the determination of the dynamic Design Space of the primary drying step during freeze-drying." *European Journal of Pharmaceutics and Biopharmaceutics*, **121**(1), 32–41.



# Chapter 5

## 5. Conclusions

In this work, freeze-drying of pharmaceuticals has been discussed, focusing the attention on freezing, the first step of the process. During freezing, the shelf temperature is decreased below 0°C to allow the complete crystallization of ice (and solute). The degree of supercooling is linked to the nucleation phenomenon that is stochastic; therefore, not all samples nucleate at the same temperature and, as a consequence, the samples can show different dimensions of ice crystals. In fact, a lower nucleation temperature leads to the formation of smaller ice crystals. Also the freezing method and the freezing rate impact on the ice crystals size. It is important to obtain samples characterized by bigger ice crystals to facilitate the ice sublimation during primary drying, allowing the optimization of the cycle in terms of energy and time. Moreover, freezing can induce some stresses on active ingredients, such as proteins, and at the same way, drying stresses are present, especially because the interface denaturation can occur. Therefore, a porous matrix with bigger pores is preferred also to preserve the stability of an active pharmaceutical ingredient (API).

So, some experiments were conducted to study the impact of freezing on the product structure, on the stability of an active pharmaceutical ingredient (API) and on the optimization of the total process via dynamic Design Space.

Firstly, the study was focused on how the freezing method can affect the product structure in terms of intra and inter-vial variability. Starting from the measurement of the nucleation temperature,  $T_n$ , two different vials configurations were compared: suspended and non-suspended vials. Furthermore, two different protocols were applied, changing the freezing rate (high cooling rate, HCR, and low cooling rate, LCR). Then, for one of the two protocols (HCR), some dried samples were analyzed by SEM in three different position of the dried cake (top, center, bottom) to estimate the pore size intra-variability, and to correlate a mean value of the pore size in the sample with the nucleation temperature both for suspended and non-suspended vials. Known the value of the mean pore size,  $D_p$ , linked to  $T_n$  for these samples, it was possible to extrapolate a function ( $D_p$  as a function of  $T_n$ ) to determine the mean pore size distribution curves. Finally, also the variability of the mass transfer resistance during primary drying,  $R_p$ , was determined. The variability is linked to the morphology of the dried samples. Taking a constant value of the pore diameter, a representative value and its variability of  $R_p$  was calculated for both vials configuration; moreover,  $R_p$  was calculated for each sample analysed by SEM as a function of  $T_n$  and taking a variable  $D_p$  in the dried cake. At last, since the investigated solution contained mannitol, the physical structure of the dried products was investigated by X-ray diffraction analysis (XRD) because mannitol tends to crystallize during freezing, but it can show three polymorphs,  $\alpha, \beta, \gamma$ ; only  $\beta$  is stable, while  $\alpha$  e  $\gamma$  are metastable.

This study suggested that the suspended-vials configuration is in general preferable to the conventional freezing, since it allows to work with fast operating conditions reaching good product quality in terms of intra-vial and inter-vial homogeneity. In fact, as first results, the suspended-vial freezing showed a narrower range of the nucleation temperature variation when the HCR protocol was applied; The most interesting result was found analyzing SEM images of some dried samples of the two vials configuration with the HCR protocol and correlating these images to the nucleation temperature. Observing these images, non-suspended vials showed a big variability, not only in the cake of each vial, but also among vials. On the other hand, SEM images of suspended vials showed bigger and similar pores independently

from the nucleation temperature and the depth of thickness of the dried cake. The mean pore size distribution curves revealed that non-suspended vials were characterized by a mean pore diameter of 41  $\mu\text{m}$ , while the value was almost 96  $\mu\text{m}$  for suspended vials. Using these mean pore diameters and the standard deviation of the gaussian curves,  $R_p$  and its variability were theoretically determined, confirming as expected:  $R_p$  and its variability were lower for the suspended vials than non-suspended vials. Nevertheless, XRD spectra indicated a major presence of the stable form of mannitol,  $\beta$ , in non-suspended vials, while a not negligible presence of the metastable polymorph  $\alpha$  was found for the suspended vials.

In the second part of this work, the impact of the freezing method on the stability of an active pharmaceutical ingredient (API), was studied choosing alcohol dehydrogenase (ADH) as model protein. The protein was subjected to freeze-thawing and freeze-drying cycles applying the conventional shelf-ramped freezing method (non-suspended vials) with two different cooling rates (1°C/min and 0.1°C/min), or using a quench freezing by immersion of the samples in liquid nitrogen for few minutes. The concentration of the protein was changed, working with 0.1 mg/ml or 0.01 mg/ml, and the efficiency of PEG and sucrose as lyoprotectant was tested. Finally, for some tests, the nucleation temperature was monitored to search if exist a correlation between the nucleation temperature and the residual activity of the enzyme.

By the first set of experiments, it was found that ADH is freeze-tolerant because preserved almost its activity after freeze-thawing in absence of any kind of protection. Moreover, working with a higher concentration of protein is a better way to preserve more activity since protein itself is able to act as a stabilizer. Nevertheless, there was no impact of freezing methods and so, of cooling rate and nucleation temperature during freeze-thawing. Since ADH did not suffer from ice interaction, the dimension of ice crystal, as consequence of the freezing method and the cooling rate, was not a cause of the deactivation of the protein. This behavior was probably due to the absence of an interface that could irreversibly compromise the denaturation of the protein. So, ADH was not revealed the right model-protein to can study the impact of freezing on its activity. In relation to the formulation, it was discovered that PEG was not able to protect ADH during drying. Instead, there is a good recovery if in the formulation sucrose was included. To stabilize if there is a correlation between nucleation temperature and the enzymatic activity, the formulation with the lower concentration of enzyme was selected because the protein seems to be more sensitive in lower concentrations and sucrose was chosen as protectant because promoted the recovery of the activity but, at the same time, it influenced the activity for the presence of an interface during drying. In fact, it was found that after drying, working with a freezing rate of 1°C/min, there was a decrease in activity with the increase of nucleation temperature. Instead, for a freezing rate of 0.1°C/min, the nucleation temperature seemed to not impact the activity because of the more uniformity of the cake structure and the bigger dimension of pores.

At last, a mechanistic model was used to determine the dynamic Design Space during primary drying, the configurational space of the process parameters, shelf temperature and chamber pressure ( $T_s$  and  $P_c$ ) as a function of the input parameters (i.e. heat and mass transfer coefficient, geometric characteristics of the vials, filling volume, critical product temperature) with the inclusion in the model of some uncertainties of these variables. The goal of the model is determining the dynamic profile of  $T_s$  and  $P_c$  that optimizes the primary drying step in terms of time (and energy) and considering three different risks of failure (1%, 50%, 99%) defined as the probability to have a collapse in one or more vials. The risk of failure is linked to the uncertainty analysis made by the model using the “simple Sobol technique”. Two case studies were examined; in the first one, the simulations were conducted on a placebo formulation using two different cooling protocols (HCR and LCR), in the second case, a formulation containing ADH was tested. Furthermore, the impact of uncertainties on model predictions was assessed running

the model also without including uncertainty, and some validation cycles were run to verify the predictions.

Simulations revealed that the inclusion of an uncertainty level impacted on the primary drying time and on the quality of the final products. If the uncertainties were not included in the model, the probability of failure was higher than 50% and closer to 99% RoF. In general terms, it is obvious that working with a higher risk of failure involves higher sublimation rate, decreasing the primary drying time and the probability of cake collapse should be higher. Comparing the predictions of HCR and LCR protocols, it was confirmed that the freezing method impacted on the optimization of the cycle also via Design Space. In fact, the prediction of the primary drying time is lower working with the LCR protocol due to the bigger dimension of pores that reduced the mass transfer resistance  $R_p$ . Regarding the second case study, two validations of the model predictions (50% and 99% RoF) were made. With these experiments, it was possible to underline that the uncertainty of the critical temperature  $T_{cr}$  was important because it is, in general, an underestimation of the real collapse temperature making the predictions more conservative. Moreover, with this second case study, the experimental primary drying time with fixed values of  $P_c$  and  $T_s$  was compared with the validations of the two dynamic design cycles. The result showed that the dynamic Design Space allowed to optimize the cycle reducing the time of primary drying and guarantying some critical attributes that depend on the uncertainty level that it was allowed.



## Acknowledgments

Here we are, at the end of my studies at Politecnico di Torino. During these years, I discovered a part of myself, a new one because staying so far from the own family and the childhood friends, from one hand, could be sad, but it allows to grow up and become independent.

If someone asked me “would you do everything again?”, Honestly, my answer would be hesitant, but I would say “yes, I do”.

With these few rows, I would like to say thank you to all the people that have been important for me during this period of my life.

First of all, thanks to my supervisor, Roberto Pisano, who allowed me to work to a so interesting project and that has been a guide with his clarifications and explanations. Thanks professor for having given me the opportunity to conduct part of my work abroad, in Ghent. I loved this experience and I would repeat it infinite times. I would also like to thank my tutor, Luigi, who always helped me in this project from the theory to the experimental work until the very last days. So, thanks to my second supervisor, Thomas De Beer, who hosted me in his University Department and dedicated part of his time to listen how proceeded my job. Thanks, also, to Pieter-Jan who was an excellent guide and always willing to help me for all the days I spent in Ghent and that conveyed serenity to me with his ever-smiling face.

A special thanks to my parents for their huge sacrifices to give me a good life in Turin. I would also like to express profound gratitude to my uncles, Anna and Enrico, behaved like second parents for me, here in Turin. And, obviously, there are no words to can say thank to my point of reference, my boyfriend, Dario, that supported and loved me for all these five years and a half.

Thanks to all the people that have always believed in me. Thanks to my old friends and to the new ones. Thanks to my Erasmus friends with whom I spent only few months, but it has been like if we knew each other since several years.

Finally, a huge to my dear grandparents. I think you every time and I will never forget you and your unconditional love.

Thank you all very much.

Valeria

